

**COIFLET-TYPE WAVELETS:  
THEORY, DESIGN, AND APPLICATIONS**

APPROVED BY  
DISSERTATION COMMITTEE:

Supervisor: \_\_\_\_\_

Supervisor: \_\_\_\_\_

\_\_\_\_\_

\_\_\_\_\_

\_\_\_\_\_

\_\_\_\_\_

Copyright  
by  
Dong Wei  
1998

To Xun, Hannah, and my parents

**COIFLET-TYPE WAVELETS:  
THEORY, DESIGN, AND APPLICATIONS**

by

**DONG WEI, B.E., M.S.**

**DISSERTATION**

Presented to the Faculty of the Graduate School of  
The University of Texas at Austin  
in Partial Fulfillment  
of the Requirements  
for the Degree of

**DOCTOR OF PHILOSOPHY**

THE UNIVERSITY OF TEXAS AT AUSTIN

August 1998

## Acknowledgments

I am deeply thankful to my supervisor Professor Al Bovik. Al has been enthusiastically inspiring and encouraging me since I joined his group. Without his excellent guidance and tremendous support, this research work would have been impossible.

My heartfelt gratitude also goes to my co-supervisor Professor Brian Evans for his great enthusiasm, interaction, friendship, and valuable advice over the years.

I wish to thank Professors Ed Powers, Joydeep Ghosh, San-qi Li, and John Gilbert, who served my Dissertation Committee.

I am grateful to Professors Sid Burrus and Ronny Wells at Rice University. It was Sid and Ronny who first introduced wavelet theory to me and planted the seed of this dissertation.

I would like to thank many former and current graduate students at the Laboratory for Image and Video Engineering (formerly the Laboratory for Vision Systems) at UT Austin. They are Güner Arslan, Barry Barnett, Niranjan Damera-Venkata, Amey Deosthali, Srikanth Gummadi, Dave Harding, Joe Havlicek, John Havlicek, Jong-il Kim, Tom Kite, Bill Klarquist, Sanghoon Lee, Biao Lu, Hung-Ta Pai, George Panayi, Marios Pattichis, Wade Schwartzkopf, Kartick Suriamoorthy, Jeff Wehnes, and Changhoon Yim. This talented group

of people has been very helpful, and I enjoyed the pleasant environment offered by them.

Most of the work in the dissertation were supported in part by grants from Schlumberger Austin Research, Southwestern Bell Technology Resources, Inc., and the Army Research Office. Their generous financial support is gratefully acknowledged.

My parents taught me many valuable “theorems of life” when I was growing up, which were important during my graduate study.

My deepest gratitude goes to my wife Xun, who showed infinite patience and understanding during my graduate study, and offered tremendous moral support and loving encouragement.

# COIFLET-TYPE WAVELETS: THEORY, DESIGN, AND APPLICATIONS

Publication No. \_\_\_\_\_

Dong Wei, Ph.D.  
The University of Texas at Austin, 1998

Supervisors: Alan C. Bovik  
Brian L. Evans

During the last decade, the explosively developing wavelet theory has proven to be a powerful mathematical tool for signal analysis and synthesis and has found a wide range of successful applications in the area of digital signal processing (DSP). Compared to their counterparts in the Fourier realm, wavelet techniques permit significantly more flexibility in system design for many applications such as multirate filtering, sampling and interpolation, signal modeling and approximation, noise reduction, signal enhancement, feature extraction, and image data compression. Most classical wavelet systems have been constructed from a primarily mathematical point of view, and they are fundamentally suitable for representing continuous-domain functions rather than discrete-domain data. From a discrete-time or DSP perspective, we develop new wavelet systems.

This dissertation focuses on the theory, design, and applications of several novel classes of one-dimensional and multi-dimensional Coiflet-type

wavelet systems. In particular, we propose a novel *generalized Coifman criterion* for designing high-performance wavelet systems, which emphasizes the vanishing moments of both wavelets and scaling functions. The resulting new wavelet systems are appropriate for representing discrete-domain data and enjoy a number of interesting and useful properties such as

- sparse representations for smooth signals,
- interpolating scaling functions,
- linear phase filterbanks, and
- dyadic fractional filter coefficients,

which are promising in solving a large variety of DSP problems. We show that some of the new wavelet systems achieve superior performance (e.g., better rate-distortion performance, better perceptual quality, and lower computational complexity) over the state-of-the-art ones in the field of image coding.



# Table of Contents

<b>Acknowledgments</b>	<b>v</b>
<b>Abstract</b>	<b>vii</b>
<b>List of Tables</b>	<b>xii</b>
<b>List of Figures</b>	<b>xiii</b>
<b>Chapter 1. Introduction</b>	<b>1</b>
1.1 Background . . . . .	1
1.2 Notation and Basic Assumptions . . . . .	2
1.3 Fundamentals of Wavelet Theory . . . . .	5
1.3.1 Wavelet Series . . . . .	5
1.3.2 The Mallat Algorithm . . . . .	6
1.3.3 Perfect Reconstruction Filterbank . . . . .	8
1.4 Vanishing Moment Property . . . . .	11
1.4.1 Vanishing Wavelet Moments . . . . .	12
1.4.2 Vanishing Scaling Function Moments . . . . .	13
1.5 Previous Work . . . . .	15
1.6 Contributions and Organization of the Dissertation . . . . .	15
<b>Chapter 2. Theory of Coiflet-Type Wavelets</b>	<b>19</b>
2.1 Equivalent Descriptions of Vanishing Wavelet Moments . . . . .	19
2.2 Equivalent Descriptions of Vanishing Scaling Function Moments . . . . .	20
2.3 Vanishing Scaling Function Moments in a Biorthogonal Wavelet System . . . . .	22
2.4 Sampling Approximation Power . . . . .	23
2.4.1 Asymptotic $L^2$ -Error of Sampling Approximation . . . . .	24
2.4.2 Computation of Asymptotic Constant . . . . .	28
2.5 Summary . . . . .	31

<b>Chapter 3. Generalized Orthogonal Coiflets</b>	<b>32</b>
3.1 Definition . . . . .	32
3.2 Design . . . . .	32
3.2.1 Filter Length versus System Order . . . . .	33
3.2.2 Newton's Method-Based Construction . . . . .	35
3.3 Near-Linear Phase Filterbanks . . . . .	37
3.4 Optimal Design for Minimum Phase Distortion . . . . .	39
3.5 Application to Sampling Approximation . . . . .	46
3.6 Summary . . . . .	47
<b>Chapter 4. Biorthogonal Coiflets</b>	<b>49</b>
4.1 Definition . . . . .	49
4.2 Design . . . . .	50
4.2.1 Constructing Synthesis Filters . . . . .	50
4.2.2 Constructing Analysis Filters . . . . .	53
4.3 Properties . . . . .	58
4.3.1 Symmetry . . . . .	58
4.3.2 Interpolating Scaling Functions . . . . .	61
4.3.3 Dyadic Rational Filter Coefficients . . . . .	62
4.4 Asymptotic Convergence of Filters . . . . .	63
4.5 Application to Image Data Compression . . . . .	66
4.6 Summary . . . . .	69
<b>Chapter 5. Generalized Biorthogonal Coiflets</b>	<b>73</b>
5.1 Definition . . . . .	73
5.2 Design . . . . .	74
5.2.1 Constructing Synthesis Filters . . . . .	74
5.2.2 Constructing Analysis Filters . . . . .	76
5.3 Properties . . . . .	77
5.3.1 Symmetry . . . . .	77
5.3.2 Extra Vanishing Moments . . . . .	78
5.3.3 Other Properties . . . . .	80
5.4 Application to Image Data Compression . . . . .	81
5.5 Summary . . . . .	83

<b>Chapter 6. Biorthogonal Quincunx Coiflets</b>	<b>86</b>
6.1 Basics of Biorthogonal Quincunx Wavelets . . . . .	87
6.2 Vanishing Moments . . . . .	88
6.3 Definition . . . . .	92
6.4 Design . . . . .	92
6.5 Properties . . . . .	94
6.5.1 Symmetry and Isotropism . . . . .	94
6.5.2 Interpolating Scaling Functions . . . . .	95
6.5.3 Asymptotic Convergence of Filters . . . . .	97
6.5.4 Dyadic Rational Filter Coefficients . . . . .	98
6.6 Application to Image Data Compression . . . . .	98
6.7 Extension to Higher Dimensions . . . . .	100
6.8 Summary . . . . .	101
<b>Chapter 7. Generalized Biorthogonal Quincunx Coiflets</b>	<b>104</b>
7.1 Design of Even-Size Filterbanks via an Extended McClellan Transformation . . . . .	105
7.2 Design of Odd-Size Filterbanks via an Extended McClellan Transformation . . . . .	107
7.3 Summary . . . . .	109
<b>Chapter 8. Conclusion</b>	<b>110</b>
<b>Appendix</b>	<b>113</b>
<b>Appendix A. Original Images</b>	<b>114</b>
<b>Bibliography</b>	<b>117</b>
<b>Vita</b>	<b>125</b>

## List of Tables

1.1	Two types of symmetry for wavelet systems . . . . .	12
1.2	Important wavelet systems . . . . .	18
3.1	Minimum phase distortion . . . . .	43
4.1	Filter coefficients of the filterbanks in some biorthogonal Coiflet systems (for some long filters we list about half the coefficients and the other can be deduced by symmetry) . . . . .	59
5.1	Filter lengths of three Coiflet-type wavelet systems . . . . .	77
5.2	Actual numbers of vanishing moments for generalized biorthogonal Coiflet systems . . . . .	80
5.3	Filter coefficients of WPB-22/14 . . . . .	81
5.4	Numbers of vanishing wavelet moments of four biorthogonal wavelet systems . . . . .	82
5.5	PSNR performance of four filterbanks . . . . .	84

# List of Figures

1.1	Block diagram of the analysis part of a two-channel iterative filterbank . . . . .	9
1.2	Block diagram of the synthesis part of a two-channel iterative filterbank . . . . .	9
3.1	Comparisons between the phase distortion of lowpass filters associated with the original Coiflet systems (dash-dotted line) and the optimized ones (solid line): (a) $L = 2$ and (b) $L = 3$ . . . .	43
3.2	Comparison between the original Coiflet and the optimal generalized Coiflet of order 3: (a) $\phi_{3,0}(t)$ ; (b) $\phi_{3,\bar{t}_w^*}(t)$ ; (c) $\psi_{3,0}(t)$ ; and (d) $\psi_{3,\bar{t}_w^*}(t)$ . . . . .	44
3.3	Comparison between the order-3 biorthogonal spline wavelet dual to the Haar wavelet and the order-3 generalized Coiflet having minimal phase distortion, as well as their scaling functions: (a) ${}_{1,3}\tilde{\phi}(t)$ ; (b) $\phi_{3,\bar{t}_h^*}(t)$ ; (c) ${}_{1,3}\tilde{\psi}(t)$ ; and (d) $\psi_{3,\bar{t}_h^*}(t)$ . . . .	45
3.4	Asymptotic constants for sampling approximation error: (a) $C_{\text{samp}}^2$ for $\phi_2$ ; (b) $C_{\text{appr}}^2$ for $\phi_2$ ; (c) $C_{\text{samp}}^2$ for $\phi_4$ ; (d) $C_{\text{appr}}^2$ for $\phi_4$ ; (e) $C_{\text{samp}}^2$ for $\phi_6$ ; and (f) $C_{\text{appr}}^2$ for $\phi_6$ . . . . .	48
4.1	Magnitude responses of the filters in biorthogonal Coiflet systems (in the order of dotted line, dashdotted line, and dashed line, with solid lines represent the limiting responses): (a) $h_2, h_4, h_6$ ; (b) $h_3, h_5, h_7$ ; (c) $\tilde{h}_{2,2}, \tilde{h}_{4,4}, \tilde{h}_{6,6}$ ; (d) $\tilde{h}_{3,3}, \tilde{h}_{5,5}, \tilde{h}_{7,7}$ . . .	65
4.2	Comparison between the magnitude responses of the filters associated with orthogonal Daubechies wavelets and those of the synthesis filters in biorthogonal Coiflet systems (in the order of dashdotted line and dashed line, with solid lines represent the limiting responses): (a) $L = 4$ and (b) $L = 5$ . . . . .	67
4.3	PSNR performance of four filterbanks (solid line: CDF-9/7; dash-dotted line: WTWB-9/7; dashed line: WTWB-13/11; dotted line: WTWB-13/11). (a) “Lena”; (b) “Boats”; (c) “Fingerprint-1”; and (d) “Fingerprint-2”. . . . .	71

4.4	The “Lena” images compressed at 0.1 bpp using the four filterbanks: (a) CDF-9/7; (b) WTWB-13/7; (c) WTWB-9/7; and (d) WTWB-13/11. . . . .	72
5.1	The “Barbara” images coded at 0.25 bpp using four filterbanks: (a) CDF-9/7; (b) VBL-6/10; (c) TVC-10/18; and (d) WPB-22/14. . . . .	85
6.1	Block diagram of the analysis part of a two-dimensional two-channel iterative filterbank . . . . .	89
6.2	Block diagram of the synthesis part of a two-dimensional two-channel iterative filterbank . . . . .	89
6.3	PSNR performance of two filterbanks: (a) “Lena”; (b) “Barbara”; (c) “Goldhill”; and (d) “Peppers”. . . . .	102
6.4	The reconstructed “Lena” and “Barbara” images with 7% and 20% of DWT coefficients, respectively. (a) “Lena” compressed by BSGAM-9/7; (b) “Lena” compressed by WEB-9/7; (c) “Barbara” compressed by BSGAM-9/7; and (d) “Barbara” compressed by WEB-9/7. . . . .	103
A.1	The original “Boats” image. . . . .	114
A.2	The original images: (a) “Lena”; (b) “Barbara”; (c) “Goldhill”; and (d) “Peppers”. . . . .	115
A.3	The original “Fingerprint-1” image. . . . .	116
A.4	The original “Fingerprint-2” image. . . . .	116

# Chapter 1

## Introduction

### 1.1 Background

A *wavelet* is a localized function that can be used to capture informative, efficient, and useful descriptions of a signal. If the signal is represented as a function of time, then wavelets provide efficient localization in both time and either frequency or scale. Despite its short history, wavelet theory has proven to be a powerful mathematical tool for analysis and synthesis of signals and has found successful applications in a remarkable diversity of disciplines such as physics, geophysics, numerical analysis, signal processing, biomedical engineering, statistics, and computer graphics. In particular, the abundance of intriguing and useful features enjoyed by the wavelet representations has led to their applications to a wide range of digital signal processing (DSP) problems.

Compared to Fourier techniques, wavelet techniques permit much more flexibility in choosing appropriate representations for particular applications. In wavelet-based DSP applications, the choice of a wavelet system<sup>1</sup> is of great

---

<sup>1</sup>The concept “wavelet system” will be defined later. Here we use the term to stand for a set of wavelet-related elements, which are necessary for a wavelet-based representation.

importance in the performance of the application. Therefore, the problem of designing wavelet systems has been the core issue in wavelet theory. Most existing wavelet systems have been designed from a primarily mathematical point of view. Many of the previous design criteria are not appropriate for DSP applications. Therefore, when those wavelet systems are applied to DSP problems, their mathematical properties are often irrelevant to performance in the application. Unfortunately, those wavelet systems are often blindly chosen by DSP engineers.

In this dissertation, we attempt to select appropriate existing criteria and propose new criteria for designing wavelet systems that are well-suited for DSP applications. As a consequence, we

- apply these criteria (old and new) to design novel wavelet systems;
- study their mathematical properties;
- provide theoretical analyses to support our design criteria; and
- conduct simulations to evaluate their potential in DSP applications.

## 1.2 Notation and Basic Assumptions

Before we continue the discussion of the work, we first introduce the notation and basic assumptions used in the dissertation.

- The symbols  $\mathbb{R}$ ,  $\mathbb{Z}$ , and  $\mathbb{N}$  denote the sets of real numbers, integers, and natural numbers, respectively.



- For any  $t \in \mathbb{R}$ , the floor operation  $\lfloor t \rfloor = \max\{n | n \leq t, n \in \mathbb{Z}\}$ , the ceiling operation  $\lceil t \rceil = \min\{n | n \geq t, n \in \mathbb{Z}\}$ , and the rounding operation  $\lceil t \rceil = \arg \min_{n \in \mathbb{Z}} |n - t|$ .
- All integrals and summations without explicit limits indicate that the actual limits are  $-\infty$  and  $+\infty$ . Similarly,  $\{h[n]\}_n \equiv \{h[n]\}_{n \in \mathbb{Z}}$ .
- Lowercase and uppercase boldfaced symbols denote vectors and matrices, respectively.
- The symbols  $\mathbf{A}^T$  and  $\mathbf{A}^{-1}$  denote the transpose and inverse of matrix  $\mathbf{A}$ , respectively.
- The constant vectors  $\mathbf{0} = [0 \ 0]^T$  and  $\boldsymbol{\pi} = [\pi \ \pi]^T$ .
- For the two-dimensional (2-D) vectors  $\mathbf{t} = [t_1 \ t_2]^T$ ,  $\mathbf{n} = [n_1 \ n_2]^T$ , and  $\mathbf{l} = [l_1 \ l_2]^T$ , we define the following multi-index notation:

$$\int d\mathbf{t} \equiv \int \int dt_1 dt_2, \quad \sum_{\mathbf{n}} \equiv \sum_{n_1} \sum_{n_2}, \quad (1.1)$$

$$\mathbf{t}^{\mathbf{n}} \equiv t_1^{n_1} t_2^{n_2}, \quad \binom{\mathbf{l}}{\mathbf{n}} \equiv \binom{l_1}{n_1} \binom{l_2}{n_2}. \quad (1.2)$$

- The symbol  $\delta[n]$  denotes the Kronecker delta sequence:  $\delta[n] = 1$  if  $n = 0$  and  $\delta[n] = 0$  otherwise. The symbol  $\delta[\mathbf{n}]$  denotes the 2-D Kronecker delta sequence:  $\delta[\mathbf{n}] = 1$  if  $\mathbf{n} = \mathbf{0}$  and  $\delta[\mathbf{n}] = 0$  otherwise.
- The Fourier transforms of a function  $\phi : \mathbb{R} \rightarrow \mathbb{R}$  and a sequence  $h$  are denoted by

$$\widehat{\phi}(\omega) = \int \phi(t) e^{-j\omega t} dt \quad (1.3)$$

and

$$H(\omega) = \sum_n h[n]e^{-j\omega n} \quad (1.4)$$

respectively.

- The Fourier transforms of a 2-D function  $\phi : \mathbb{R}^2 \rightarrow \mathbb{R}$  and a 2-D sequence  $h$  are denoted by

$$\hat{\phi}(\boldsymbol{\omega}) = \int \phi(\mathbf{t})e^{-j\boldsymbol{\omega}^T \mathbf{t}} d\mathbf{t} \quad (1.5)$$

and

$$H(\boldsymbol{\omega}) = \sum_{\mathbf{n}} h[\mathbf{n}]e^{-j\boldsymbol{\omega}^T \mathbf{n}} \quad (1.6)$$

respectively.

- Every time-domain function  $f$  studied in the dissertation is assumed to be square integrable; i.e.,

$$\int |f(t)|^2 dt < \infty. \quad (1.7)$$

The norm of a function  $f$  over the interval  $[a, b]$  is defined as

$$\|f\|_{[a,b]} = \left( \int_a^b |f(t)|^2 dt \right)^{\frac{1}{2}} \quad (1.8)$$

and the norm of a sequence  $h$  is defined as

$$\|h\| = \left( \sum_n |h[n]|^2 \right)^{\frac{1}{2}}. \quad (1.9)$$

- We define the following shorthand notation for the dyadic scaling and translates of a function  $\phi$ :

$$\phi_{i,n}(t) = 2^{i/2} \phi(2^i t - n) \quad (1.10)$$

where  $i \in \mathbb{Z}$  and  $n \in \mathbb{Z}$ .

- The  $l$ th-order,  $t_0$ -centered moment of a function  $\phi$  is defined as

$$\mathcal{M}_\phi(t_0, l] = \int (t - t_0)^l \phi(t) dt \quad (1.11)$$

where  $t_0 \in \mathbb{R}$  and  $l \in \mathbb{N}$ .

- Since all the filters discussed in the dissertation are real-valued discrete-time filters, we shall simply use the term “filter” instead of “discrete-time filter” and only consider their frequency responses over the interval  $[0, \pi]$ .
- Since all the filterbanks discussed in the dissertation are multirate filterbanks [44], we shall simply use the term “filterbank” instead of “multirate filterbank”.

### 1.3 Fundamentals of Wavelet Theory

In this section, we briefly review those fundamentals of wavelet theory, on which the work in the dissertation is based. More detailed discussions may be found in many textbooks on wavelets, e.g., [6], [13], [36], [46]. While many variations of wavelet systems exist, we focus on *two-channel, compactly supported, and real-valued wavelet systems*. These systems are the most fundamental and widely used wavelet systems in DSP applications such as data compression [30], noise reduction [16], signal enhancement [50], and singularity detection [24].

#### 1.3.1 Wavelet Series

We define a *wavelet series* expansion to approximate a function  $f$ :

$$f(t) \approx \sum_n s_{i_0}[n] \phi_{i_0,n}(t) + \sum_{i=i_0}^{i_1} \sum_n w_i[n] \psi_{i,n}(t) \quad (1.12)$$

where  $\{s_{i_0}[n]\}_n$  are the *scaling coefficients* at scale  $2^{i_0}$ ,

$$s_{i_0}[n] = \int f(t)\tilde{\phi}_{i_0,n}(t) dt \quad (1.13)$$

and  $\{w_i[n]\}_n$  are the *wavelet coefficients* at scale  $2^i$ ,

$$w_i[n] = \int f(t)\tilde{\psi}_{i,n}(t) dt. \quad (1.14)$$

There are four functions in the above linear expansion: the analysis scaling function  $\tilde{\phi}$ , the synthesis scaling function  $\phi$ , the analysis wavelet  $\tilde{\psi}$ , and the synthesis wavelet  $\psi$ . The scaling functions  $\tilde{\phi}$  and  $\phi$  are of lowpass nature, and the scaling coefficients  $\{s_{i_0}[n]\}_n$  capture the coarse information of  $f$ . The wavelets  $\tilde{\psi}$  and  $\psi$  are of bandpass nature, and the wavelet coefficients  $\{w_i[n]\}_{i,n}$  weight the detail features of  $f$ . Since multiple scales are used in (1.12), the wavelet series is a multiscale or multiresolution representation.

### 1.3.2 The Mallat Algorithm

The definitions of the scaling coefficients in (1.13) and the wavelet coefficients in (1.14) are not appealing from a computational perspective. Since the analytic forms of the functions being studied are not available in many practical problems, it is difficult, if not impossible, to use (1.13) and (1.14) to compute the expansion coefficients. Even if we have the analytic forms, the complexity of numerically computing the expansion coefficients is impractically high. Hence, in order to make the wavelet series useful in practice, we need fast algorithms to compute the expansion coefficients  $\{s_{i_0}[n]\}_n$  and  $\{w_i[n]\}_{i,n}$  efficiently. The *Mallat algorithm* is one such algorithm. If the scaling functions

satisfy the so-called *dilation equations*

$$\phi(t) = \sum_n 2h[n] \phi(2t - n) \quad (1.15)$$

$$\tilde{\phi}(t) = \sum_n 2\tilde{h}[n] \tilde{\phi}(2t - n) \quad (1.16)$$

and the wavelets satisfy the so-called *wavelet equations*

$$\psi(t) = \sum_n 2g[n] \phi(2t - n) \quad (1.17)$$

$$\tilde{\psi}(t) = \sum_n 2\tilde{g}[n] \tilde{\phi}(2t - n) \quad (1.18)$$

with some sequences (or filters)  $h$ ,  $\tilde{h}$ ,  $g$ , and  $\tilde{g}$ , then

- the scaling coefficients and the wavelet coefficients at scale  $2^i$  can be computed from the scaling coefficients at the finer scale  $2^{i+1}$  via a discrete-time filtering followed by a two-fold downsampling [26]:

$$s_i[m] = \sum_n \tilde{h}[n - 2m] s_{i+1}[n] \quad \text{and} \quad w_i[m] = \sum_n \tilde{g}[n - 2m] s_{i+1}[n] \quad (1.19)$$

- the scaling coefficients at the scale  $2^{i+1}$  can be synthesized from the scaling coefficients and wavelet coefficients at the coarser scale  $2^i$  via a two-fold upsampling [26] followed by a discrete-time filtering:

$$s_{i+1}[n] = 2 \sum_m (h[n - 2m] s_i[m] + g[n - 2m] w_i[m]). \quad (1.20)$$

Both the analysis and synthesis can be performed recursively, which yields a pyramid-structured set of expansion coefficients. For instance, we start with  $\{s_{i_1+1}[n]\}_n$  and perform the decomposition  $(i_1 + 1 - i_0)$  times:

$$\begin{array}{ccccccc} s_{i_1+1}[n] & \longrightarrow & s_{i_1}[n] & \longrightarrow & s_{i_1-1}[n] & \longrightarrow & \dots & \longrightarrow & s_{i_0}[n] \\ & & \searrow & & \searrow & & \searrow & & \searrow \\ & & w_{i_1}[n] & & w_{i_1-1}[n] & & \dots & & w_{i_0}[n] \end{array} \quad (1.21)$$

and we can recover  $\{s_{i_1+1}[n]\}_n$  by performing the reconstruction  $(i_1 + 1 - i_0)$  times:

$$\begin{array}{ccccccc} s_{i_0}[n] & \longrightarrow & s_{i_0+1}[n] & \longrightarrow & \dots & \longrightarrow & s_{i_1}[n] & \longrightarrow & s_{i_1+1}[n] \\ & \nearrow & & \nearrow & & \nearrow & & \nearrow & \\ w_{i_0}[n] & & w_{i_0+1}[n] & & \dots & & w_{i_1}[n] & & \end{array} \quad (1.22)$$

Such a pyramid filtering algorithm is called *Mallat algorithm*, which provides an efficient discrete-time approach to compute the wavelet series expansion in (1.12), provided that  $\{s_{i_1+1}[n]\}_n$ , the scaling coefficients at the finest scale, are available. However, the Mallat algorithm does not provide a way to compute  $\{s_{i_1+1}[n]\}_n$ . When applied to discrete-time signals, Mallat algorithm is also called the *discrete wavelet transform* (DWT).

### 1.3.3 Perfect Reconstruction Filterbank

From a multirate system theory point of view, the Mallat algorithm can be implemented with a two-channel iterative filterbank, whose analysis and synthesis parts are depicted in Figures 1.1 and 1.2, respectively. The symbols  $\downarrow 2$  and  $\uparrow 2$  denote two-fold downsampling and upsampling, respectively. In the Mallat algorithm, if we require that the  $s_{i+1}[n]$  in (1.20) be identical to the  $s_{i+1}[n]$  in (1.19) following the analysis and synthesis stages, then the four filters  $h$ ,  $\tilde{h}$ ,  $g$ , and  $\tilde{g}$  must satisfy the *conjugate quadrature filter* condition

$$g[n] = (-1)^n \tilde{h}[-n] \quad \text{and} \quad \tilde{g}[n] = (-1)^n h[-n] \quad (1.23)$$

and the *perfect reconstruction* condition

$$\sum_n h[n] \tilde{h}[n - 2m] = \frac{1}{2} \delta[m] \quad \forall m \in \mathbb{Z} \quad (1.24)$$

or equivalently, in the frequency domain,

$$H(\omega) \tilde{H}(-\omega) + H(\omega + \pi) \tilde{H}(-\omega + \pi) = 1. \quad (1.25)$$

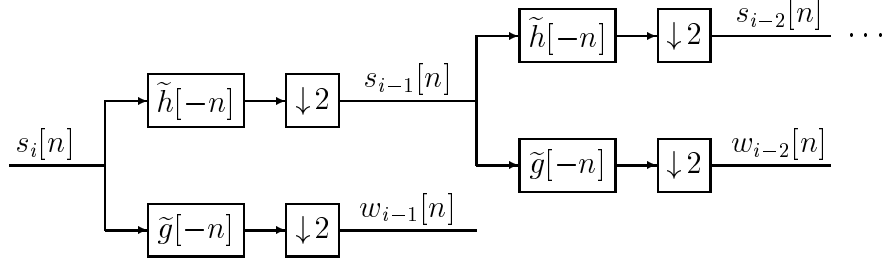


Figure 1.1: Block diagram of the analysis part of a two-channel iterative filterbank

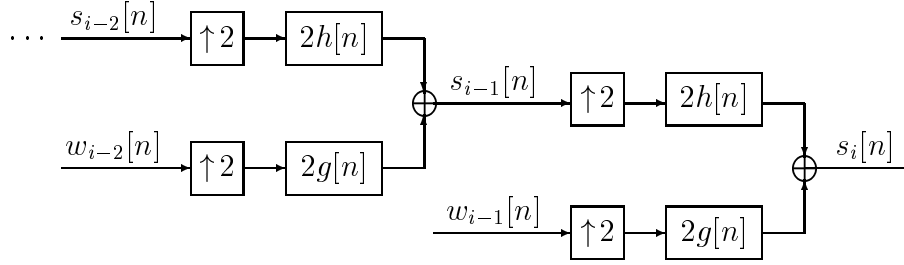


Figure 1.2: Block diagram of the synthesis part of a two-channel iterative filterbank

We call the set  $\{\phi, \tilde{\phi}, \psi, \tilde{\psi}, h, \tilde{h}, g, \tilde{g}\}$  a *wavelet system*. Such a system is *biorthogonal* in the sense that for any  $k \in \mathbb{Z}$  and  $n \in \mathbb{Z}$ ,

$$\int \phi(t-k) \tilde{\phi}(t-n) dt = \int \psi(t-k) \tilde{\psi}(t-n) dt = \delta[k-n] \quad (1.26)$$

$$\int \tilde{\phi}(t-k) \psi(t-n) dt = \int \phi(t-k) \tilde{\psi}(t-n) dt = 0. \quad (1.27)$$

If the analysis elements are identical to their synthesis counterparts, i.e.,

$$\tilde{\phi} = \phi, \quad \tilde{\psi} = \psi, \quad \tilde{h} = h, \quad \tilde{g} = g \quad (1.28)$$

then the wavelet system becomes *orthogonal* in the sense that, for any integers

$k$  and  $n$ ,

$$\int \phi(t - k)\phi(t - n) dt = \int \psi(t - k)\psi(t - n) dt = \delta[k - n] \quad (1.29)$$

$$\int \phi(t - k)\psi(t - n) dt = 0 \quad (1.30)$$

and the associated DWT is an orthogonal transform. The perfect reconstruction condition becomes

$$\sum_n h[n] h[n - 2m] = \frac{1}{2}\delta[m] \quad \forall m \in \mathbb{Z} \quad (1.31)$$

or equivalently, in the frequency domain,

$$H(\omega)H(-\omega) + H(\omega + \pi)H(-\omega + \pi) = 1. \quad (1.32)$$

Orthogonal wavelet systems are special cases of biorthogonal wavelet systems, and the design of the former is more restrictive than that of the latter.

The following describes a generic procedure for designing a biorthogonal wavelet system:

*Step 1:* translate a set of desired properties of the wavelet system into an equivalent set of properties of  $h$  and  $\tilde{h}$ ;

*Step 2:* design  $h$  and  $\tilde{h}$  satisfying (1.24) and other desired properties of the filters  $h$  and  $\tilde{h}$ ;

*Step 3:* derive  $g$  and  $\tilde{g}$  using (1.23);

*Step 4:* derive  $\phi$  and  $\tilde{\phi}$  using (1.15) and (1.16);

*Step 5:* derive  $\psi$  and  $\tilde{\psi}$  using (1.17) and (1.18).



Apparently, the core of the procedure is a filter design problem, in which we attempt to design a pair of lowpass filters  $h$  and  $\tilde{h}$ . If the wavelet system is required to be orthogonal, we only need to design a single filter.

The functions  $\phi$ ,  $\tilde{\phi}$ ,  $\psi$ , and  $\tilde{\psi}$  are compactly supported if and only if the filters  $h$ ,  $\tilde{h}$ ,  $g$ , and  $\tilde{g}$  are finite impulse response (FIR) [36]. Therefore, all the filters discussed in the dissertation are FIR, which permits us to ignore causality when we design filters.

In audio, image, and many other DSP applications, one of the highly desirable filter characteristics is linear phase, which corresponds to symmetry of the associated wavelet system [36]. There are two types of symmetry which can be possessed by wavelet systems: *whole-point symmetry* (WPS) and *half-point symmetry* (HPS). Table 1.1 summarizes the two types of symmetry for wavelet systems. For a WPS (HPS) wavelet system, all four filters have odd (even) lengths [36]. Unfortunately, there does not exist any non-trivial WPS or HPS two-channel orthogonal wavelet system [13]; i.e., for any non-trivial two-channel wavelet system, symmetry and orthogonality cannot be achieved simultaneously.

## 1.4 Vanishing Moment Property

While the design of a wavelet system may be converted to a filter design problem, the design criteria for wavelet systems are fundamentally different from those encountered in traditional filter design. Next, we shall discuss two key properties of wavelet systems, which are at the heart of wavelet theory.

Table 1.1: Two types of symmetry for wavelet systems

whole-point symmetry	half-point symmetry
$\tilde{h}[n] = \tilde{h}[-n]$	$\tilde{h}[n] = \tilde{h}[1 - n]$
$\tilde{g}[n] = \tilde{g}[-n]$	$\tilde{g}[n] = -\tilde{g}[1 - n]$
$h[n] = h[-n]$	$h[n] = h[1 - n]$
$g[n] = g[-n]$	$g[n] = -g[1 - n]$
$\tilde{\phi}(t) = \tilde{\phi}(-t)$	$\tilde{\phi}(t) = \tilde{\phi}(1 - t)$
$\tilde{\psi}(t) = \tilde{\psi}(-t)$	$\tilde{\psi}(t) = -\tilde{\psi}(1 - t)$
$\phi(t) = \phi(-t)$	$\phi(t) = \phi(1 - t)$
$\psi(t) = \psi(-t)$	$\psi(t) = -\psi(1 - t)$

#### 1.4.1 Vanishing Wavelet Moments

One of the most important properties of wavelet systems is that the first  $L$  moments of the analysis wavelet  $\tilde{\psi}$  vanish; i.e.,

$$\mathcal{M}_{\tilde{\psi}}(0, l] = 0 \quad \text{for } l = 0, 1, \dots, L - 1 \quad (1.33)$$

where we have used the notation given in (1.11). The consequences of this property are that

- all polynomials of degree up to  $(L - 1)$  can be expressed as a linear combination of  $\{\phi(t - n)\}_n$  [36];
- a sufficiently smooth function  $f$  can be approximated with error  $O(2^{-i_0 L})$  by a linear combination of  $\{\phi_{i_0, n}\}_n$  [43]:

$$\|f - \mathcal{P}_{i_0} f\| = C_{\text{proj}} \cdot 2^{-i_0 L} \cdot \|f^{(L)}\| + O(2^{-i_0(L+1)}) \quad (1.34)$$

where

$$(\mathcal{P}_{i_0} f)(t) = \sum_n s_{i_0}[n] \phi_{i_0,n}(t) \quad (1.35)$$

and

$$C_{\text{proj}} = \frac{1}{L!} \left( \sum_{m \neq 0} |\widehat{\phi}^{(L)}(2m\pi)|^2 \right)^{1/2}; \quad (1.36)$$

- the wavelet coefficients of a smooth function  $f$  decay rapidly [36]:

$$|w_i[n]| \leq C \cdot 2^{-iL}; \quad (1.37)$$

- (1.33) is a necessary condition (but not sufficient) for the wavelet  $\tilde{\psi}$  to be differentiable  $L$  times [13].

The property of vanishing wavelet moments makes the wavelet series of a smooth function  $f$  in (1.12) a *sparse* representation of  $f$ ; i.e., only a small portion of the expansion coefficients are needed to approximate  $f$  accurately. In fact, this is the fundamental reason for the success of wavelet representations in certain applications where data is selectively discarded, such as data compression and noise reduction.

Because of the importance of vanishing wavelet moments, most families of wavelet system are indexed by the degree of vanishing wavelet moments. For instance, a biorthogonal wavelet system of order  $(L, \tilde{L})$  has  $L$  and  $\tilde{L}$  vanishing moments for the synthesis and analysis wavelets, respectively.

#### 1.4.2 Vanishing Scaling Function Moments

A lesser known property of wavelet systems is that the first moment of the analysis scaling function  $\tilde{\phi}$  is one for normalization and its next  $L - 1$  moments

vanish; i.e.,

$$\mathcal{M}_{\tilde{\phi}}(0, l) = \delta[l] \quad \text{for } l = 0, 1, \dots, L - 1. \quad (1.38)$$

The consequences of this property are that

- the scaling coefficients  $\{s_{i_1+1}[n]\}_n$  in (1.21) can be accurately approximated by the uniform samples of the function  $f$  [4]:

$$s_{i_1+1}[n] = f(2^{-(i_1+1)}n) + O(2^{-(i_1+1)L}); \quad (1.39)$$

- the property makes  $\tilde{\phi}$  exactly or nearly symmetric [13].

The property implies that one can apply the Mallat algorithm directly on the uniform function samples to generate a nearly valid wavelet representation.

This property was first proposed by the numerical analysis community for wavelet-based numerical methods. However, we show that it is also extremely important for wavelet-based DSP applications. In typical DSP applications, only uniform function samples rather than analytic functions are available. It is generally invalid to treat function samples as the expansion coefficients of a wavelet series [36, pp. 232–233]. The samples must be preprocessed before they can be treated as approximated expansion coefficients [1], [38], [58]. However, due to the approximation in (1.39), preprocessing is not necessary, and the combination of Mallat algorithm and the property of vanishing scaling function moments yields a valid, purely discrete-domain, and fast algorithm for computing scaling coefficients and wavelet coefficients.

## 1.5 Previous Work

In her celebrated paper [12], Daubechies proposed the following design criterion for orthogonal wavelet systems: given a degree of freedom, maximize the degree  $L$  in (1.33). This *Daubechies criterion* only emphasizes vanishing wavelet moments. The primary motivation of the criterion was to obtain smooth wavelets with a sufficiently large  $L$ . Such a criterion was used in the design of several wavelet systems, including orthogonal Daubechies wavelet systems [12], biorthogonal spline wavelet systems [11], [45], and biorthogonal quincunx spline wavelet systems [10], [20].

Motivated by wavelet-based numerical analysis, Coifman chose a different criterion: given a degree of freedom, maximize the degree  $L$  in both (1.33) and (1.38) [4]. This *Coifman criterion* emphasizes the vanishing moments of both the wavelet and scaling function. Daubechies used such a criterion to construct orthogonal Coiflet systems of even orders [14]. Tian and Wells constructed odd-ordered ones [41].

## 1.6 Contributions and Organization of the Dissertation

The following summarizes the contributions of the dissertation, supplies related publications by the author, in which partial results of the dissertation were presented, and describes the organization of the rest of the dissertation.

- We extend the Coifman criterion to a more general form by replacing the zero-centered vanishing scaling function moments by *nonzero-centered* ones. Our new criterion is, given a degree of freedom, to maximize  $L$

such that

$$\mathcal{M}_{\tilde{\psi}}(0, l] = 0 \quad \text{for } l = 0, 1, \dots, L - 1 \quad (1.40)$$

$$\mathcal{M}_{\tilde{\phi}}(t_0, l] = \delta[l] \quad \text{for } l = 0, 1, \dots, L - 1 \quad (1.41)$$

which we refer to as *generalized Coifman criterion*. Such an extension allows a more general and flexible sampling approximation with an arbitrary sampling offset  $t_0$ . Also, the parameter  $t_0$  provides one extra degree of freedom in designing wavelet systems.

- In Chapter 2, we present a theory of the wavelet systems satisfying the generalized Coifman criterion. We generally refer to such systems as *Coiflet-type wavelet systems*.
- In Chapter 3, we apply the generalized Coifman criterion to extend the existing class of original orthogonal Coiflet systems to the novel class of generalized orthogonal Coiflet systems, and design a subclass having optimal phase responses, which are significantly better than those of the original orthogonal Coiflet systems. We prove that generalized Coiflet systems are an excellent choice for the sampling and approximation of smooth functions, and can be shown to perform better than the original Coiflet systems by choosing  $t_0$  appropriately [51], [52], [54].
- In Chapter 4, we design the novel class of biorthogonal Coiflet systems, study their properties, and propose three promising filterbanks in the family having both excellent rate-distortion performance and extremely low computational complexity for wavelet transform-based image data compression [57]. We also conduct systematic comparisons between

biorthogonal Coiflet systems and orthogonal Daubechies wavelet systems [48], [49].

- In Chapter 5, we apply the generalized Coifman criterion to design the novel class of generalized biorthogonal Coiflet systems, study their properties, and discover one promising filterbank in the family to be the best filterbank to date in the rate-distortion sense for image data compression [56].
- In Chapter 6, we extend the class of one-dimensional biorthogonal Coiflet systems in Chapter 4 to the quincunx sampling pattern, and evaluate the properties of the resulting two-dimensional nonseparable Coiflet systems [53]. We find that a novel biorthogonal quincunx Coiflet system significantly outperforms the state-of-the-art quincunx wavelet system for image data compression.
- In Chapter 7, we raise an open problem regarding the existence of multidimensional generalized biorthogonal Coiflet systems. We prove that such systems, if they exist, cannot be derived via the two types of extended McClellan transformations [55].
- In Chapter 8, we conclude the dissertation.

Table 1.2 lists a number of important wavelet systems, including several existing ones and the new ones proposed and developed in the dissertation.

Table 1.2: Important wavelet systems

Criterion	1-D Orthogonal	1-D Biorthogonal	2-D Biorthogonal
<i>Daubechies Criterion</i>	<b>Orthogonal Daubechies Wavelets</b> (Daubechies '88)	<b>Biorthogonal Spline Wavelets</b> (Cohen, Daubechies, & Feauveau '92; Vetterli & Herley '92)	<b>Biorthogonal Quincunx Spline Wavelets</b> (Kovačević & Vetterli '92; Cohen & Daubechies '93)
<i>Coifman Criterion</i>	<b>Orthogonal Coiflets</b> (Daubechies '93)	<b>Biorthogonal Coiflets</b> (Sweldens '96; Wei, Tian, Wells, Jr., & Burrus '98)	<b>Biorthogonal Quincunx Coiflets</b> (Wei, Evans, & Bovik '97)
<i>Generalized Coifman Criterion</i>	<b>Generalized Orthogonal Coiflets</b> (Wei & Bovik '98)	<b>Generalized Biorthogonal Coiflets</b> (Wei, Pai, & Bovik '98)	<b>Preliminary Result</b> (Wei, Evans, & Bovik '97)



## Chapter 2

### Theory of Coiflet-Type Wavelets

In this chapter, we present a fundamental theory of Coiflet-type wavelets. Except for Theorem 1, which we include for completeness, all of the results in this chapter are new. The theory serves as a mathematical foundation on which the results in the following chapters are based. In particular, the theory provides the analytic framework for designing Coiflet-type wavelet systems, studying their mathematical properties, evaluating their potential in various applications, and comparing them with other existing wavelet systems.

#### 2.1 Equivalent Descriptions of Vanishing Wavelet Moments

The following theorem states a set of equivalent descriptions of vanishing wavelet moments.

**Theorem 1** *For a wavelet system  $\{\phi, \tilde{\phi}, \psi, \tilde{\psi}, h, \tilde{h}, g, \tilde{g}\}$ , the following three equations are equivalent:*

$$\mathcal{M}_{\tilde{\psi}}(0, l] = 0 \quad \text{for } l = 0, 1, \dots, L - 1 \quad (2.1)$$

$$\sum_n (-1)^n n^l h[n] = 0 \quad \text{for } l = 0, 1, \dots, L - 1 \quad (2.2)$$

$$H^{(l)}(\pi) = 0 \quad \text{for } l = 0, 1, \dots, L - 1; \quad (2.3)$$

and similar equivalence holds between  $\psi$  and  $\tilde{h}$ .

One importance of Theorem 1 is that it translates the vanishing moment property of a wavelet into an equivalent property of the corresponding lowpass filter (in either the time domain or the frequency domain). The latter can be directly used in the filter design procedure for the wavelet system. The theorem is one of the most fundamental results in wavelet theory. Its proof can be found in many textbooks on wavelets, e.g., [6], [13], [36], [46].

## 2.2 Equivalent Descriptions of Vanishing Scaling Function Moments

The following theorem states a set of equivalent descriptions of vanishing scaling function moments.

**Theorem 2** *For a wavelet system  $\{\phi, \tilde{\phi}, \psi, \tilde{\psi}, h, \tilde{h}, g, \tilde{g}\}$ , the following six equations are equivalent:*

$$\mathcal{M}_\phi(t_0, l) = \delta[l] \quad \text{for } l = 0, 1, \dots, L - 1 \quad (2.4)$$

$$\mathcal{M}_\phi(0, l) = t_0^l \quad \text{for } l = 0, 1, \dots, L - 1 \quad (2.5)$$

$$\hat{\phi}^{(l)}(0) = (-jt_0)^l \quad \text{for } l = 0, 1, \dots, L - 1 \quad (2.6)$$

$$\sum_n (n - t_0)^l h[n] = \delta[l] \quad \text{for } l = 0, 1, \dots, L - 1 \quad (2.7)$$

$$\sum_n n^l h[n] = t_0^l \quad \text{for } l = 0, 1, \dots, L - 1 \quad (2.8)$$

$$H^{(l)}(0) = (-jt_0)^l \quad \text{for } l = 0, 1, \dots, L - 1; \quad (2.9)$$

and similar equivalence holds between  $\tilde{\phi}$  and  $\tilde{h}$ .

**Proof:** Due to the similarity between  $\{\phi, h\}$  and  $\{\tilde{\phi}, \tilde{h}\}$ , we only need to prove the first equivalence. It is trivial to check that (2.4) and (2.5) are equivalent and (2.7) and (2.8) are equivalent.

Using the dilation equation (1.15), we infer that

$$\mathcal{M}_\phi(t_0, l) = \int (t - t_0)^l \left[ \sum_n 2h[n] \phi(2t - n) \right] dt \quad (2.10)$$

$$= 2^{-l} \sum_n h[n] \int (s + n - 2t_0)^l \phi(s) ds \quad (2.11)$$

$$= 2^{-l} \sum_n h[n] \int \sum_{p=0}^l \binom{l}{p} (s - t_0)^p (n - t_0)^{l-p} \phi(s) ds \quad (2.12)$$

for  $l = 0, 1, \dots, L - 1$ . If  $h$  satisfies (2.7), then for  $l = 0, 1, \dots, L - 1$ ,

$$\mathcal{M}_\phi(t_0, l) = 2^{-l} \int \sum_{p=0}^l \binom{l}{p} (s - t_0)^p \delta[l - p] \phi(s) ds \quad (2.13)$$

$$= 2^{-l} \int (s - t_0)^l \phi(s) ds \quad (2.14)$$

which implies (2.4).

On the other hand, if  $\phi$  satisfies (2.4), then

$$\mathcal{M}_\phi(t_0, l) = 2^{-l} \sum_n h[n] \sum_{p=0}^l \binom{l}{p} (n - t_0)^{l-p} \delta[p] \quad (2.15)$$

$$= 2^{-l} \sum_n (n - t_0)^l h[n] \quad (2.16)$$

$$= \delta[l] \quad (2.17)$$

for  $l = 0, 1, \dots, L - 1$ , which implies (2.8). Hence, (2.4) and (2.8) are equivalent.

According to the *differentiation in frequency* property of the continuous-time Fourier transform and the discrete-time Fourier transform [26, pp. 58], it is trivial to show that (2.5) is equivalent to (2.6) and (2.8) is equivalent to (2.9). ■

One importance of Theorem 2 is that it translates the vanishing moment property of a scaling function into an equivalent property of the corresponding lowpass filter (in either the time domain or the frequency domain). The latter can be directly used in the filter design procedure of wavelet system design.

### 2.3 Vanishing Scaling Function Moments in a Biorthogonal Wavelet System

The next theorem describes a relationship between the vanishing moments of the two scaling functions in a biorthogonal wavelet system.

**Theorem 3** *For a biorthogonal wavelet system  $\{\phi, \psi, \tilde{\phi}, \tilde{\psi}\}$ , if either  $\tilde{\psi}$  or  $\psi$  possesses a degree  $L$  of vanishing moments, then the following two equations are equivalent:*

$$\mathcal{M}_{\tilde{\phi}}(t_0, l) = \delta[l] \quad \text{for } l = 0, 1, \dots, \bar{L} - 1 \quad (2.18)$$

$$\mathcal{M}_{\phi}(t_0, l) = \delta[l] \quad \text{for } l = 0, 1, \dots, \bar{L} - 1 \quad (2.19)$$

for any  $\bar{L}$  such that  $\bar{L} \leq L$ .

**Proof:** Due to the symmetry between  $\tilde{\psi}$  and  $\psi$ , without loss of generality, we assume that  $\tilde{\psi}$  satisfies (2.1). According to Theorem 1,  $H(\omega)$  satisfies (2.3). Assume that  $\tilde{\phi}$  satisfies (2.18). Therefore, according to Theorem 2, it follows that

$$\tilde{H}^{(l)}(0) = (-jt_0)^l \quad \text{for } l = 0, 1, \dots, \bar{L} - 1. \quad (2.20)$$

We shall show by means of induction that  $\phi$  satisfies (2.19), or equivalently,

$$H^{(l)}(0) = (-jt_0)^l \quad \text{for } l = 0, 1, \dots, \bar{L} - 1. \quad (2.21)$$

Checking the base case is trivial:  $H(0) = 1$  due to (1.25) and (2.20). Assume that for some integer  $l$  such that  $0 \leq l \leq \bar{L} - 1$ ,  $h$  satisfies that

$$H^{(p)}(0) = (-jt_0)^p \quad \text{for } p = 0, 1, \dots, l - 1. \quad (2.22)$$

We differentiate (1.25)  $l$  times with respect to  $\omega$ :

$$\sum_{p=0}^l \binom{l}{p} (-1)^{l-p} \left[ H^{(p)}(\omega) \tilde{H}^{(l-p)}(-\omega) + H^{(p)}(\omega + \pi) \tilde{H}^{(l-p)}(-\omega + \pi) \right] = 0. \quad (2.23)$$

Evaluating (2.23) at  $\omega = 0$  and applying (2.3), (2.20), and (2.22), we conclude that

$$H^{(l)}(0) + (-jt_0)^l \sum_{p=0}^{l-1} \binom{l}{p} (-1)^{l-p} = 0 \quad (2.24)$$

which implies that

$$H^{(l)}(0) = (-jt_0)^l \quad (2.25)$$

and completes the induction. Similarly, it can be shown that if  $\phi$  satisfies (2.19), then  $\tilde{\phi}$  satisfies (2.18). Thus, we have completed the proof.  $\blacksquare$

Theorem 3 states that for a biorthogonal wavelet system, if one of the two wavelets possesses a sufficient number of vanishing moments, then the two scaling functions must have the same degree of vanishing moments. We will see later that this fact helps us manipulate the degrees of freedom in designing Coiflet-type biorthogonal wavelet systems.

## 2.4 Sampling Approximation Power

We now study the sampling approximation of smooth functions via compactly supported wavelet systems satisfying the generalized Coifman criterion.

### 2.4.1 Asymptotic $L^2$ -Error of Sampling Approximation

A key problem in wavelet-based multiresolution approximation theory is to measure the decay of the approximation error as the resolution increases, given some *a priori* knowledge on the smoothness of the function being approximated [9], [19], [22], [35], [39], [40], [43]. We first establish three lemmas that are necessary to our primary result given by Theorem 4.

For a wavelet system satisfying the generalized Coifman criterion given in (1.40) and (1.41), we define a function  $\rho_l$  as

$$\rho_l(t) = \sum_n (t - n - t_0)^l \phi(t - n) \quad (2.26)$$

for  $l \in \mathbb{Z}$  and  $l \geq 0$ . It is obvious that  $\rho_l$  is a periodic function with unit period. In addition, if the scaling function  $\phi$  is compactly supported,  $\rho_l$  is bounded and well-defined.

**Lemma 1** *If a wavelet system satisfies the generalized Coifman criterion given in (1.40) and (1.41), then for any  $t \in \mathbb{R}$  and  $l = 0, 1, \dots, L - 1$ ,*

$$\rho_l(t) = \delta[l]. \quad (2.27)$$

**Proof:** Since  $\tilde{\psi}$  has  $L$  vanishing moments,  $\phi$  satisfies [38]

$$\sum_n (t - n)^l \phi(t - n) = \mathcal{M}_\phi(0, l) \quad \text{for } l = 0, 1, \dots, L - 1. \quad (2.28)$$

Using (2.28) and Theorem 2, we infer that for  $l = 0, 1, \dots, L - 1$ ,

$$\rho_l(t) = \sum_k \sum_{p=0}^l \binom{l}{p} (t - n)^p (-t_0)^{l-p} \phi(t - n) \quad (2.29)$$

$$= \sum_{p=0}^l \binom{l}{p} (-t_0)^{l-p} t_0^p \quad (2.30)$$

$$= \delta[l]. \quad (2.31)$$

which gives the desired result. ■

Since the scaling function  $\phi$  is compactly supported, only a finite number of terms in  $\rho_l(t)$  for a given  $t$  contribute to the constant value of the summation. Consequently, we arrive at the following lemma, which can be shown easily using Lemma 1.

**Lemma 2** *If a wavelet system satisfies the generalized Coifman criterion given in (1.40) and (1.41), then for any  $K_1 \in \mathbb{Z}$  and  $K_2 \in \mathbb{Z}$  such that  $K_1 < K_2$ , and any  $t \in \mathbb{R}$  such that  $K_1 + B - 1 \leq t \leq K_2 + A + 1$ , where  $[A, B]$  is the smallest interval that contains the support of  $\phi$  with  $A \in \mathbb{Z}$  and  $B \in \mathbb{Z}$ ,*

$$\sum_{n=K_1}^{K_2} (t - n - t_0)^l \phi(t - n) = \delta[l] \quad (2.32)$$

for  $l = 0, 1, \dots, L - 1$ .

The generalized Coifman criterion generalizes a significant advantage of the original Coifman criterion: the projection coefficients of a sufficiently smooth function  $f$  on the subspace spanned by the basis  $\{\phi_{i,n}\}_n$  can be approximated accurately by the uniform samples of  $f$  (up to a scaling constant)  $\{f(2^{-i}(n + t_0))\}_n$ . Such an extension also allows a more general and flexible sampling approach, called *shifted sampling*, in which uniform samples with a sampling period  $2^{-i}$ ,  $\{f(2^{-i}(n + t_0))\}_n$ , are used for some  $t_0 \in \mathbb{R}$ . This can be useful when samples at the dyadic points  $\{2^{-i}n\}_n$  are not available.

For a given smooth function  $f$ , we intend to recover  $f$  over a given interval  $[a, b]$ ,  $a \in \mathbb{Z}$ ,  $b \in \mathbb{Z}$ ,  $a \leq b$ , using its uniform samples  $\{f(2^{-i}(n + t_0))\}_n$ . We define a subset of integers

$$\mathbb{K} = \{n : n \in \mathbb{Z}, 2^i a - B + 1 \leq n \leq 2^i b - A - 1\} \quad (2.33)$$

and a function  $\tilde{\rho}_l$  with  $l \in \mathbb{Z}$  and  $l \geq 0$ ,

$$\tilde{\rho}_l(t) = \sum_{n \in \mathbb{K}} (t - n - t_0)^l \phi(t - n). \quad (2.34)$$

According to Lemma 2, we conclude that, for any  $t \in [2^i a, 2^i b]$  and  $l = 0, 1, \dots, L - 1$ ,

$$\tilde{\rho}_l(t) = \delta[l]. \quad (2.35)$$

We define a sequence of functions  $\{f_i : [a, b] \rightarrow \mathbb{R}, i \in \mathbb{Z}\}$ ,

$$f_i(t) = 2^{-\frac{i}{2}} \sum_{n \in \mathbb{K}} f(2^{-i}(n + t_0)) \phi_{i,n}(t) \quad (2.36)$$

which can be viewed as successive approximations of  $f$  over the interval  $[a, b]$  with the scaled and translated versions of the scaling function  $\phi$  being used as the interpolants. The following lemma gives the convergence rate of the pointwise approximation error.

**Lemma 3** *If  $f^{(L+1)}$  exists and is bounded, then the approximation error at any  $t \in [a, b]$  has the asymptotic form*

$$f_i(t) - f(t) = \frac{f^{(L)}(t) \tilde{\rho}_L(2^i t)}{(-1)^L 2^{iL} L!} + O(2^{-i(L+1)}). \quad (2.37)$$

**Proof:** Perform a Taylor expansion of  $f(s)$  around  $t$  and evaluate it at  $s = 2^{-i}(n + t_0)$ ,

$$f\left(\frac{n + t_0}{2^i}\right) = \sum_{l=0}^L \frac{f^{(l)}(t)}{2^{il} l!} (-1)^l (2^i t - n - t_0)^l + \frac{f^{(L+1)}(\xi_n)}{2^{i(L+1)} (L+1)!} (n + t_0 - 2^i t)^{L+1} \quad (2.38)$$



with some  $\xi_n \in (t, 2^{-i}(n + t_0))$ . Inserting (2.38) into (2.36) and using (2.35), we infer that

$$f_i(t) = f(t) + \sum_{n \in \mathbb{K}} \left( \frac{f^{(L)}(t)}{2^{iL} L!} (n + t_0 - 2^i t)^L + \frac{f^{(L+1)}(\xi_n)}{2^{i(L+1)} (L+1)!} (n + t_0 - 2^i t)^{L+1} \right) \times \phi(2^i t - n) \quad (2.39)$$

$$= f(t) + \frac{f^{(L)}(t) \tilde{\rho}_L(2^i t)}{(-1)^L 2^{iL} L!} + \sum_{n \in \mathbb{K}} \frac{f^{(L+1)}(\xi_n)}{2^{i(L+1)} (L+1)!} (n + t_0 - 2^i t)^{L+1} \times \phi(2^i t - n). \quad (2.40)$$

Therefore,

$$\left| f_i(t) - f(t) - \frac{f^{(L)}(t) \tilde{\rho}_L(2^i t)}{(-1)^L 2^{iL} L!} \right| \leq C \cdot 2^{-i(L+1)} \quad (2.41)$$

where

$$C = \frac{\|f^{(L+1)}\|_\infty}{(L+1)!} \sup_{t \in [a, b]} \left( \sum_{n \in \mathbb{K}} \left| (n + t_0 - 2^i t)^{L+1} \phi(2^i t - n) \right| \right) \quad (2.42)$$

which gives the desired result. ■

Based on Lemma 3, in the next theorem we develop the convergence rate for the  $\mathbf{L}^2$ -error of the approximation.

**Theorem 4** *If  $f^{(L+1)}$  exists and is bounded, then the  $\mathbf{L}^2$ -norm of the reconstruction error over  $[a, b]$  has the asymptotic form*

$$\|f - f_i\|_{[a, b]} = C_{\text{appr}} \cdot 2^{-iL} \cdot \|f^{(L)}\|_{[a, b]} + O(2^{-i(L+1)}) \quad (2.43)$$

where the constant  $C_{\text{appr}}$  is given as

$$C_{\text{appr}} = (L!)^{-1} \cdot \|\rho_L\|_{[0, 1]}. \quad (2.44)$$

**Proof:** For  $i$  sufficiently large, the  $O(2^{-i(L+1)})$  error term in (2.37) becomes negligible, and we can use the pointwise estimate in Lemma 3 to obtain the asymptotic form of the  $\mathbf{L}^2$ -error,

$$\lim_{i \rightarrow +\infty} \left( \frac{\|f - f_i\|_{[a,b]}}{2^{-iL}} \right)^2 = \frac{1}{(L!)^2} \lim_{i \rightarrow +\infty} \int_a^b |f^{(L)}(t) \tilde{\rho}_L(2^i t)|^2 dt \quad (2.45)$$

$$= \frac{1}{(L!)^2} \lim_{i \rightarrow +\infty} \sum_{m=2^i a+1}^{2^i b} \int_{\frac{m-1}{2^i}}^{\frac{m}{2^i}} \left| f^{(L)}\left(\frac{m}{2^i}\right) \rho_L(2^i t) \right|^2 dt \quad (2.46)$$

$$= \frac{1}{(L!)^2} \lim_{i \rightarrow +\infty} \left( \int_0^{2^{-i}} |\rho_L(2^i t)|^2 dt \right) \times \left( \sum_{m=2^i a+1}^{2^i b} \left| f^{(L)}\left(\frac{m}{2^i}\right) \right|^2 \right) \quad (2.47)$$

$$= \frac{1}{(L!)^2} \cdot \|\rho_L\|_{[0,1]}^2 \cdot \|f^{(L)}\|_{[a,b]}^2 \quad (2.48)$$

where we have used (2.35) and the periodicity of  $\rho_L$ . Thus, we have proved (2.43). ■

Theorem 4 provides a *localized* measure for the asymptotic  $\mathbf{L}^2$ -error, which depends on the scaling function  $\phi$ , the scale  $2^i$ , the wavelet system order  $L$ , and the local smoothness of the function.

### 2.4.2 Computation of Asymptotic Constant

In order to compare the asymptotic performance of various Coiflet-type wavelet systems in sampling approximation, it is necessary to study the dependence of the asymptotic constant  $C_{\text{appr}}$  on a particular wavelet system. Since the scaling function  $\phi$  is often not explicitly available, we need to develop a method to compute  $C_{\text{appr}}$  based on the filter coefficients  $\{h[n]\}_n$ , which are known after the wavelet system is constructed. We first develop the following theorem.

**Theorem 5** *The asymptotic constant  $C_{\text{appr}}$  can be expressed as*

$$C_{\text{appr}}^2 = C_{\text{proj}}^2 + C_{\text{samp}}^2 \quad (2.49)$$

where  $C_{\text{proj}}$  is given in (1.36) and

$$C_{\text{samp}} = (L!)^{-1}(\mathcal{M}_\phi(0, L] - t_0^L). \quad (2.50)$$

**Proof:** Since  $\rho_L$  is a periodic function with a unit period, it follows from Parseval's theorem that

$$\int_0^1 \rho_L^2(t) dt = \sum_m |D_m|^2 \quad (2.51)$$

where the Fourier series coefficients are given as

$$D_m = \int_0^1 \sum_n (t - n - t_0)^L \phi(t - n) e^{-j2\pi mt} dt \quad (2.52)$$

$$= \sum_n \int_{-n}^{1-n} (s - t_0)^L \phi(s) e^{-j2\pi ms} ds \quad (2.53)$$

$$= \int \sum_{l=0}^L \binom{L}{l} s^l (-t_0)^{L-l} \phi(s) e^{-j2\pi ms} ds \quad (2.54)$$

$$= \sum_{l=0}^L \binom{L}{l} (-t_0)^{L-l} j^l \hat{\phi}^{(l)}(2m\pi). \quad (2.55)$$

Hence, according to (2.6) in Theorem 2, we have

$$D_0 = j^L \hat{\phi}^{(L)}(0) + \sum_{l=0}^{L-1} \binom{L}{l} (-t_0)^{L-l} j^l \hat{\phi}^{(l)}(0) \quad (2.56)$$

$$= \mathcal{M}_\phi(0, L] - t_0^L. \quad (2.57)$$

The dilation equation (1.15) is equivalent to

$$\hat{\phi}(\omega) = H(\omega/2) \hat{\phi}(\omega/2). \quad (2.58)$$

Applying the chain rule, we differentiate both sides of (2.58)  $l$  times

$$\widehat{\phi}^{(l)}(\omega) = \sum_{p=0}^l \binom{l}{p} \frac{1}{2^l} H^{(p)}(\omega/2) \widehat{\phi}^{(l-p)}(\omega/2). \quad (2.59)$$

Now we evaluate  $\widehat{\phi}^{(l)}(2m\pi)$ , for  $l = 0, 1, \dots, L - 1$ . If  $m$  is odd, then from Theorem 1 we conclude that  $\widehat{\phi}^{(l)}(2m\pi) = 0$ . If  $m$  is even, then

$$\widehat{\phi}^{(l)}(2m\pi) = \frac{1}{2^l} \sum_{p=0}^l \binom{l}{p} (-jt_0)^p \widehat{\phi}^{(l-p)}(m\pi). \quad (2.60)$$

Recursively applying (2.60), we finally conclude that  $\widehat{\phi}^{(l)}(2m\pi) = 0$ , if  $m$  is even but not zero. Therefore,  $D_m = j^L \widehat{\phi}^{(L)}(2m\pi)$ , if  $m \neq 0$ . We thus obtain (2.49). ■

In fact, the above theorem not only indicates a way to compute the asymptotic constant  $C_{\text{appr}}$ , but also possesses an interesting interpretation. The squared  $\mathbf{L}^2$ -error for Coiflet-type wavelets-based sampling approximation can be represented as

$$\|f - f_i\|^2 = \|f - \mathcal{P}_i f\|^2 + \|\mathcal{P}_i f - f_i\|^2. \quad (2.61)$$

Since we have known that  $\|f - f_i\|^2$  and  $\|f - \mathcal{P}_i f\|^2$  have the same convergence rate  $2^{-2iL}$ ,  $\|\mathcal{P}_i f - f_i\|^2$  has the same convergence rate, too. Thus, it is interesting to compare the associated asymptotic constants of the latter two. According to (1.34) and (1.36), the asymptotic constant for  $\|f - \mathcal{P}_i f\|^2$ , which is the  $\mathbf{L}^2$ -error due to projection, is apparently  $C_{\text{proj}}$ . Therefore,  $C_{\text{samp}}$  is the asymptotic constant for  $\|\mathcal{P}_i f - f_i\|^2$ , which is the error due to the approximation of the projection coefficients by the function samples.

A method to compute  $C_{\text{proj}}$  was proposed in [43]. Thus, we only need to compute  $C_{\text{samp}}$ , or equivalently to compute  $\mathcal{M}_\phi(0, L)$ , based on the given

filter coefficients. From (2.59), it follows that

$$\widehat{\phi}^{(L)}(0) = \frac{H^{(L)}(0)}{2^L - 1}. \quad (2.62)$$

Since

$$H^{(L)}(0) = (-j)^L \sum_n n^L h[n], \quad (2.63)$$

it follows that

$$\mathcal{M}_\phi(0, L) = j^L \widehat{\phi}^{(L)}(0) = \frac{\sum_n n^L h[n]}{2^L - 1}. \quad (2.64)$$

## 2.5 Summary

By presenting a theory of Coiflet-type wavelets, we have built a mathematical foundation for the rest of the dissertation. Every Coiflet-type wavelet system possesses unique mathematical properties. All of these new results have significantly enriched wavelet theory.

# Chapter 3

## Generalized Orthogonal Coiflets

Orthogonal Coiflet systems have been popular in numerical analysis due to their sampling approximation property [4], [14] and in digital signal processing due to their associated near-linear phase filterbanks [13]. In this chapter, we generalize the original orthogonal Coiflet systems by using the generalized Coifman criterion. With the resulting extra degree of freedom, we achieve improved properties over the original systems.

### 3.1 Definition

**Definition 1** *An orthogonal wavelet system is a **generalized orthogonal Coiflet (GOC)** system of order  $L$  if it satisfies the generalized Coifman criterion given in (1.40) and (1.41).*

### 3.2 Design

According to Theorem 1 and Theorem 2, (1.40) is equivalent to

$$\sum_n (-1)^n n^l h[n] = 0 \quad \text{for } l = 0, 1, \dots, L - 1 \quad (3.1)$$

and (1.41) is equivalent to

$$\sum_n n^l h[n] = t_0^l \quad \text{for } l = 0, 1, \dots, L - 1. \quad (3.2)$$

In addition to the above equations,  $h$  needs to satisfy the perfect reconstruction condition given in (1.31). For a given  $t_0$ , the filter coefficients  $\{h[n]\}_n$  can be obtained by solving the equations given in (1.31), (3.1), and (3.2) simultaneously.

### 3.2.1 Filter Length versus System Order

Let  $N$  be the length of the filter  $h$  in a GOC system of order  $L$  for some  $t_0$ . We require  $h$  to have the minimal length among all filters satisfying (1.31), (3.1), and (3.2). The perfect reconstruction condition (1.31) gives  $\frac{N}{2}$  equations. The vanishing moment conditions (3.1) and (3.2) provide a total of  $2L$  equations, which are, however, redundant according to the following theorem.

**Theorem 6** *If a filter  $h$  satisfies*

$$\sum_n (-1)^n n^l h[n] = 0 \quad \text{for } l = 0, 1, \dots, 2p - 1 \quad (3.3)$$

*and*

$$\sum_n n^l h[n] = t_0^l \quad \text{for } l = 0, 1, \dots, 2p - 1, \quad (3.4)$$

*then  $h$  satisfies*

$$\sum_n n^{2p} h[n] = t_0^{2p}. \quad (3.5)$$

**Proof:** Define

$$F(\omega) = H(\omega)H(-\omega). \quad (3.6)$$

Then (1.32) becomes

$$F(\omega) + F(\omega + \pi) = 1. \quad (3.7)$$

From Theorem 2, it follows that

$$F^{(2p)}(0) = \sum_{l=0}^{2p} \binom{2p}{l} (-1)^{2p-l} H^{(l)}(0) H^{(2p-l)}(0) \quad (3.8)$$

$$= (-jt_0)^{2p} \sum_{l=1}^{2p-1} \binom{2p}{l} (-1)^l + 2H^{(2p)}(0) \quad (3.9)$$

$$= -2(-jt_0)^{2p} + 2H^{(2p)}(0). \quad (3.10)$$

Taking the  $2p$ th derivative of both sides of (3.7) and evaluating it at  $\omega = 0$  using Theorem 1, we have

$$F^{(2p)}(0) = 0 \quad (3.11)$$

or

$$H^{(2p)}(0) = (-jt_0)^{2p} \quad (3.12)$$

which implies (3.5). ■

The theorem indicates that the equations in (3.2) with even-order vanishing moments can be derived from (1.31), (3.1), and the conditions in (3.2) with lower odd-order vanishing moments. Thus, (3.1) and (3.2) yield  $\frac{3L-1}{2}$  independent equations if  $L$  is odd and  $\frac{3L}{2}$  equations if  $L$  is even. Hence, the minimal  $N$  is given by

$$N = 2 \left\lfloor \frac{3L}{2} \right\rfloor = \begin{cases} 3L - 1 & \text{if } L \text{ is odd} \\ 3L & \text{if } L \text{ is even.} \end{cases} \quad (3.13)$$

Such a phenomenon of extra vanishing scaling function moments was also observed by Burrus and Odegard [6], [7] for the original Coiflet systems.



### 3.2.2 Newton's Method-Based Construction

Similar to [14] and [41], we apply Newton's method [27, pp. 181-188] to solve the multivariate nonlinear equations iteratively. We note that  $h[n]$  satisfies (1.31), (3.1), and (3.2) if and only if  $h'[n]$  satisfies

$$\sum_n h'[n] h'[n - 2m] = \frac{1}{2} \delta[m] \quad \forall m \in \mathbb{Z} \quad (3.14)$$

$$\sum_n (-1)^n n^l h'[n] = 0 \quad \text{for } l = 0, 1, \dots, L - 1 \quad (3.15)$$

$$\sum_n n^l h'[n] = (t_0 + k)^l \quad \text{for } l = 0, 1, \dots, L - 1 \quad (3.16)$$

where  $h'[n] = h[n - k]$  for some  $k \in \mathbb{Z}$ . This fact implies that any solution  $h$  to (1.31), (3.1), and (3.2), with some support interval and sampling offset  $t_0$ , corresponds to another solution with a *fixed* support interval and an appropriate sampling offset. Therefore, the support interval of  $h$  can be arbitrarily chosen without loss of generality. Thus, we choose the same support interval as that of the original orthogonal Coiflets for the convenience of comparison [14]; i.e., the impulse response  $h$  starts with  $h[-L]$  and ends with  $h[N - L - 1]$ . Define an  $N \times 1$  vector

$$\mathbf{h} = [h[-L] \ h[-L + 1] \ \dots \ h[N - L - 1]]^T \quad (3.17)$$

and a vector-valued function  $\mathbf{f} : \mathbb{R}^N \rightarrow \mathbb{R}^N$ ,

$$\mathbf{f}(\mathbf{h}) = \begin{bmatrix} \sum_n h^2[n] - 1 \\ \sum_n h[n]h[n+2] \\ \vdots \\ \sum_n h[n]h[n+N-2] \\ \sum_n nh[n] - t_0 \\ \sum_n n^3 h[n] - t_0^3 \\ \vdots \\ \sum_n n^{\lfloor N/3 \rfloor - 1} h[n] - t_0^{\lfloor N/3 \rfloor - 1} \\ \sum_n (-1)^n h[n] \\ \sum_n (-1)^n n h[n] \\ \vdots \\ \sum_n (-1)^n n^{L-1} h[n] \end{bmatrix} \quad (3.18)$$

where all the summations are from  $n = -L$  to  $n = N - L - 1$ . Therefore,

$$\mathbf{f}(\mathbf{h}) = \mathbf{0}_N \quad (3.19)$$

gives a set of  $N$  independent equations in (1.24), (4.11), and (4.14), where  $\mathbf{0}_N$  denotes the zero vector of length  $N$ . The approximated solution to (3.19) in the  $k$ th iteration is denoted by  $\mathbf{h}_k$ . With an initial guess of  $\mathbf{h}_0$ , Newton's iteration is then

$$\mathbf{h}_{k+1} = \mathbf{h}_k - (\mathbf{f}'(\mathbf{h}_k))^{-1} \mathbf{f}(\mathbf{h}_k) \quad (3.20)$$

where  $\mathbf{f}'$  denotes the Gateaux-derivative of  $\mathbf{f}$  [27]. The initial choice of  $\mathbf{h}_0$  is not arbitrary because some choices may cause the iteration to diverge. In our design, we choose the filter in the original orthogonal Coiflet system of the same order as the starting solution. The iteration stops when the difference between  $\mathbf{h}_{k+1}$  and  $\mathbf{h}_k$  is small enough (e.g., its norm is smaller than a given

threshold). In our experiments, we found that with such an initialization scheme the Newton iteration always converges.

From the above discussion, we notice that the extension from zero-centered vanishing scaling function moments to nonzero-centered ones does not increase the computational complexity of wavelet design.

### 3.3 Near-Linear Phase Filterbanks

The lowpass filters of the original orthogonal Coiflet systems are close to whole-point symmetric [13]. We now study the phase response of the lowpass filter  $h$  in GOC systems.

**Theorem 7** *If  $|\omega|$  is sufficiently small, then the phase response of the lowpass filter in the GOC system of order  $L$  has the asymptotic form*

$$\angle H(\omega) = -t_0\omega + C \cdot \omega^{L'} + O(\omega^{L'+2}) \quad (3.21)$$

where  $L' = 2\lfloor L/2 \rfloor + 1$  and the constant  $C$  is given by

$$C = \frac{\sum_n (n - t_0)^{L'} h[n]}{(-1)^{(L'+1)/2} L!}; \quad (3.22)$$

in addition,  $h$  possesses asymptotically linear phase; i.e., for each  $\omega \in [0, \pi)$ ,

$$\lim_{L \rightarrow \infty} \angle H(\omega) = -t_0\omega. \quad (3.23)$$

**Proof:** Since

$$H(\omega)e^{j\omega t_0} = \sum_n h[n]e^{-j\omega(n-t_0)}, \quad (3.24)$$

we infer that

$$\tan(\angle H(\omega) + t_0\omega) = -\frac{\sum_n h[n] \sin(\omega(n-t_0))}{\sum_n h[n] \cos(\omega(n-t_0))}. \quad (3.25)$$

Taking the Taylor expansions of  $\sin(\omega(n-t_0))$  and  $\cos(\omega(n-t_0))$  around  $\omega = 0$ , and applying (2.7), we have

$$\begin{aligned} & \sum_n h[n] \sin(\omega(n-t_0)) \\ &= \sum_n h[n] \left( \sum_{l=0}^{\lfloor L/2 \rfloor} \frac{(\omega(n-t_0))^{2l+1}}{(-1)^l (2l+1)!} + \frac{\cos(\xi_1(n-t_0))(\omega(n-t_0))^{L'+2}}{(-1)^{\lfloor L/2 \rfloor+1} (L'+2)!} \right) \end{aligned} \quad (3.26)$$

$$= \sum_n \frac{h[n](\omega(n-t_0))^{L'}}{(-1)^{\lfloor L/2 \rfloor} L!} + \sum_n \frac{h[n] \cos(\xi_1(n-t_0))(\omega(n-t_0))^{L'+2}}{(-1)^{\lfloor L/2 \rfloor+1} (L'+2)!} \quad (3.27)$$

and

$$\begin{aligned} & \sum_n h[n] \cos(\omega(n-t_0)) \\ &= \sum_n h[n] \left( \sum_{l=0}^{\lceil L/2 \rceil-1} \frac{(\omega(n-t_0))^{2l}}{(-1)^l (2l)!} + \frac{\cos(\xi_2(n-t_0))(\omega(n-t_0))^{2\lceil L/2 \rceil}}{(-1)^{\lceil L/2 \rceil} (2\lceil L/2 \rceil)!} \right) \end{aligned} \quad (3.28)$$

$$= 1 + \sum_n \frac{h[n] \cos(\xi_2(n-t_0))(\omega(n-t_0))^{2\lceil L/2 \rceil}}{(-1)^{\lceil L/2 \rceil} (2\lceil L/2 \rceil)!} \quad (3.29)$$

where  $0 < \xi_1 < \omega$  and  $0 < \xi_2 < \omega$ . Therefore,

$$\left| \sum_n h[n] \sin(\omega(n-t_0)) - \sum_n \frac{h[n](\omega(n-t_0))^{L'}}{(-1)^{\lfloor L/2 \rfloor} L!} \right| \leq \frac{\sum_n |h[n](n-t_0)^{L'+2}|}{(L'+2)!} \cdot |\omega|^{L'+2} \quad (3.30)$$

i.e.,

$$\sum_n h[n] \sin(\omega(n-t_0)) = \sum_n \frac{h[n](\omega(n-t_0))^{L'}}{(-1)^{\lfloor L/2 \rfloor} L!} + O(\omega^{L'+2}). \quad (3.31)$$

Then,

$$\tan(\angle H(\omega) + t_0\omega) = \frac{\sum_n (n-t_0)^{L'} h[n]}{(-1)^{\lfloor L/2 \rfloor+1} L!} \cdot \omega^{L'} + O(\omega^{L'+2}). \quad (3.32)$$

Again, considering that for  $|x| < 1$ ,

$$\arctan x = \sum_{m=0}^{\infty} \frac{(-1)^m x^{2m+1}}{2m+1} \quad (3.33)$$

we obtain

$$\angle H(\omega) + t_0\omega = \frac{\sum_n (n - t_0)^{L'} h[n]}{(-1)^{\lfloor L/2 \rfloor + 1} L!} \cdot \omega^{L'} + O(\omega^{L'+2}) \quad (3.34)$$

which gives the desired result. Since

$$\lim_{L \rightarrow \infty} C = 0, \quad (3.35)$$

the asymptotic form (3.23) follows immediately. ■

Theorem 7 states that the phase response of the lowpass filter  $h$  in a GOC system is close to linear phase at low frequencies. While Theorem 7 is true for all real  $t_0$ , only integers and half-integers are of interest for filters. An advantage of introducing a half-integer  $t_0$  is that filters close to half-point symmetric can be constructed, which are impossible for the original orthogonal Coiflet systems.

### 3.4 Optimal Design for Minimum Phase Distortion

From Theorem 7 we know that the filter  $h$  has near-zero phase distortion, i.e., deviation from linear phase, at low frequencies. However, the phase distortion at the other frequencies can be much larger. The resulting phase response may not be satisfactory in applications that require uniformly insignificant phase distortion over a broad frequency band.

From the proof of Theorem 7, we find that the phase response at low frequencies is primarily characterized by the first several moments of the scaling function, and hence by the parameter  $t_0$ . Thus, we attempt to use that

parameter to obtain smaller phase distortion. Although for non-integer  $t_0$  or non-half-integer  $t_0$ , the property of near-zero phase distortion around DC will be lost, the gain lies in the fact that phase distortion can be largely reduced over a broad frequency band.

Since in a typical DWT-based DSP application, the input signal is convolved with a filterbank, the phase response of the output signal is the sum of the phase responses of the input signal and the filterbank. Therefore, the phase distortion of the output signal, which is additive and caused by the non-linearity of the phase response of the filterbank, can be viewed as the difference between the desired linear phase response for the filterbank and its actual phase response. In DWT-based analysis-processing-synthesis applications, after reconstruction, the aliasing part of the frequency response  $H(\omega)$ , for  $\omega \in (\pi/2, \pi]$ , is cancelled or at least largely attenuated. Thus, the phase distortion in the passband is crucial.

We are interested in both the optimal near-WPS filters and the optimal near-HPS filters; i.e., we attempt to find

$$t_{0,w}^* = \arg \min_{t_0} \mathcal{D}_w(t_0) = \arg \min_{t_0} \left( \max_{\omega \in [0, \frac{\pi}{2})} |\angle H(\omega) - (-[t_0]\omega)| \right) \quad (3.36)$$

and

$$t_{0,h}^* = \arg \min_{t_0} \mathcal{D}_h(t_0) = \arg \min_{t_0} \left( \max_{\omega \in [0, \frac{\pi}{2})} \left| \angle H(\omega) - \left( \frac{1}{2} - \left[ t_0 + \frac{1}{2} \right] \right) \omega \right| \right) \quad (3.37)$$

where the subscripts “w” and “h” indicate “WPS” and “HPS”, respectively.

Although the objective functions in the optimization problem are functions of  $t_0$ , they do not have explicit forms. Thus, we have to resort to a

brute-force search of the one-dimensional parameter space. For a given  $h$ , we apply a fast Fourier transform (FFT) to obtain dense samples of its phase response  $\angle H(\omega)$ .

We list the resulting maximum phase distortion over the passband  $[0, \frac{\pi}{2})$  in Table 3.1. The table shows that the optimal near-WPS GOC filters have consistently smaller maximum phase distortion over  $[0, \frac{\pi}{2})$  than their counterpart original orthogonal Coiflets. Since the lowpass filters of even-ordered original orthogonal Coiflets are closer to linear phase than the odd-ordered counterparts, the improvement is more significant in the odd-ordered GOC systems. The odd-ordered optimal near-HPS lowpass filters have the smallest phase distortion among this entire class of new filters. Both the even-ordered, nearly HPS, and the odd-ordered, nearly WPS filters possess relatively large phase distortion. Figure 3.1 illustrates the comparisons between the phase distortions of the lowpass filters for the original orthogonal Coiflets and those for the optimal GOC systems when  $L = 2$  and  $L = 3$ .

In Figure 3.2, we plot the original orthogonal Coiflet and the optimal GOC of order 3 as well as their scaling functions. The optimal GOC appears more symmetric than the original orthogonal Coiflet. Table 3.1 shows that the optimal parameter  $t_{0,w}^*$  is close to the origin and  $t_{0,h}^*$  is close to -0.5. As  $L$  increases with the same parity,  $t_{0,w}^*$  and  $t_{0,h}^*$  approach zero and -0.5, respectively, the phase distortion of the original orthogonal Coiflets decreases, and the improvement of using  $t_{0,w}^*$  over using zero reduces, which can be explained by the fact that the original orthogonal Coiflet filters  $h$  have asymptotically zero phase distortion.

In [11], it was pointed out that the lowpass filters of the even-ordered original orthogonal Coiflets are very close to the Laplacian pyramid filters [8], which are associated with some symmetric biorthogonal wavelet bases and are widely used in applications of image processing and computer vision. Since the optimal near-WPS filters of the even-ordered GOC systems are close to those of the even-ordered original orthogonal Coiflets, they are also close to the Laplacian pyramid filters. The optimal near-HPS filters of the GOC systems with odd orders are close to the Haar filter except for their “oscillating tails” (small filter coefficients other than the biggest two). On the other hand, they are surprisingly similar to the filters of some biorthogonal spline wavelets,<sup>1</sup> referred to as  ${}_{1,\tilde{N}}\tilde{h}$  in Table 6.1 in [11]. In fact, they may be regarded as the filters of the biorthogonal Coiflets with the same orders (see the next chapter or [57]). Like the Laplacian pyramid filters, these biorthogonal wavelets are popular in image processing applications. In Figure 3.3, we plot the order-3 biorthogonal spline wavelet dual to the Haar wavelet and the order-3 GOC having the minimal phase distortion, as well as their scaling functions. The two scaling functions are indeed surprisingly similar to each other; so are the two wavelets.

Additional design criteria are possible. The work in [32] is related to but different from ours. Besides imposing a number of moment constraints as in our work, the authors used the extra degree of freedom due to  $t_0$  to maximize the flatness of group delay at DC and solved the resulting nonlinear polynomial equations using Gröbner bases.

---

<sup>1</sup>In fact, they are the dual wavelets with respect to the Haar wavelet.



Table 3.1: Minimum phase distortion

$L$	$\mathcal{D}(0)$	$t_{0,w}^*$	$\mathcal{D}_w(t_{0,w}^*)$	$t_{0,h}^*$	$\mathcal{D}_h(t_{0,h}^*)$
2	$.019922\pi$	-.0540	$.006542\pi$	-.7342	$.035134\pi$
3	$.075167\pi$	.0874	$.009084\pi$	-.4586	$.004589\pi$
4	$.017518\pi$	-.0323	$.008156\pi$	-.6702	$.036083\pi$
5	$.041155\pi$	.0595	$.008959\pi$	-.4720	$.006360\pi$
6	$.016155\pi$	-.0239	$.008645\pi$	-.6420	$.035447\pi$
7	$.028955\pi$	.0359	$.009859\pi$	-.4783	$.007118\pi$

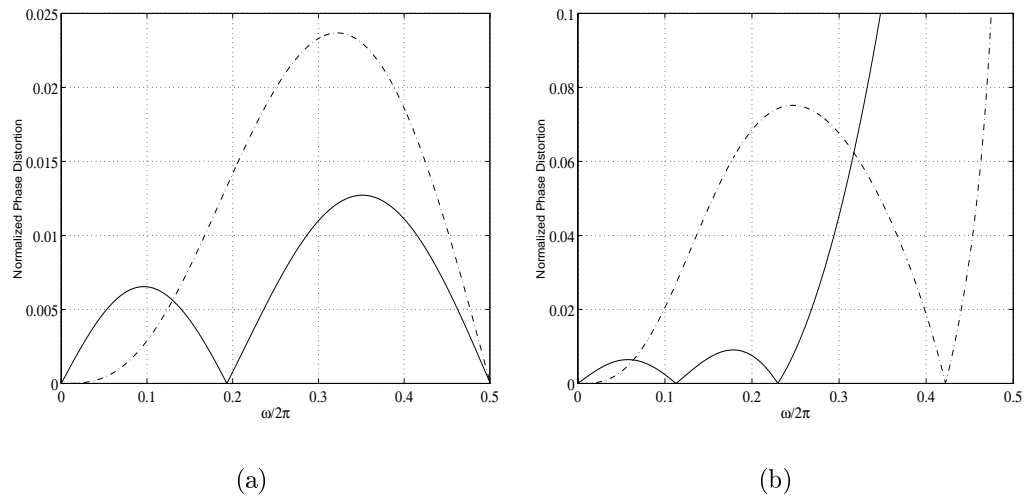


Figure 3.1: Comparisons between the phase distortion of lowpass filters associated with the original Coiflet systems (dash-dotted line) and the optimized ones (solid line): (a)  $L = 2$  and (b)  $L = 3$ .

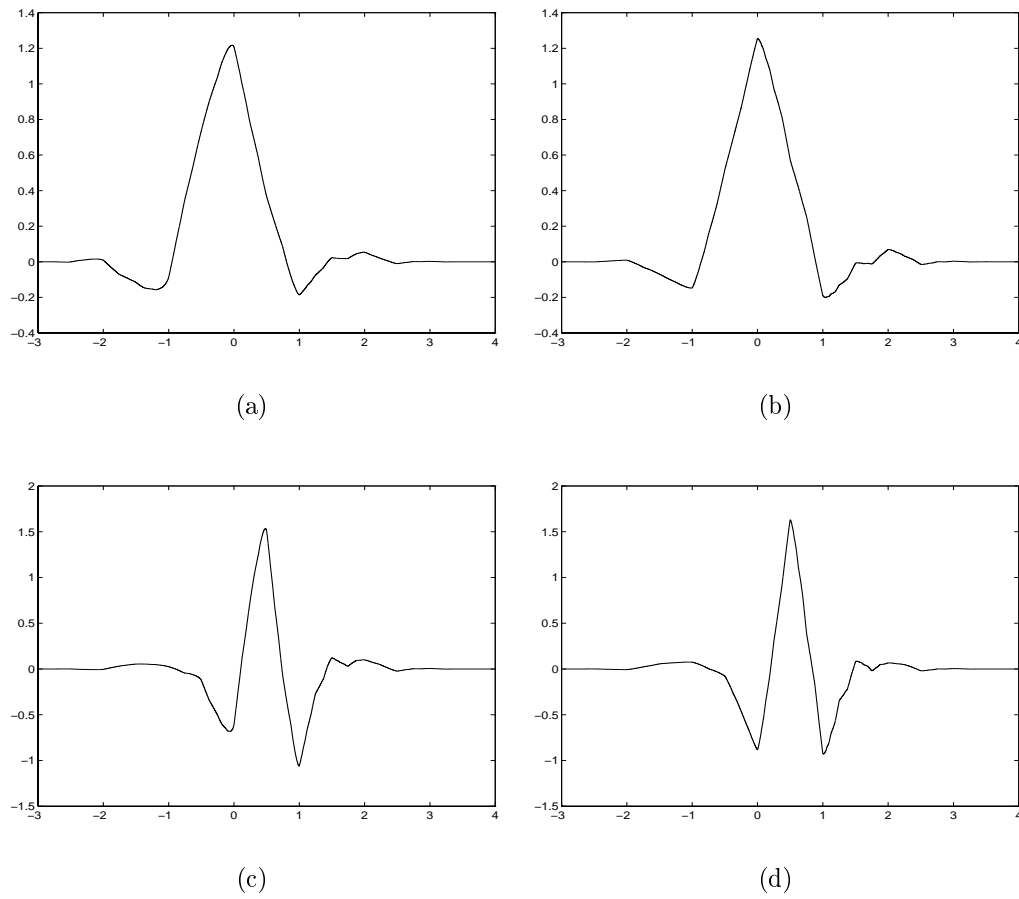


Figure 3.2: Comparison between the original Coiflet and the optimal generalized Coiflet of order 3: (a)  $\phi_{3,0}(t)$ ; (b)  $\phi_{3,\tilde{t}_w^*}(t)$ ; (c)  $\psi_{3,0}(t)$ ; and (d)  $\psi_{3,\tilde{t}_w^*}(t)$ .

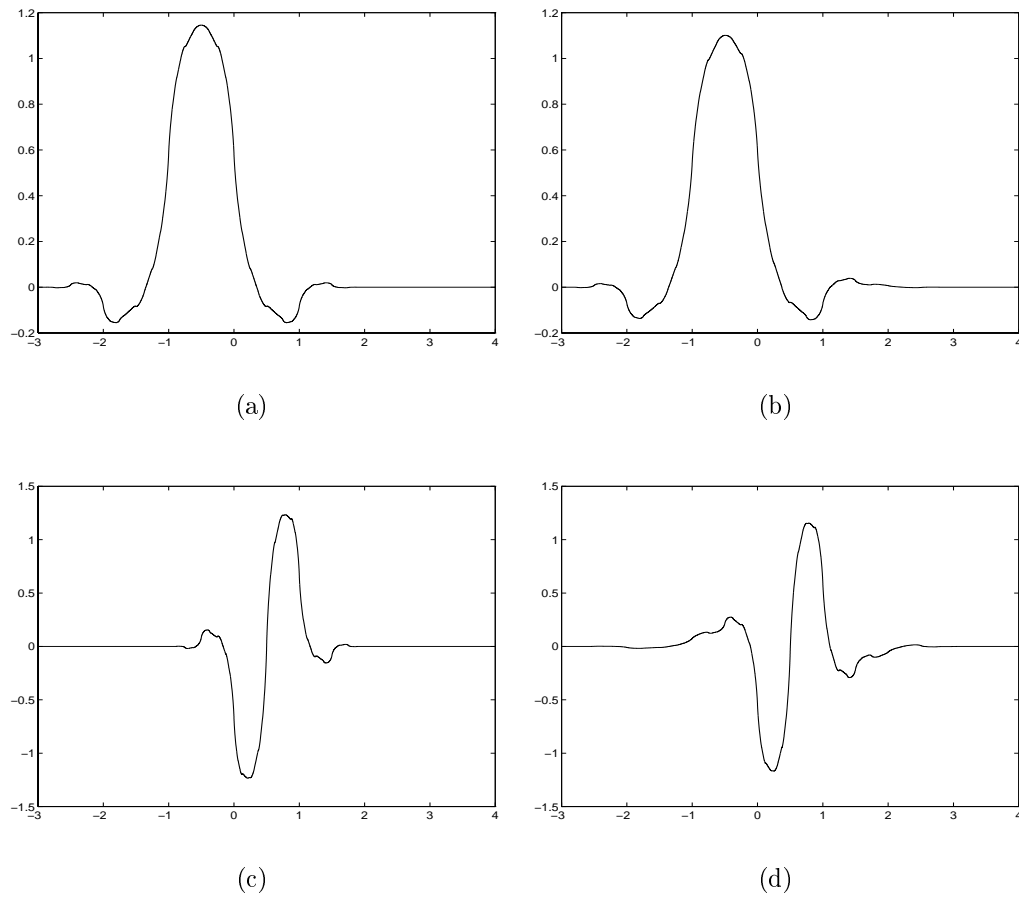


Figure 3.3: Comparison between the order-3 biorthogonal spline wavelet dual to the Haar wavelet and the order-3 generalized Coiflet having minimal phase distortion, as well as their scaling functions: (a)  ${}_{1,3}\tilde{\phi}(t)$ ; (b)  $\phi_{3,\tilde{h}}(t)$ ; (c)  ${}_{1,3}\tilde{\psi}(t)$ ; and (d)  $\psi_{3,\tilde{h}}(t)$ .

### 3.5 Application to Sampling Approximation

In the previous chapter, we have addressed the sampling approximation of smooth functions via Coiflet-type wavelet systems. Based on those results, we now study the performance of GOC systems in sampling approximation. In Figure 3.4, we plot the squared asymptotic constants  $C_{\text{samp}}^2$  and  $C_{\text{appr}}^2$  versus sampling offset  $t_0$  for the GOC systems of orders 2, 4, and 6. From the figure, we observe the following facts.

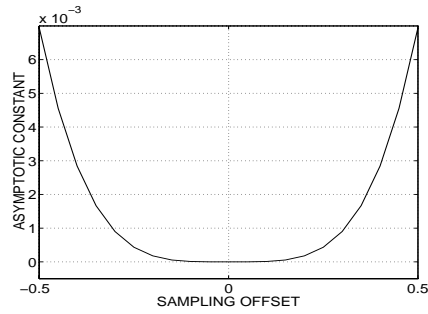
- The constants  $C_{\text{samp}}$  and  $C_{\text{appr}}$  both decrease as the order of GOC system increases.
- The constant  $C_{\text{samp}}$  is much smaller than  $C_{\text{appr}}$  for all the three orders. According to Theorem 5, this implies that the  $\mathbf{L}^2$ -error due to the approximation of the projection coefficients by the function samples is asymptotically negligible compared to that due to the projection, because the two types of errors have the same convergence rate.
- The constant  $C_{\text{samp}}$  is negligibly small if the sampling offset  $t_0$  is in a neighborhood of the origin, regardless of the order of the GOC system. The length of such a neighborhood increases as the order increases.
- There is a unique minimum value of  $C_{\text{appr}}$  for  $t_0 \in [-0.5, 0.5]$  and for every order. However, the minimum value of  $C_{\text{appr}}$  does not occur at  $t_0 = 0$  for any of the three orders, which implies that for a given order, a unique member in the GOC family other than the original orthogonal Coiflet is asymptotically optimal in terms of  $\mathbf{L}^2$ -error.

### 3.6 Summary

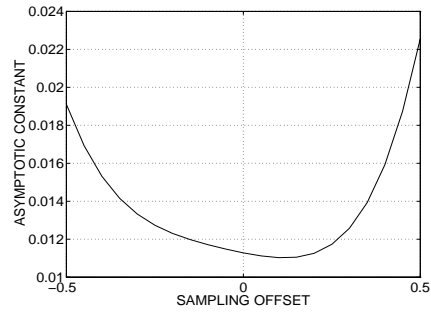
We have presented a new, general class of orthogonal Coiflet systems. The new wavelet systems can

- result in smaller phase distortion in associated filterbanks;
- permit the design of nearly half-point symmetric filterbanks; and
- achieve a better sampling approximation property.

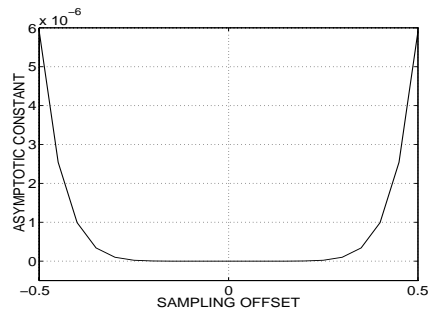
They can be useful in a broad range of DSP applications where the original orthogonal Coiflet systems are successful. Since the new wavelet systems provide a better tradeoff between the two desirable but conflicting properties of compactly-supported, real-valued wavelets, i.e., orthogonality versus symmetry, than the original orthogonal Coiflet systems, and possess better sampling approximation power, we expect that they will achieve improved performance over their original counterparts.



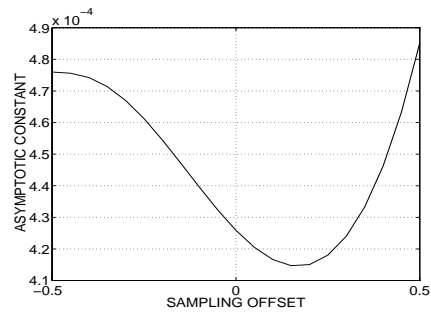
(a)



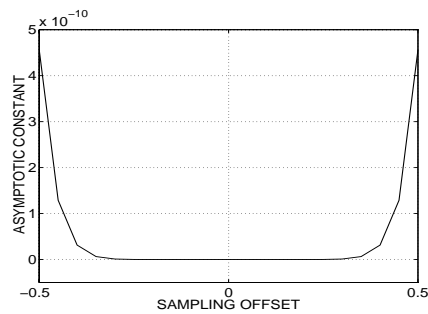
(b)



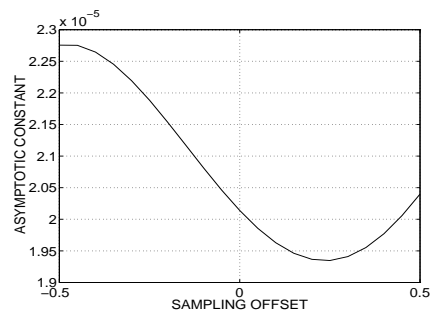
(c)



(d)



(e)



(f)

Figure 3.4: Asymptotic constants for sampling approximation error: (a)  $C_{\text{samp}}^2$  for  $\phi_2$ ; (b)  $C_{\text{appr}}^2$  for  $\phi_2$ ; (c)  $C_{\text{samp}}^2$  for  $\phi_4$ ; (d)  $C_{\text{appr}}^2$  for  $\phi_4$ ; (e)  $C_{\text{samp}}^2$  for  $\phi_6$ ; and (f)  $C_{\text{appr}}^2$  for  $\phi_6$ .

# Chapter 4

## Biorthogonal Coiflets

Historically, the Coifman criterion was first used to design orthogonal wavelet systems [14]. In this chapter, we extend it to design of a novel class of biorthogonal wavelet systems, which we refer to as biorthogonal Coiflet systems. We study the properties possessed by these new wavelet systems and evaluate their performance in image data compression, which has been one of the most successful applications of biorthogonal wavelet systems.

### 4.1 Definition

**Definition 2** *A biorthogonal wavelet system is a **biorthogonal Coiflet system** of order  $(L, \tilde{L})$  if*

$$\mathcal{M}_{\tilde{\phi}}(0, l) = \delta[l] \quad \text{for } l = 0, 1, \dots, L - 1 \quad (4.1)$$

$$\mathcal{M}_{\tilde{\psi}}(0, l) = 0 \quad \text{for } l = 0, 1, \dots, L - 1 \quad (4.2)$$

$$\mathcal{M}_{\psi}(0, l) = 0 \quad \text{for } l = 0, 1, \dots, \tilde{L} - 1. \quad (4.3)$$

According to Theorem 3, it follows that

$$\mathcal{M}_{\phi}(0, l) = \delta[l] \quad \text{for } l = 0, 1, \dots, L - 1. \quad (4.4)$$

## 4.2 Design

According to Theorem 1 and Theorem 2, (4.2) is equivalent to

$$\sum_n (-1)^n n^l h[n] = 0 \quad \text{for } l = 0, 1, \dots, L-1 \quad (4.5)$$

(4.3) is equivalent to

$$\sum_n (-1)^n n^l \tilde{h}[n] = 0 \quad \text{for } l = 0, 1, \dots, \tilde{L}-1 \quad (4.6)$$

and (4.4) is equivalent to

$$\sum_n n^l h[n] = \delta[l] \quad \text{for } l = 0, 1, \dots, L-1. \quad (4.7)$$

In addition to the above equations,  $h$  and  $\tilde{h}$  need to satisfy the perfect reconstruction condition given in (1.24).

### 4.2.1 Constructing Synthesis Filters

We first use (4.5) and (4.7) to design  $h$ . Combining (4.5) and (4.7), we conclude that

$$\sum_m (2m)^l h[2m] = \sum_m (2m+1)^l h[2m+1] = \frac{1}{2} \delta[m] \quad \text{for } l = 0, 1, \dots, L-1. \quad (4.8)$$

We require  $h$  to have the shortest length among all of the filters satisfying (4.8). Since there are  $2L$  independent conditions on  $h$  in (4.8), we define that the extent of  $h$  to be  $[1-L, L]$ . Note that these linear conditions on the filter coefficients naturally divide into two parts: conditions on the even-indexed coefficients and conditions on the odd-indexed coefficients. The first set of



conditions can be expressed as

$$\begin{bmatrix} 1 & 1 & \cdots & 1 \\ 2-L & 4-L & \cdots & L \\ \vdots & \vdots & \ddots & \vdots \\ (2-L)^{L-1} & (4-L)^{L-1} & \cdots & L^{L-1} \end{bmatrix} \begin{bmatrix} h[2-L] \\ h[4-L] \\ \vdots \\ h[L] \end{bmatrix} = \begin{bmatrix} \frac{1}{2} \\ 0 \\ \vdots \\ 0 \end{bmatrix}$$

if  $L$  is even; (4.9)

$$\begin{bmatrix} 1 & 1 & \cdots & 1 \\ 1-L & 3-L & \cdots & L-1 \\ \vdots & \vdots & \ddots & \vdots \\ (1-L)^{L-1} & (3-L)^{L-1} & \cdots & (L-1)^{L-1} \end{bmatrix} \begin{bmatrix} h[1-L] \\ h[3-L] \\ \vdots \\ h[L-1] \end{bmatrix} = \begin{bmatrix} \frac{1}{2} \\ 0 \\ \vdots \\ 0 \end{bmatrix}$$

if  $L$  is odd. (4.10)

It is easy to see that the solution is exactly that

$$h[2m] = \frac{1}{2}\delta[m]. \quad (4.11)$$

The second part can be written as

$$\begin{bmatrix} 1 & 1 & \cdots & 1 \\ 1-L & 3-L & \cdots & L-1 \\ \vdots & \vdots & \ddots & \vdots \\ (1-L)^{L-1} & (3-L)^{L-1} & \cdots & (L-1)^{L-1} \end{bmatrix} \begin{bmatrix} h[1-L] \\ h[3-L] \\ \vdots \\ h[L-1] \end{bmatrix} = \begin{bmatrix} \frac{1}{2} \\ 0 \\ \vdots \\ 0 \end{bmatrix}$$

if  $L$  is even; (4.12)

$$\begin{bmatrix} 1 & 1 & \cdots & 1 \\ 2-L & 4-L & \cdots & L \\ \vdots & \vdots & \ddots & \vdots \\ (2-L)^{L-1} & (4-L)^{L-1} & \cdots & L^{L-1} \end{bmatrix} \begin{bmatrix} h[2-L] \\ h[4-L] \\ \vdots \\ h[L] \end{bmatrix} = \begin{bmatrix} \frac{1}{2} \\ 0 \\ \vdots \\ 0 \end{bmatrix}$$

if  $L$  is odd. (4.13)

Since the coefficient matrix of these simultaneous linear equations is a non-singular Vandermonde matrix, there exists a unique solution. The closed-form expressions for the odd-indexed non-zero coefficients are given by

- if  $L = 1$ , then  $h[2m + 1] = \delta[m]/2$ , which gives the Haar filter [6], [36];

- if  $L = 2K$ ,  $K \in \mathbb{Z}$ , then for  $-K \leq m \leq K - 1$ ,

$$h[2m + 1] = \frac{(-1)^m}{2m + 1} \binom{2K - 2}{K - 1} \binom{2K - 1}{K + m} \frac{2K - 1}{2^{4K - 2}}; \quad (4.14)$$

- if  $L = 2K + 1$ ,  $K \in \mathbb{Z}$ , then for  $-K \leq m \leq K$ ,

$$h[2m + 1] = \frac{(-1)^m}{2m + 1} \binom{2K - 1}{K - 1} \binom{2K}{K + m} \frac{2K + 1}{2^{4K}}. \quad (4.15)$$

From (4.11), it is easy to see that the actual length of  $h$  is  $2L - 1$  for  $L > 1$ . In particular, the indices are from  $1 - L$  to  $L - 1$  if  $L$  is even and from  $2 - L$  to  $L$  if  $L$  is odd.

Filters satisfying (4.11) are commonly called *interpolating filters* or *à trous filters*, which are used in the à trous algorithm to compute quickly the samples of a continuous wavelet transform [29], [33]. If  $L = 2K$  for  $K = 1, 2, \dots$ , then  $h$  coincides with the *Lagrange halfband lowpass filter* of order  $K$  [2]. Its frequency response is given by

$$H_{2K}(\omega) = Q_K\left(\sin^2\left(\frac{\omega}{2}\right)\right) \quad (4.16)$$

where the subscript  $2K$  denotes the order of the biorthogonal Coiflet system and

$$Q_K(y) = (1 - y)^K \sum_{k=0}^{K-1} \binom{K - 1 + k}{k} y^k. \quad (4.17)$$

If  $L = 2K - 1$  for  $K = 1, 2, \dots$ , then using (4.11), (4.14), and (4.15), we derive that

$$H_{2K-1}(\omega) = H_{2K}(\omega) + j \frac{H_{2K}^{(1)}(\omega)}{2K - 1}. \quad (4.18)$$

### 4.2.2 Constructing Analysis Filters

Now we use (1.24) and (4.6) to design  $\tilde{h}$ . Assume that the lengths of the filters  $h$  and  $\tilde{h}$  are  $N$  and  $\tilde{N}$ , respectively. Hence,  $N = 2L - 1$  and we have a total of  $\tilde{N}$  degrees of freedom to design  $\tilde{h}$ . For a given  $h$ , (1.24) provides  $(\tilde{N} + N - 2)/2$  linear conditions on  $\tilde{h}$ . According to Theorem 3, since the conditions in (4.4) are satisfied, the conditions given in (4.1) are automatically satisfied by  $\tilde{h}$ . Hence, there are  $(\tilde{N} - N + 2)/2$  degrees of freedom remaining. We use all the remaining degrees of freedom to maximize the number of vanishing moments of  $\psi$ , or equivalently, to maximize  $\tilde{L}$  in (4.6); i.e., we set  $\tilde{L} = (\tilde{N} - N + 2)/2$ . Thus, we infer that  $\tilde{N} = 2L + 2\tilde{L} - 3$ . Assume that the extent of  $\tilde{h}$  is  $[-L - \tilde{L} + 2, L + \tilde{L} - 2]$ . We attempt to solve (1.24) and (4.6), which give a total of  $\tilde{N}$  simultaneous linear equations, to determine the coefficients of  $\tilde{h}$ .

Using (4.11), we can rewrite the  $L + \tilde{L} - 1$  equations in (1.24), which all contain some explicit terms of even-indexed coefficients, as, for  $m = (-L - \tilde{L} + 2)/2, (-L - \tilde{L} + 4)/2, \dots, (L + \tilde{L} - 2)/2$ ,

$$\tilde{h}[2m] = \delta[m] - 2 \sum_k \tilde{h}[2k + 1]h[2k + 1 - 2m] \quad (4.19)$$

which implies that the  $L + \tilde{L} - 1$  even-indexed coefficients of  $\tilde{h}$  can be uniquely determined by the odd-indexed coefficients of  $h$  and  $\tilde{h}$  with the above  $L + \tilde{L} - 1$  equations. Hence, we intend to determine the odd-indexed coefficients first. For any filter  $h$  and  $l \in \mathbb{Z}$ , we define the notation

$$\mathcal{S}_h[l] = \sum_m (2m + 1)^l h[2m + 1]. \quad (4.20)$$

We use (4.19) to rewrite the left-hand side of (4.6) as

$$\sum_n (-1)^n n^l \tilde{h}[n] = \sum_m (2m)^l \tilde{h}[2m] - \mathcal{S}_{\tilde{h}}[l] \quad (4.21)$$

$$= \sum_m (2m)^l \left( \delta[m] - 2 \sum_k \tilde{h}[2k+1] h[2k+1-2m] \right) - \mathcal{S}_{\tilde{h}}[l] \quad (4.22)$$

$$= \delta[l] - 2 \sum_m \sum_k [(2k+1) - (2k+1-2m)]^l \times h[2k+1-2m] \tilde{h}[2k+1] - \mathcal{S}_{\tilde{h}}[l] \quad (4.23)$$

$$= \delta[l] - 2 \sum_m \sum_k \sum_{p=0}^l \binom{l}{p} (-1)^{l-p} (2k+1-2m)^{l-p} \times (2k+1)^p h[2k+1-2m] \tilde{h}[2k+1] - \mathcal{S}_{\tilde{h}}[l] \quad (4.24)$$

$$= \delta[l] - 2 \mathcal{S}_{\tilde{h}}[l] - 2 \sum_{p=0}^{l-1} \binom{l}{p} (-1)^{l-p} \mathcal{S}_{\tilde{h}}[l-p] \mathcal{S}_{\tilde{h}}[p] \quad (4.25)$$

for  $l = 0, 1, \dots, \tilde{L}-1$ . Therefore, if  $L \geq 2$ , then we can determine the  $L + \tilde{L} - 2$  odd-indexed coefficients by solving a total of  $L + \tilde{L} - 2$  simultaneous linear equations, i.e.,  $L - 2$  equations without explicit terms of those even-indexed coefficients from (1.24) and  $\tilde{L}$  equations from (4.6) using the above rewritten forms. Next, we discuss how to solve these linear equations for two cases  $\tilde{L} \leq L$  and  $\tilde{L} > L$ .

*The case  $\tilde{L} \leq L$ :* Due to (4.8), (4.6) becomes

$$\mathcal{S}_{\tilde{h}}[l] = \frac{1}{2} \delta[l] \quad (4.26)$$

for  $l = 0, 1, \dots, \tilde{L}-1$ . We express these equations and those from (1.24) using a matrix format,  $\mathbf{A}\mathbf{h} = \mathbf{b}$ , or

$$\begin{bmatrix} \mathbf{A}_{11} & \mathbf{A}_{12} & \mathbf{A}_{13} \\ \mathbf{A}_{21} & \mathbf{A}_{22} & \mathbf{A}_{23} \\ \mathbf{A}_{31} & \mathbf{A}_{32} & \mathbf{A}_{33} \end{bmatrix} \begin{bmatrix} \tilde{h}[-L - \tilde{L} + 3] \\ \tilde{h}[-L - \tilde{L} + 5] \\ \vdots \\ \tilde{h}[L + \tilde{L} - 3] \end{bmatrix} = \begin{bmatrix} \mathbf{b}_1 \\ \mathbf{b}_2 \\ \mathbf{b}_3 \end{bmatrix} \quad (4.27)$$

where  $\mathbf{A}_{11}$  and  $\mathbf{A}_{33}$  are a  $(\lceil L/2 \rceil - 1) \times (\lceil L/2 \rceil - 1)$  lower-triangle matrix and

a  $(\lfloor L/2 \rfloor - 1) \times (\lfloor L/2 \rfloor - 1)$  upper-triangle matrix, respectively,

$$\mathbf{A}_{11} = \begin{cases} \begin{bmatrix} h[L-1] & 0 & 0 & \cdots & 0 \\ h[L-3] & h[L-1] & 0 & \cdots & 0 \\ \vdots & \vdots & & & \\ h[3] & h[5] & h[7] & \cdots & h[L-1] \end{bmatrix} & \text{if } L \text{ is even} \\ \begin{bmatrix} h[L] & 0 & 0 & \cdots & 0 \\ h[L-2] & h[L] & 0 & \cdots & 0 \\ \vdots & \vdots & & & \\ h[3] & h[5] & h[7] & \cdots & h[L] \end{bmatrix} & \text{if } L \text{ is odd;} \end{cases} \quad (4.28)$$

$$\mathbf{A}_{33} = \begin{cases} \begin{bmatrix} h[1-L] & h[3-L] & \cdots & h[-5] & h[-3] \\ 0 & h[1-L] & \cdots & h[-7] & h[-5] \\ \vdots & & & & \vdots \\ 0 & 0 & \cdots & 0 & h[1-L] \end{bmatrix} & \text{if } L \text{ is even} \\ \begin{bmatrix} h[2-L] & h[4-L] & \cdots & h[-5] & h[-3] \\ 0 & h[2-L] & \cdots & h[-7] & h[-5] \\ \vdots & & & & \vdots \\ 0 & 0 & \cdots & 0 & h[2-L] \end{bmatrix} & \text{if } L \text{ is odd;} \end{cases} \quad (4.29)$$

the matrix  $\mathbf{A}_{22}$  is an  $\tilde{L} \times \tilde{L}$  Vandermonde matrix,

$$\mathbf{A}_{22} = \begin{cases} \begin{bmatrix} 1 & 1 & \cdots & 1 \\ 1 - \tilde{L} & 3 - \tilde{L} & \cdots & \tilde{L} - 1 \\ \vdots & \vdots & & \vdots \\ (1 - \tilde{L})^{\tilde{L}-1} & (3 - \tilde{L})^{\tilde{L}-1} & \cdots & (\tilde{L} - 1)^{\tilde{L}-1} \end{bmatrix} & \text{if } L \text{ is even} \\ \begin{bmatrix} 1 & 1 & \cdots & 1 \\ 2 - \tilde{L} & 4 - \tilde{L} & \cdots & \tilde{L} \\ \vdots & \vdots & & \vdots \\ (2 - \tilde{L})^{\tilde{L}-1} & (4 - \tilde{L})^{\tilde{L}-1} & \cdots & \tilde{L}^{\tilde{L}-1} \end{bmatrix} & \text{if } L \text{ is odd;} \end{cases} \quad (4.30)$$

the matrices  $\mathbf{A}_{12}$ ,  $\mathbf{A}_{13}$ ,  $\mathbf{A}_{31}$ , and  $\mathbf{A}_{32}$  are zero matrices of proper sizes; the vectors  $\mathbf{b}_1$  and  $\mathbf{b}_3$  are zero vectors of lengths  $\lfloor L/2 \rfloor - 1$  and  $\lfloor L/2 \rfloor - 1$ , respectively;

$\mathbf{b}_2$  is a vector of length  $\tilde{L}$  and is given by  $\mathbf{b}_2 = [\frac{1}{2} 0 0 \dots 0]^T$ .

Since the determinant of  $\mathbf{A}$  is the product of the determinants of  $\mathbf{A}_{11}$ ,  $\mathbf{A}_{22}$ , and  $\mathbf{A}_{33}$ , which are all non-singular matrices, the matrix  $\mathbf{A}$  is also non-singular. Thus, there always exists a unique solution  $\mathbf{h} = \mathbf{A}^{-1}\mathbf{b}$ . We give the formulae for all of the non-zero odd-indexed coefficients of  $\tilde{h}$  in three cases:

- if  $\tilde{L} = 1$ , then  $\tilde{h}[2m + 1] = \delta[m]/2$ ;
- if  $\tilde{L} = 2\tilde{K}$ ,  $\tilde{K} = 1, 2, \dots$ , then for  $-\tilde{K} \leq m \leq \tilde{K} - 1$ ,

$$\tilde{h}[2m + 1] = \frac{(-1)^m}{2m + 1} \binom{2\tilde{K} - 2}{\tilde{K} - 1} \binom{2\tilde{K} - 1}{\tilde{K} + m} \frac{2\tilde{K} - 1}{2^{4\tilde{K} - 2}}; \quad (4.31)$$

- if  $\tilde{L} = 2\tilde{K} + 1$ ,  $\tilde{K} = 1, 2, \dots$ , then for  $-\tilde{K} \leq m \leq \tilde{K}$ ,

$$\tilde{h}[2m + 1] = \frac{(-1)^m}{2m + 1} \binom{2\tilde{K} - 1}{\tilde{K} - 1} \binom{2\tilde{K}}{\tilde{K} + m} \frac{2\tilde{K} + 1}{2^{4\tilde{K}}}. \quad (4.32)$$

We observe that, because the matrix  $\mathbf{A}_{22}$  only depends on  $\tilde{L}$ , the odd-indexed coefficients of  $\tilde{h}_{N, \tilde{N}}$  only depend on  $\tilde{L}$ , too. Furthermore, by comparing (4.14) and (4.15) with (4.31) and (4.32), we conclude that if  $\tilde{L} \leq L$ , then

$$\tilde{h}_{L, \tilde{L}}[2m + 1] = h_{\tilde{L}}[2m + 1] \quad \forall m. \quad (4.33)$$

Since we have known that for any  $\tilde{L}$  the coefficients of  $h_{\tilde{L}}$  are all dyadic fractions, from (4.33) and (4.19) we conclude that the coefficients of  $\tilde{h}_{L, \tilde{L}}$  are all dyadic fractions as well.

*The case  $\tilde{L} > L$ :* The structure of those simultaneous linear equations is more involved for this case. We use an indirect approach to solve those equations. In fact, (4.25) provides a way to calculate  $\mathcal{S}_{\tilde{h}}[l]$  recursively:

$$\mathcal{S}_{\tilde{h}}[l] = -\frac{1}{2} \sum_{p=0}^{l-1} \binom{l}{p} (-1)^{l-p} \mathcal{S}_h[l-p] \mathcal{S}_{\tilde{h}}[p] \quad \text{for } l = 1, 2, \dots, \tilde{L} - 1 \quad (4.34)$$

where  $\mathcal{S}_{\tilde{h}}[0] = 1/2$ . Now we write

$$\sum_m (2m+1)^l \tilde{h}[2m+1] = \mathcal{S}_{\tilde{h}}[l] \quad (4.35)$$

for  $l = 0, 1, \dots, \tilde{L} - 1$ , and those from (1.24) using the matrix format  $\mathbf{A}\mathbf{h} = \tilde{\mathbf{b}}$ , where the vector  $\tilde{\mathbf{b}}$  is given by

$$\tilde{\mathbf{b}} = \begin{bmatrix} \tilde{\mathbf{b}}_1^T & \tilde{\mathbf{b}}_2^T & \tilde{\mathbf{b}}_3^T \end{bmatrix}^T = \begin{bmatrix} \tilde{\mathbf{b}}_1^T & \mathcal{S}_{\tilde{h}}[0] & \mathcal{S}_{\tilde{h}}[1] & \dots & \mathcal{S}_{\tilde{h}}[\tilde{L}-1] & \tilde{\mathbf{b}}_3^T \end{bmatrix}^T, \quad (4.36)$$

$\tilde{\mathbf{b}}_1$  and  $\tilde{\mathbf{b}}_3$  are zero vectors of lengths  $\lceil L/2 \rceil - 1$  and  $\lfloor L/2 \rfloor - 1$ , respectively, and,  $\mathbf{A}$  and  $\mathbf{h}$  are the same as those given for the case  $\tilde{L} \leq L$ . Therefore, there always exists a unique solution  $\mathbf{h} = \mathbf{A}^{-1}\tilde{\mathbf{b}}$  for this case, although its closed form may be quite complicated.

The actual length of  $\tilde{h}$  is  $2(L + \tilde{L}) - 3$  for  $L > 1$ . In particular, the indices are from  $-L - \tilde{L} + 2$  to  $L + \tilde{L} - 2$ .

If  $L \geq \tilde{L}$ , then

$$\tilde{H}_{L,\tilde{L}}(\omega) = \sum_m \tilde{h}_{L,\tilde{L}}[2m+1]e^{-j(2m+1)\omega} + \sum_m \tilde{h}_{L,\tilde{L}}[2m]e^{-j2m\omega} \quad (4.37)$$

$$\begin{aligned} &= \sum_m h_{\tilde{L}}[2m+1]e^{-j(2m+1)\omega} \\ &\quad + \sum_m \left( \delta[m] - 2 \sum_k h_{\tilde{L}}[2k+1]h_L[2k+1-2m] \right) e^{-j2m\omega} \end{aligned} \quad (4.38)$$

$$\begin{aligned} &= H_{\tilde{L}}(\omega) - \frac{1}{2} + 1 - 2 \sum_k h_{\tilde{L}}[2k+1]e^{-j(2k+1)\omega} \\ &\quad \times \left( \sum_m h_L[2k+1-2m]e^{j(2k+1-2m)\omega} \right) \end{aligned} \quad (4.39)$$

$$= H_{\tilde{L}}(\omega) + \frac{1}{2} - 2 \sum_k h_{\tilde{L}}[2k+1]e^{-j(2k+1)\omega} \left( H_L(-\omega) - \frac{1}{2} \right) \quad (4.40)$$

$$= H_{\tilde{L}}(\omega) + \frac{1}{2} - 2 \left( H_{\tilde{L}}(\omega) - \frac{1}{2} \right) \left( H_L(-\omega) - \frac{1}{2} \right) \quad (4.41)$$

i.e.,

$$\widetilde{H}_{L,\widetilde{L}}(\omega) = 2H_{\widetilde{L}}(\omega) + H_L(-\omega) - 2H_{\widetilde{L}}(\omega)H_L(-\omega). \quad (4.42)$$

For some biorthogonal Coiflet systems, we list the coefficients of  $h$  and  $\widetilde{h}$  in Table 4.1.

### 4.3 Properties

We shall show that biorthogonal Coiflet systems enjoy several interesting and desirable properties: symmetry, interpolating scaling functions, and dyadic rational filter coefficients.

#### 4.3.1 Symmetry

From (4.11), (4.14), and (4.15),  $h$  is whole-point symmetric about the origin, i.e.,

$$h[n] = h[-n] \quad (4.43)$$

if and only if  $L$  is even. A question naturally arises: can one construct some new  $h$  by increasing the length of  $h$  to obtain more degrees of freedom so that the resulting  $h$  is: (a) half-point symmetric; or (b) whole-point symmetric for odd  $L$ ?

The answer to the first part lies in (4.8). If  $h[n] = h[2n_0 + 1 - n]$  for some  $n_0 \in \mathbb{Z}$ , and  $L > 1$ , then according to (4.8),

$$\sum_m (2m + 1)h[2m + 1] = \sum_m (2m)h[2n_0 - 2m] + \sum_m h[2m + 1] \quad (4.44)$$

$$= (2n_0 + 1)/2 \quad (4.45)$$



Table 4.1: Filter coefficients of the filterbanks in some biorthogonal Coiflet systems (for some long filters we list about half the coefficients and the other can be deduced by symmetry)

$L$	$\sum_n h[n]z^{-n}$	$\tilde{L}$	$\sum_n \tilde{h}[n]z^{-n}$
1	$2^{-1}(1 + z^{-1})$	1	$2^{-1}(1 + z^{-1})$
		3	$2^{-4}(-z^2 + z + 8 + 8z^{-1} + z^{-2} - z^{-3})$
2	$2^{-2}(z + 2 + z^{-1})$	2	$2^{-3}(-z^2 + 2z + 6 + 2z^{-1} - z^{-2})$
		4	$2^{-7}(3z^4 - 6z^3 - 16z^2 + 38z + 90 + 38z^{-1} - 16z^{-2} - 6z^{-3} + 3z^{-4})$
3	$2^{-4}(3z + 8 + 6z^{-1} - z^{-3})$	1	$2^{-4}(z^2 + 10 + 8z^{-1} - 3z^{-2})$
		3	$2^{-7}(3z^4 - 12z^2 + 24z + 82 + 48z^{-1} - 12z^{-2} - 8z^{-3} + 3z^{-4})$
4	$2^{-5}(-z^3 + 9z + 16 + 9z^{-1} - z^{-3})$	2	$2^{-6}(z^4 - 8z^2 + 16z + 46 + 16z^{-1} - 8z^{-2} + z^{-4})$
		4	$2^{-9}(-z^6 + 18z^4 - 16z^3 - 63z^2 + 144z + 348 + 144z^{-1} + \dots)$
		6	$2^{-14}(9z^8 - 140z^6 + 144z^5 + 756z^4 - 944z^3 - 1908z^2 + 4896z + 10758 + 4896z^{-1} + \dots)$
5	$2^{-8}(-5z^3 + 60z + 128 + 90z^{-1} - 20z^{-3} + 3z^{-5})$	1	$2^{-8}(-3z^4 + 20z^2 + 166 + 128z^{-1} - 60z^{-2} + 5z^{-4})$
		3	$2^{-11}(-9z^6 + 42z^4 - 147z^2 + 384z + 1308 + 768z^{-1} - 255z^{-2} - 128z^{-3} + 90z^{-4} - 5z^{-6})$
		5	$2^{-15}(15z^8 - 280z^6 + 1380z^4 - 640z^3 - 3240z^2 + 7680z + 20634 + 11520z^{-1} - 3240z^{-2} - 2560z^{-3} + 1380z^{-4} + 384z^{-5} - 280z^{-6} + 15z^{-8})$
6	$2^{-9}(3z^5 - 25z^3 + 150z + 256 + 150z^{-1} + \dots)$	2	$2^{-10}(-3z^6 + 22z^4 - 125z^2 + 256z + 724 + 256z^{-1} + \dots)$
		4	$2^{-13}(3z^8 - 52z^6 + 348z^4 - 256z^3 - 972z^2 + 2304z + 5442 + 2304z^{-1} + \dots)$
		6	$2^{-17}(-9z^{10} + 150z^8 - 1525z^6 + 768z^5 + 6600z^4 - 6400z^3 - 14850z^2 + 38400z + 84804 + 38400z^{-1} + \dots)$

which cannot be zero and conflicts with (4.8). Therefore,  $h$  cannot be half-point symmetric if  $L > 1$ .

We now answer the second part. If  $h[n] = h[2n_0 - n]$  for some  $n_0 \in \mathbb{Z}$ , and the order  $L$  is odd, then using (4.5) and (4.7) we deduce that

$$\sum_n (-1)^n n^L h[n] = \sum_n (-1)^n n^L h[2n_0 - n] \quad (4.46)$$

$$= \sum_m (-1)^m (2n_0 - m)^L h[m] \quad (4.47)$$

$$= \sum_m \sum_{l=0}^L \binom{L}{l} (-1)^{m+L-l} (2n_0)^l m^{L-l} h[m] \quad (4.48)$$

$$= - \sum_m (-1)^m m^L h[m] \quad (4.49)$$

which implies  $\sum_n (-1)^n n^L h[n] = 0$ , and

$$\sum_n n^L h[n] = \sum_n n^L h[2n_0 - n] \quad (4.50)$$

$$= \sum_m (2n_0 - m)^L h[m] \quad (4.51)$$

$$= \sum_m \sum_{l=0}^L \binom{L}{l} (-1)^{L-l} (2n_0)^l m^{L-l} h[m] \quad (4.52)$$

$$= - \sum_m m^L h[m] \quad (4.53)$$

which implies  $\sum_n (-1)^n n^L h[n] = 0$ . This conflicts with the assumption that the degree of wavelet and scaling function vanishing moments is  $L$ . Therefore, if  $L$  is odd, then  $h$  cannot be whole-point symmetric.

If  $h[n] = h[-n]$  and  $\tilde{h}[n]$  satisfies (1.24) and (4.6),  $\tilde{h}[-n]$  also satisfies (1.24) and (4.6). Since  $\tilde{h}[n]$  is the unique solution,  $\tilde{h}$  must satisfy

$$\tilde{h}[n] = \tilde{h}[-n] \quad (4.54)$$

if  $L$  is even.

### 4.3.2 Interpolating Scaling Functions

A scaling function  $\phi$  is *interpolating* or *cardinal* if

$$\phi(n) = \delta[n] \quad \forall n \in \mathbb{Z}. \quad (4.55)$$

Interpolating functions are desirable in sampling and interpolation. If we use the uniform samples of a function  $f$  and an interpolating function  $\phi$  to reconstruct  $f$  as

$$\tilde{f}(t) = \sum_n f(2^{-i}n) \phi(2^i t - n) \quad (4.56)$$

for any  $i \in \mathbb{Z}$ , then

$$\tilde{f}(2^{-i}n) = f(2^{-i}n) \quad \forall n \in \mathbb{Z} \quad (4.57)$$

i.e., we obtain an exact reconstruction at those sampling points. For example, the scaling function of the Shannon wavelet system [36], which is given by

$$\phi(t) = \frac{\sin(\pi t)}{\pi t}, \quad (4.58)$$

satisfies (4.55) and is therefore interpolating.

Based on Theorem 10 in [37], it is straightforward to verify that the synthesis scaling functions in biorthogonal Coiflet systems are interpolating. However, there are two key differences between the two types of interpolating scaling functions:

- The integer-shifted versions of Shannon scaling function are orthogonal and those of a biorthogonal Coiflet scaling function are not.
- A biorthogonal Coiflet scaling function is compactly supported and the Shannon scaling function is not. This is a highly desirable property of a

biorthogonal Coiflet scaling function because no truncation is necessary when it is used in practice.

### 4.3.3 Dyadic Rational Filter Coefficients

Since  $[\sin(\omega/2)]^2 = (2 - e^{j\omega} - e^{-j\omega})/4$ , we conclude from (4.16) that the filter coefficients of  $h_{2K}$  are all dyadic fractions of the form  $2^a(2b + 1)$ ,  $a \in \mathbb{Z}$  and  $b \in \mathbb{Z}$ . From (4.11) and (4.14), we know that the coefficients of the polynomial  $H_{2K}^{(1)}(\omega)/(2K - 1)$  in  $e^{j\omega}$  are dyadic fractions. Therefore, according to (4.18), the coefficients of  $h_{2K-1}$  are dyadic fractions, too. Thus, the synthesis lowpass filter  $h_L$  has dyadic fractional coefficients for each  $L$ .

Since  $h_{\tilde{L}}$  has dyadic fractional coefficients, so does  $\tilde{h}_{L,\tilde{L}}$  due to (4.33) and (4.19), if  $L \geq \tilde{L}$ . In the case  $L < \tilde{L}$ , since no closed-form formula of  $\tilde{h}_{L,\tilde{L}}[n]$  is available, it is not clear whether  $\tilde{h}_{L,\tilde{L}}$  has dyadic fractional coefficients. However, we have designed many examples for this case and found that every resulting  $\tilde{h}_{L,\tilde{L}}$  has dyadic fractional coefficients. Thus, we conjecture that for any integers  $L$  and  $\tilde{L}$ , the filter coefficients of  $h_L$  and  $\tilde{h}_{L,\tilde{L}}$  are all dyadic fractions.

Dyadic rational filter coefficients are extremely appealing in the hardware implementation of the discrete wavelet transform (DWT). For instance, if the signals  $x$  and  $y$  are the input and output of the filter  $h_4$ , respectively, whose coefficients are dyadic fractions, then we infer that

$$y[n] = \sum_m h_4[m]x[n - m] \quad (4.59)$$

$$= -\frac{1}{32}x[n + 3] + \frac{9}{32}x[n + 1] + \frac{1}{2}x[n] + \frac{9}{32}x[n - 1] - \frac{1}{32}x[n - 3] \quad (4.60)$$

$$\begin{aligned}
&= \frac{1}{2}x[n] + \frac{1}{4}(x[n+1] + x[n-1]) \\
&\quad + \frac{1}{32}(x[n+1] + x[n-1] - x[n+3] - x[n-3]). \tag{4.61}
\end{aligned}$$

If  $\{x[n]\}$  are integer-valued, the only integer additions and binary shifts are required. If  $\{x[n]\}$  are real and fixed-point, then only fixed-point additions and binary shifts are needed. In both cases, multiplications, which are more computationally expensive and power-consuming operations, can be entirely avoided. Therefore, filterbanks having dyadic rational filter coefficients permit a *multiplication-free* DWT, which possesses a dramatically lower computational complexity than a standard implementation of the DWT.

#### 4.4 Asymptotic Convergence of Filters

Based on (4.16), (4.18), and (4.42), we establish the following theorem on the asymptotic behavior of the filterbanks in biorthogonal Coiflet systems.

**Theorem 8** *The frequency responses of the filters in biorthogonal Coiflet systems converge pointwise to ideal halfband lowpass frequency responses as the orders of the biorthogonal Coiflet systems tend to infinity:*

$$\lim_{L \rightarrow \infty} H_L(\omega) = \begin{cases} 1 & \text{if } 0 \leq \omega < \pi/2 \\ 1/2 & \text{if } \omega = \pi/2 \\ 0 & \text{if } \pi/2 < \omega \leq \pi \end{cases} \tag{4.62}$$

$$\lim_{L, \tilde{L} \rightarrow \infty} \tilde{H}_{L, \tilde{L}}(\omega) = \begin{cases} 1 & \text{if } 0 \leq \omega \leq \pi/2 \\ 0 & \text{if } \pi/2 < \omega \leq \pi \end{cases} \tag{4.63}$$

if  $L$  is even, the convergence of  $H_L(\omega)$  is monotonic in the sense that

$$H_L(\omega) \leq H_{L+2}(\omega) \quad \text{if } 0 \leq \omega < \pi/2 \tag{4.64}$$

$$H_L(\omega) \geq H_{L+2}(\omega) \quad \text{if } \pi/2 < \omega \leq \pi; \tag{4.65}$$

*the convergence of  $H_L(\boldsymbol{\omega})$  does not exhibit any Gibbs-like phenomenon and the convergence of  $\widetilde{H}_{L,\widetilde{L}}(\boldsymbol{\omega})$  exhibits a one-sided Gibbs-like phenomenon.*

The theorem states that biorthogonal Coiflet systems are finite-order (or compactly supported) realizable approximations of the ideal sinc wavelet system [36], which is orthogonal, not compactly supported, and not realizable in practice. Figure 4.1 illustrates some examples of the convergence.

We note that Figure 4.1(c) shows a *one-sided* Gibbs-like phenomenon. There are some significant differences between the one-sided Gibbs-like phenomenon and a typical Gibbs phenomenon:

- the overshoot occurs only in passband of the former and occurs in both passband and stopband in the latter;
- there is no oscillation in the former, but oscillation always occurs in the latter and becomes faster during the converging process;
- the maximum amount of overshoot in the former is exactly 12.5% and larger than that in the latter, which is approximately 9%; and
- the two limiting frequency responses have different values at  $\omega = \pi/2$ .

Because both the magnitude responses of the filters associated with orthogonal Daubechies wavelets [21] and those of the synthesis filters associated with biorthogonal Coiflet systems monotonically converge to the ideal halfband lowpass frequency response without Gibbs-like phenomenon, it may be interesting to compare the behavior of their convergence. In particular,

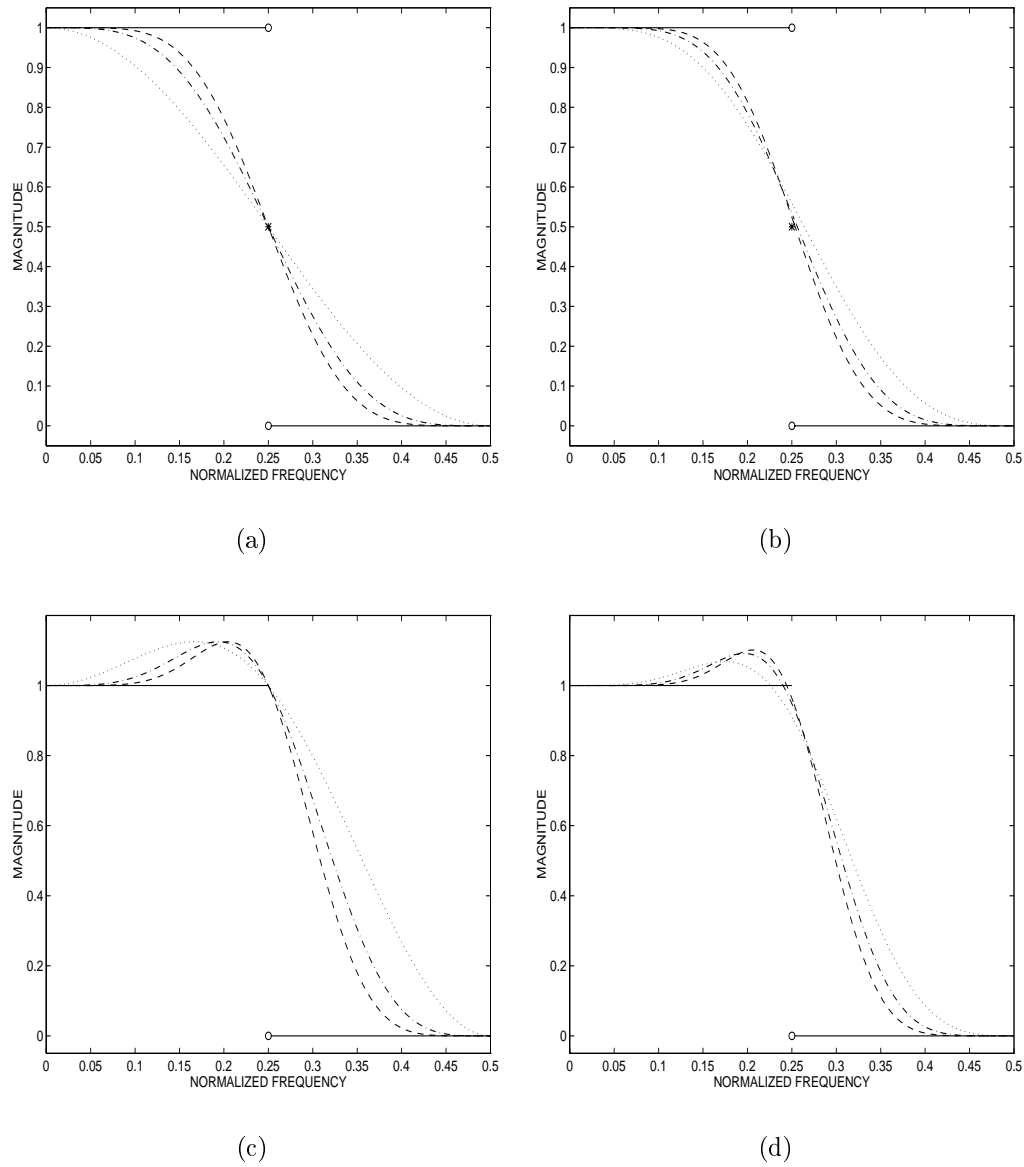


Figure 4.1: Magnitude responses of the filters in biorthogonal Coiflet systems (in the order of dotted line, dashdotted line, and dashed line, with solid lines represent the limiting responses): (a)  $h_2, h_4, h_6$ ; (b)  $h_3, h_5, h_7$ ; (c)  $\tilde{h}_{2,2}, \tilde{h}_{4,4}, \tilde{h}_{6,6}$ ; (d)  $\tilde{h}_{3,3}, \tilde{h}_{5,5}, \tilde{h}_{7,7}$ .

we are interested in the following question: for a given order  $L$ , which is the better approximation of the ideal HBLP frequency response:  $|H_L^{\text{Daub}}(\omega)|$  or  $|H_L^{\text{Coif}}(\omega)|$ ? The theorem below answers the question.

**Theorem 9** *For any integer  $L$  such that  $L > 1$ , the frequency responses of the filter associated with an  $L$ th-order orthogonal Daubechies wavelet and the synthesis filter in an  $L$ th-order biorthogonal Coiflet system satisfy*

$$|H_L^{\text{Daub}}(\omega)| \geq |H_L^{\text{Coif}}(\omega)| \quad (4.66)$$

where equality holds if and only if  $\omega = 0$  or  $\omega = \pi$ .

The complete proof can be found in [49]. The theorem implies that for a given order  $N$ ,  $|H_L^{\text{Daub}}(\omega)|$  approximates the ideal HBLP frequency response better than  $|H_L^{\text{Coif}}(\omega)|$  in the passband and worse than it in the stopband. However,  $H_L^{\text{Coif}}(\omega)$  possesses zero phase if  $L$  is even and asymptotically zero phase if  $L$  is odd, but  $H_L^{\text{Daub}}(\omega)$  always has nonlinear phase for any  $L$  such that  $L > 1$ . Figure 4.2 illustrates two examples of this comparison.

## 4.5 Application to Image Data Compression

We shall show that the symmetric filterbanks in biorthogonal Coiflet systems are well-suited to image transform coding. The biorthogonal Coiflet systems of orders 1 and 2 are the same as the biorthogonal spline wavelet systems of the same orders [11], in which there are a few short filterbanks that have been shown to have good compression capability [47]. We propose that three filterbanks in the family of biorthogonal Coiflet systems have remarkable compression potential. They are the 9/7-tapped, 13/7-tapped, and 13/11-tapped



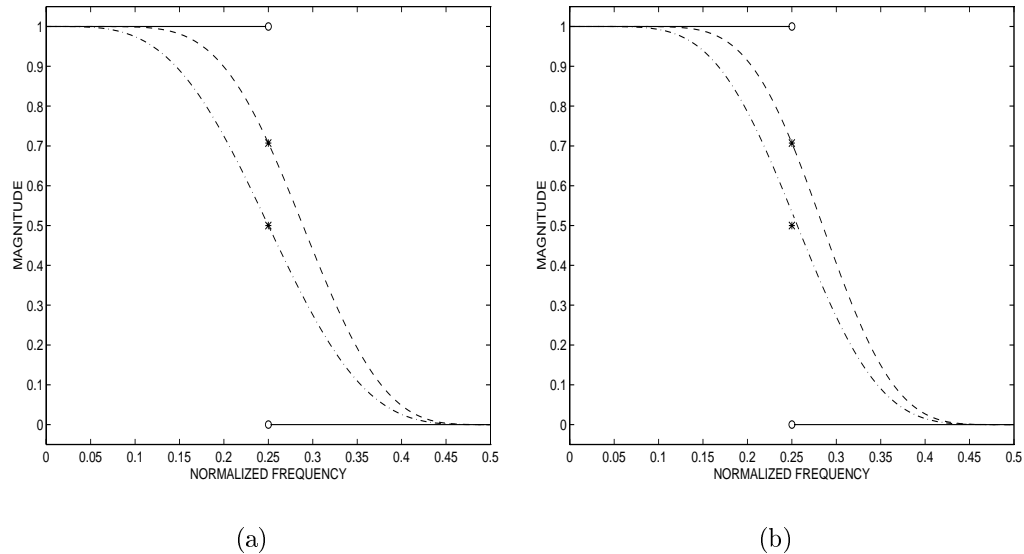


Figure 4.2: Comparison between the magnitude responses of the filters associated with orthogonal Daubechies wavelets and those of the synthesis filters in biorthogonal Coiflet systems (in the order of dashdotted line and dashed line, with solid lines represent the limiting responses): (a)  $L = 4$  and (b)  $L = 5$ .

filterbanks, corresponding to the biorthogonal Coiflet systems of orders (4,2), (4,4), and (6,2), respectively. We refer to them as WTWB-9/7, WTWB-13/7, and WTWB-13/11, respectively, for they were first studied by Wei, Tian, Wells, and Burrus in [57]. We compare them with the 9/7-tapped filterbank designed by Cohen, Daubechies, and Feauveau [11], which we call CDF-9/7. CDF-9/7 has been the most widely used filterbank in the wavelet transform coding literature and was the only approved filterbank in the FBI's fingerprint image compression standard [5]. In [47], Villasenor, Belzer, and Liao tested the compression performance of over 4300 candidate filterbanks and showed that CDF-9/7 was one of the best filterbanks for image data compression. One

major disadvantage of CDF-9/7 lies in the fact that, because its filter coefficients are irrational, it does not permit multiplication-free DWT. Therefore, the computational complexity of its associated DWT is much higher than that of WTWB-9/7, WTWB-13/7, and WTWB-13/11.

We choose four 8-bit grayscale test images: “Lena” of size  $512 \times 512$ , “Boats” of size  $576 \times 720$ , “Fingerprint-1” of size  $768 \times 768$ , and “Fingerprint-2” of size  $480 \times 384$ . We apply the *Set Partitioning in Hierarchical Trees* (SPIHT) algorithm by Said and Pearlman [30] to evaluate the rate-distortion performance of the four filterbanks. The SPIHT algorithm has been regarded by the image coding community as one of the state-of-the-art wavelet transform coding algorithms for image data compression. We choose *bit rate* in bits per pixel (bpp) and *peak signal-to-noise ratio* (PSNR), which is the most popular metric for objective image quality, to measure rate and distortion, respectively. For an 8-bit grayscale image  $x[m, n]$  and its compressed version  $y[m, n]$ ,  $m = 0, 1, \dots, M - 1$  and  $n = 0, 1, \dots, N - 1$ , the PSNR in dB is defined as

$$\text{PSNR} = 10 \log_{10} \left( \frac{255^2}{\frac{1}{MN} \sum_{m=0}^{M-1} \sum_{n=0}^{N-1} (x[m, n] - y[m, n])^2} \right). \quad (4.67)$$

In Figure 4.3, we plot the PSNR performance for the four filterbanks. The figure indicates that, for the four test images, the four filterbanks achieved comparable rate-distortion performance. Figure 4.4 depicts the “Lena” images coded at 0.1 bpp by the four filterbanks. The figure shows that the four coded “Lena” images have comparable perceptual quality.

## 4.6 Summary

Some of the wavelet systems reported by other researchers are related to our work. The synthesis lowpass filters of even-ordered biorthogonal Coiflet systems have already been known in different forms in the literature [2], [15], [28], [31], [33], [36]. After finishing this work the author realized that, in [37], even-ordered biorthogonal Coiflet systems were constructed via a lifting scheme. Nevertheless, the novelty of our work lies in the following aspects:

- the construction scheme used in this work is quite different from those used in the previous published work such as [37];
- the odd-ordered biorthogonal Coiflet systems can be constructed with our scheme, which form a new wavelet family to the best of our knowledge;
- the explicit formulae for the analysis lowpass filters for the case  $L \geq \tilde{L}$  are novel; and
- the systematic analysis of the compression potential of three biorthogonal Coiflet systems shows that they are promising in transform coding applications.

We have presented the design of a novel class of biorthogonal wavelet systems, which possess several remarkable properties. In particular, three filterbanks in this family have been shown to have a competitive rate-distortion performance to CDF-9/7 in DWT-based image data compression and enjoy much lower computational complexity. Furthermore, the multiplication-free

implementation of the DWT using biorthogonal Coiflet systems are promising for the efficient realization of real-time image and video codecs. Therefore, we feel that these biorthogonal Coiflet systems are serious candidates for the choice of wavelet systems in future image/video transform coding standards.

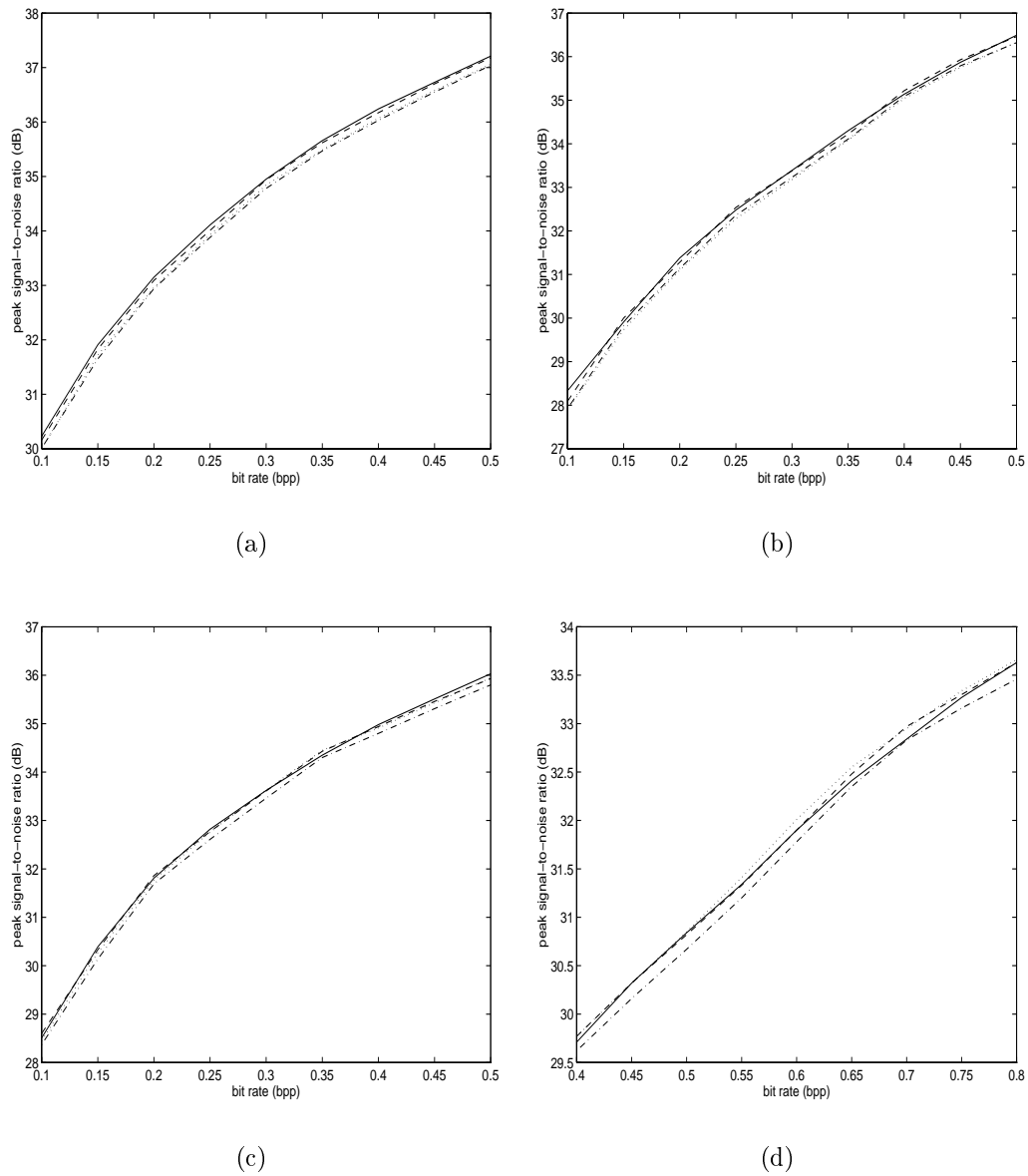


Figure 4.3: PSNR performance of four filterbanks (solid line: CDF-9/7; dash-dotted line: WTWB-9/7; dashed line: WTWB-13/11; dotted line: WTWB-13/11). (a) "Lena"; (b) "Boats"; (c) "Fingerprint-1"; and (d) "Fingerprint-2".



Figure 4.4: The “Lena” images compressed at 0.1 bpp using the four filterbanks: (a) CDF-9/7; (b) WTWB-13/7; (c) WTWB-9/7; and (d) WTWB-13/11.

## Chapter 5

### Generalized Biorthogonal Coiflets

In signal processing applications, half-point symmetric (HPS) filters are about as popular as whole-point symmetric (WPS) filters. In the last chapter, we have shown that biorthogonal Coiflet (BC) systems have a limitation: their filterbanks cannot be HPS due to the Coifman criterion. In this chapter, we use the generalized Coifman criterion and exploit its extra degree of freedom to overcome such a limitation. In particular, we choose  $\frac{1}{2}$ -centered vanishing moment conditions on the scaling function to design HPS filterbanks and anti-symmetric wavelets. We evaluate the performance of the resulting filterbanks in image data compression.

#### 5.1 Definition

**Definition 3** *A biorthogonal wavelet system is a **generalized biorthogonal Coiflet (GBC)** system of order  $(L, \tilde{L})$  if*

$$\mathcal{M}_{\tilde{\phi}}(1/2, l) = \delta[l] \quad \text{for } l = 0, 1, \dots, L - 1 \quad (5.1)$$

$$\mathcal{M}_{\tilde{\psi}}(0, l) = 0 \quad \text{for } l = 0, 1, \dots, L - 1 \quad (5.2)$$

$$\mathcal{M}_{\psi}(0, l) = 0 \quad \text{for } l = 0, 1, \dots, \tilde{L} - 1. \quad (5.3)$$

The definition is very similar to that of BC systems except for the  $\frac{1}{2}$ -centered vanishing moment conditions on the scaling function  $\tilde{\phi}$ . However, it is such a subtle difference that leads to an entirely new family of biorthogonal wavelet systems.

According to Theorem 3, it follows that

$$\mathcal{M}_\phi(1/2, l) = \delta[l] \quad \text{for } l = 0, 1, \dots, L - 1. \quad (5.4)$$

## 5.2 Design

According to Theorem 1 and Theorem 2, (5.2) is equivalent to

$$\sum_n (-1)^n n^l h[n] = 0 \quad \text{for } l = 0, 1, \dots, L - 1, \quad (5.5)$$

(5.3) is equivalent to

$$\sum_n (-1)^n n^l \tilde{h}[n] = 0 \quad \text{for } l = 0, 1, \dots, \tilde{L} - 1, \quad (5.6)$$

and (5.4) is equivalent to

$$\sum_n n^l h[n] = 2^{-l} \quad \text{for } l = 0, 1, \dots, L - 1. \quad (5.7)$$

In addition to the above equations,  $h$  and  $\tilde{h}$  need to satisfy the perfect reconstruction condition given in (1.24).

### 5.2.1 Constructing Synthesis Filters

We first use (5.5) and (5.7) to design  $h$ . Combining (5.5) and (5.7), we conclude that

$$\sum_m (2m)^l h[2m] = \sum_m (2m + 1)^l h[2m + 1] = 2^{-l-1} \quad \text{for } l = 0, 1, \dots, L - 1. \quad (5.8)$$



We require  $h$  to have the shortest length among all filters satisfying (5.8). Since there are  $2L$  independent conditions on  $h$  in (5.8), we define the extent of  $h$  to be  $[1-L, L]$ . Note that these linear conditions on the filter coefficients naturally divide into two parts: conditions on the even-indexed coefficients and conditions on the odd-indexed coefficients. The first part can be expressed as

$$\begin{bmatrix} 1 & 1 & \cdots & 1 \\ 2-L & 4-L & \cdots & L \\ \vdots & \vdots & \ddots & \vdots \\ (2-L)^{L-1} & (4-L)^{L-1} & \cdots & L^{L-1} \end{bmatrix} \begin{bmatrix} h[2-L] \\ h[4-L] \\ \vdots \\ h[L] \end{bmatrix} = \begin{bmatrix} 2^{-1} \\ 2^{-2} \\ \vdots \\ 2^{-L} \end{bmatrix} \quad \text{if } L \text{ is even;} \quad (5.9)$$

$$\begin{bmatrix} 1 & 1 & \cdots & 1 \\ 1-L & 3-L & \cdots & L-1 \\ \vdots & \vdots & \ddots & \vdots \\ (1-L)^{L-1} & (3-L)^{L-1} & \cdots & (L-1)^{L-1} \end{bmatrix} \begin{bmatrix} h[1-L] \\ h[3-L] \\ \vdots \\ h[L-1] \end{bmatrix} = \begin{bmatrix} 2^{-1} \\ 2^{-2} \\ \vdots \\ 2^{-L} \end{bmatrix} \quad \text{if } L \text{ is odd.} \quad (5.10)$$

The second part can be written as

$$\begin{bmatrix} 1 & 1 & \cdots & 1 \\ 1-L & 3-L & \cdots & L-1 \\ \vdots & \vdots & \ddots & \vdots \\ (1-L)^{L-1} & (3-L)^{L-1} & \cdots & (L-1)^{L-1} \end{bmatrix} \begin{bmatrix} h[1-L] \\ h[3-L] \\ \vdots \\ h[L-1] \end{bmatrix} = \begin{bmatrix} 2^{-1} \\ 2^{-2} \\ \vdots \\ 2^{-L} \end{bmatrix} \quad \text{if } L \text{ is even;} \quad (5.11)$$

$$\begin{bmatrix} 1 & 1 & \cdots & 1 \\ 2-L & 4-L & \cdots & L \\ \vdots & \vdots & \ddots & \vdots \\ (2-L)^{L-1} & (4-L)^{L-1} & \cdots & L^{L-1} \end{bmatrix} \begin{bmatrix} h[2-L] \\ h[4-L] \\ \vdots \\ h[L] \end{bmatrix} = \begin{bmatrix} 2^{-1} \\ 2^{-2} \\ \vdots \\ 2^{-L} \end{bmatrix} \quad \text{if } L \text{ is odd.} \quad (5.12)$$

Note that the difference between the above equations and (4.9) and (4.10) is their right-hand sides. For both parts, since the coefficient matrices of these simultaneous linear equations are non-singular Vandermonde matrices, there

exist unique solutions  $\{h[2m]\}_m$  and  $\{h[2m+1]\}_m$ . Hence, the minimum-length solution  $h[n]$  is unique.

### 5.2.2 Constructing Analysis Filters

Now we use (5.6) and (1.24) to design  $\tilde{h}$ . Assume that the lengths of the filters  $h$  and  $\tilde{h}$  are  $N$  and  $\tilde{N}$ , respectively. Hence,  $N = 2L$  and we have a total of  $\tilde{N}$  degrees of freedom to design  $\tilde{h}$ . For a given  $h$ , (1.24) provides  $(\tilde{N} + N - 2)/2$  linear conditions on  $\tilde{h}$ . According to Theorem 3, since the conditions in (5.4) are satisfied, the conditions given in (5.1) are automatically satisfied by  $\tilde{h}$ . Hence, there are  $(\tilde{N} - N + 2)/2$  degrees of freedom remaining. We use all the remaining degrees of freedom to maximize the number of vanishing moments of  $\psi$ , or equivalently, to maximize  $\tilde{L}$  in (5.6); i.e., we set  $\tilde{L} = (\tilde{N} - N + 2)/2$ . Thus, we infer that  $\tilde{N} = 2(L + \tilde{L} - 1)$ . Assume that  $\tilde{h}$  starts with  $\tilde{h}[-L - \tilde{L} + 2]$  and ends with  $\tilde{h}[L + \tilde{L} - 1]$ . We solve (1.24) and (5.6), which give a total of  $\tilde{N}$  simultaneous linear equations, to determine the coefficients of  $\tilde{h}$ .

Unlike the BC systems, it is quite difficult to prove the existence and uniqueness of the solution to the above set of linear equations. However, in our numerical design, we have discovered that for any  $L$  and  $\tilde{L}$  with the same parity, there exists a unique solution for  $\tilde{h}$ .

In Table 5.1, we list the filter lengths of generalized orthogonal Coiflet (GOC) systems, BC systems, and GBC systems. We notice that the length of the lowpass filter in the  $L$ th-order GOC system is about 50% longer and 25% shorter than those of the synthesis and analysis lowpass filters in the BC and GBC systems of order  $(L, L)$ , respectively.

Table 5.1: Filter lengths of three Coiflet-type wavelet systems

GOC	BC		GBC	
$N$	$N$	$\tilde{N}$	$N$	$\tilde{N}$
$2 \lfloor \frac{3L}{2} \rfloor$	$2L - 1$	$2(L + \tilde{L}) - 3$	$2L$	$2(L + \tilde{L} - 1)$

### 5.3 Properties

We now derive some interesting and desirable properties possessed by GBC systems: symmetry and extra vanishing moments.

#### 5.3.1 Symmetry

If  $h[n]$  is the minimum-length solution to (5.5) and (5.7), then

$$\sum_n (-1)^n n^l h[1-n] = \sum_m (-1)^{1-m} (1-m)^l h[m] \quad (5.13)$$

$$= \sum_m (-1)^{1+m} \sum_{p=0}^l \binom{l}{p} (-m)^{l-p} h[m] \quad (5.14)$$

$$= \sum_{p=0}^l \binom{l}{p} (-1)^{l-p+1} \left( \sum_m (-1)^m m^{l-p} h[m] \right) \quad (5.15)$$

$$= 0 \quad (5.16)$$

and

$$\sum_n n^l h[1-n] = \sum_m (1-m)^l h[m] \quad (5.17)$$

$$= \sum_m \sum_{p=0}^l \binom{l}{p} (-m)^{l-p} h[m] \quad (5.18)$$

$$= \sum_{p=0}^l \binom{l}{p} (-1)^{l-p} \left( \sum_m m^{l-p} h[m] \right) \quad (5.19)$$

$$= \sum_{p=0}^l \binom{l}{p} (-1)^{l-p} 2^{p-l} \quad (5.20)$$

$$= 2^{-l} \quad (5.21)$$

i.e.,  $h[1 - n]$  is a minimum-length solution, too. Since  $h[n]$  is unique,  $h$  must satisfy

$$h[1 - n] = h[n]. \quad (5.22)$$

It can be shown in a similar way that

$$\tilde{h}[1 - n] = \tilde{h}[n] \quad (5.23)$$

assuming the existence and uniqueness of  $\tilde{h}$ . Therefore, the filters in GBC systems are half-point symmetric.

### 5.3.2 Extra Vanishing Moments

We have shown that our definition of GBC systems automatically leads to the half-point symmetry of their filterbanks. We shall see that, more interestingly, such a symmetry in turn provides a bonus of extra vanishing moments to GBC systems.

Based on the above definition and the symmetry of  $h$ , we infer that

$$\sum_n (-1)^n n^L h[n] = \sum_n (-1)^n n^L h[1 - n] \quad (5.24)$$

$$= \sum_m (-1)^{1-m} (1 - m)^L h[m] \quad (5.25)$$

$$= \sum_m (-1)^{1+m} \sum_{l=0}^L \binom{L}{l} (-m)^{L-l} h[m] \quad (5.26)$$

$$= \sum_{l=0}^L \binom{L}{l} (-1)^{L-l+1} \left( \sum_m (-1)^m m^{L-l} h[m] \right) \quad (5.27)$$

$$= (-1)^{L+1} \sum_m (-1)^m m^L h[m] \quad (5.28)$$

and

$$\sum_n n^L h[n] = \sum_n n^L h[1-n] \quad (5.29)$$

$$= \sum_m (1-m)^L h[m] \quad (5.30)$$

$$= \sum_m \sum_{l=0}^L \binom{L}{l} (-m)^{L-l} h[m] \quad (5.31)$$

$$= \sum_{l=0}^L \binom{L}{l} (-1)^{L-l} \left( \sum_m m^{L-l} h[m] \right) \quad (5.32)$$

$$= (-1)^L \sum_m m^L h[m] + \sum_{l=1}^L \binom{L}{l} \left( -\frac{1}{2} \right)^{L-l} \quad (5.33)$$

$$= (-1)^L \sum_m m^L h[m] + \left( \frac{1}{2} \right)^L - \left( -\frac{1}{2} \right)^L. \quad (5.34)$$

Similarly, due to the symmetry of  $\tilde{h}$ , we deduce that

$$\sum_n n^L \tilde{h}[n] = (-1)^L \sum_n n^L \tilde{h}[n] + \left( \frac{1}{2} \right)^L - \left( -\frac{1}{2} \right)^L. \quad (5.35)$$

Therefore, if  $L$  is even, then

$$\sum_n (-1)^n n^L h[n] = 0 \quad (5.36)$$

and if  $L$  is odd, then

$$\sum_n n^L h[n] = \sum_n n^L \tilde{h}[n] = 2^{-L}. \quad (5.37)$$

That is, the half-point symmetry of  $h$  and  $\tilde{h}$  yields an extra degree of vanishing moment for either  $\tilde{\psi}$  or  $\phi$  and  $\tilde{\phi}$ . This fact implies that after design, the actual degrees of vanishing moment for  $\psi$  and  $\tilde{\psi}$  must be odd and those for  $\phi$  and  $\tilde{\phi}$  must be even. In this sense, even though we applied the generalized Coifman criterion in our design, the resulting GBC systems do not possess exactly the same degree of vanishing moments for a pair of scaling function and wavelet.

Table 5.2: Actual numbers of vanishing moments for generalized biorthogonal Coiflet systems

$L$	$L_{\tilde{\psi}}$	$L_{\tilde{\phi}}$	$L_{\phi}$
2	3	2	2
3	3	4	4
4	5	4	4
5	5	6	6

We list some examples in Table 5.2, where the symbols  $L_{\tilde{\psi}}$ ,  $L_{\tilde{\phi}}$ , and  $L_{\phi}$  denote the actual degrees of vanishing moment for  $\tilde{\psi}$ ,  $\tilde{\phi}$ , and  $\phi$ , respectively.

Since the filterbanks in BC systems cannot be HPS, BC systems do not possess this type of extra degree of vanishing moment.

### 5.3.3 Other Properties

Unlike BC systems, the synthesis scaling function  $\phi$  in GBC systems is not interpolating. In general, the filter coefficients of the filterbanks in GBC systems are not dyadic rationals. The asymptotic convergence property of the filterbanks in GBC systems is not clear, since no closed-form formulae for either their impulse responses or their frequency responses are available. While GBC systems lose some of the nice properties possessed by BC systems, we shall see what GBC systems gain over BC systems is a significantly improved performance of image data compression.

## 5.4 Application to Image Data Compression

We conducted a comparative study of applying the filterbanks having short lengths in GBC systems to image data compression. We concluded that the 22/14-tapped filterbank corresponding to the GBC system of order (7,5) achieved the best rate-distortion performance in terms of bit rate versus PSNR. This filterbank is denoted by WPB-22/14, for it was first designed and studied by Wei, Pai, and Bovik [56]. We list its filter coefficients in Table 5.3.

Table 5.3: Filter coefficients of WPB-22/14

$n$		$h[n]$	$\tilde{h}[n]$
0	1	0.45822144	0.51620125
-1	2	0.11455536	0.05573021
-2	3	-0.06873322	-0.10097515
-3	4	-0.01963806	0.01279669
-4	5	0.01527405	0.02604553
-5	6	0.00208282	-0.00659508
-6	7	-0.00176239	-0.00465364
-7	8		0.00085361
-8	9		0.00068975
-9	10		-0.00005047
-10	11		-0.00004270

We compare our WPB-22/14 filterbank with three other state-of-the-art filterbanks in terms of compression performance. They are CDF-9/7 which we have introduced in the last chapter, the 6/10-tapped filterbank studied by Villasenor, Belzer, and Liao [47] (referred to as VBL-6/10), and the 10/18-tapped filterbank studied by Tsai, Villasenor, and Chen [42] (referred to as TVC-10/18). VBL-6/10 and TVC-10/18 are the even-length filterbanks having the best coding performance reported in the literature. All the three

existing filterbanks can be constructed from factoring the polynomial  $Q(\cdot)$  given in (4.17), and they possess the maximum degrees of vanishing wavelet moments. Table 5.4 lists the numbers of vanishing wavelet moments of the four biorthogonal wavelet systems and shows that all the four systems have reasonable degrees of vanishing wavelet moments.

Table 5.4: Numbers of vanishing wavelet moments of four biorthogonal wavelet systems

	CDF-9/7	VBL-6/10	TVC-10/18	WPB-22/14
$\tilde{\psi}$	4	3	5	5
$\psi$	4	5	9	7

WPB-22/14 has a long analysis lowpass filter (LPF), and relatively short analysis highpass and synthesis lowpass filters. This is a highly desirable property for filterbanks used in image coding. In general, natural images are composed of both large homogeneous regions and edges having small spatial supports, which correspond to low-frequency and high-frequency components, respectively. At the analysis stage of a subband decomposition, a long LPF and a short highpass filter (HPF) match the two types of components the most appropriately. At the synthesis stage, since most image energy is packed into low-frequency subbands and the human visual system is essentially a lowpass system, the synthesis LPF is much more important than the synthesis HPF in terms of the quality of reconstructed images. Since a short LPF accumulates fewer quantization errors than a long one, the former results in less ringing artifacts, which are the most significant perceptual distortion in wavelet transform-coded images.



The images used in our simulations are “Lena”, “Barbara”, and “Gold-hill”, which are all  $512 \times 512$  8-bit grayscale images. We apply a wavelet transform coding algorithm similar to the SPIHT algorithm [30].

We list the PSNR (defined in (4.67)) versus bit rate results in Table 5.5 and highlight the best result for each case. From the table, we conclude that

- WPB-22/14 consistently outperforms CDF-9/7 and VBL-6/10. The largest improvements are above 0.5 dB over CDF-9/7 and 0.7 dB over VBL-6/10.
- WPB-22/14 is remarkably better than TVC-10/18 for the “Barbara” image and the two filterbanks achieve about the same performance for the other two images.

In the last chapter, we found that WTWB-9/7, WTWB-13/7, and WTWB-13/11 achieved about the same PSNR performance as CDF-9/7. Therefore, WPB-22/14 is significantly better than the three filterbanks in BC systems in the rate-distortion sense.

Figure 5.1 illustrates the “Barbara” images coded at 0.25 bpp using the four filterbanks. While the four coded images have comparable perceptual qualities, WPB-22/14 resulted in slightly less severe ringing effect.

## 5.5 Summary

In this chapter, we have presented a novel class of antisymmetric biorthogonal wavelet systems and discovered that the 22/14-tapped filterbank in this new

Table 5.5: PSNR performance of four filterbanks

image	bit rate	CDF-9/7	VBL-6/10	TVC-10/18	WPB-22/14
Lena	0.500	36.98	36.92	37.04	<b>37.12</b>
	0.250	33.82	33.76	<b>34.01</b>	<b>34.01</b>
	0.125	30.74	30.82	<b>30.98</b>	30.97
Barbara	0.500	31.41	31.21	31.82	<b>31.93</b>
	0.250	27.29	27.10	27.39	<b>27.54</b>
	0.125	24.61	24.48	24.55	<b>24.71</b>
Goldhill	0.500	32.71	32.69	32.77	<b>32.78</b>
	0.250	30.31	30.26	30.31	<b>30.34</b>
	0.125	28.27	28.36	<b>28.37</b>	28.36

family has a superior coding performance over several state-of-the-art filterbanks and thus it is the *best* filterbank to date in the rate-distortion sense. Therefore, we feel that it is a serious candidate for the wavelet system in future image/video compression standards. We have also demonstrated that for image coding, the generalized Coifman criterion is more appropriate than the traditional criterion of maximizing wavelet vanishing moments.



(a)



(b)



(c)



(d)

Figure 5.1: The “Barbara” images coded at 0.25 bpp using four filterbanks: (a) CDF-9/7; (b) VBL-6/10; (c) TVC-10/18; and (d) WPB-22/14.

## Chapter 6

### Biorthogonal Quincunx Coiflets

Most existing developments in wavelet theory and its applications have concentrated on one-dimensional (1-D) systems. The multidimensional (M-D) case has been handled via the tensor product to yield separable systems [23]. For example, a separable two-dimensional (2-D) filter is given as the tensor product of two 1-D filters:

$$h[\mathbf{n}] = h[n_1, n_2] = h[n_1] h[n_2]. \quad (6.1)$$

Separable M-D wavelet systems preserve some properties of 1-D wavelet systems, such as finite support, perfect reconstruction (PR), orthogonality, symmetry, and regularity, and often leads to simple implementations and low computational complexity due to separable processing. However, it imposes a severe limitation on the resulting M-D wavelet representation in the sense that it gives a particular importance to the two directions of coordinates. Therefore, when dealing with M-D signals, *true* M-D processing (allowing both nonseparable sampling and filtering) is more appropriate. Though nonseparable wavelet representations suffer from higher computational complexity, they offer more flexibility (e.g. near-isotropic processing) in multiresolution analysis, more degrees of freedom in design, finer multiscale/multiresolution analysis, better

adaption to the human visual system, and consequently better performance. In particular, nonseparable 2-D wavelet systems are of great importance in image processing applications. On the other hand, since orthogonality and symmetry/antisymmetry are a pair of conflicting properties for compactly supported wavelets [13], biorthogonal symmetric/antisymmetric wavelet systems whose associated filterbanks possess linear phase are the most widely used in practice. Linear phase is often a highly desirable property in image processing.

The construction of nonseparable 2-D wavelet systems has been a challenging problem. This is because *spectral factorization*, which is the fundamental method used in the design of 1-D wavelet systems, cannot be extended to construct 2-D nonseparable wavelet systems. This is because 2-D polynomials cannot always be factored. For this reason, there exist much fewer nonseparable wavelet systems than 1-D wavelet systems.

In this chapter, we study the theory, design, and applications of a novel class of 2-D nonseparable wavelet systems.

## 6.1 Basics of Biorthogonal Quincunx Wavelets

In multiple dimensions, the change in resolution and sampling rate is given by an integer *dilation matrix*  $\mathbf{D}$ . For *quincunx* wavelet systems, it is required that  $\mathbf{D}\mathbf{n}$ ,  $\mathbf{n} \in \mathbb{Z}^2$ , is a quincunx sublattice of  $\mathbb{Z}^2$ ,  $|\det \mathbf{D}| = 2$ , and the two eigenvalues of  $\mathbf{D}$  have magnitude strictly greater than 1 so that there is indeed a dilation in each dimension [10], [20]. The following are two typical choices:

$$\mathbf{D} = \mathbf{D}_1 = \begin{bmatrix} 1 & 1 \\ 1 & -1 \end{bmatrix} \quad \text{or} \quad \mathbf{D} = \mathbf{D}_2 = \begin{bmatrix} 1 & -1 \\ 1 & 1 \end{bmatrix}. \quad (6.2)$$

The dilation equations for the 2-D scaling functions  $\phi(\mathbf{t})$  and  $\tilde{\phi}(\mathbf{t})$  becomes

$$\phi(\mathbf{t}) = \sum_{\mathbf{n}} 2h[\mathbf{n}]\phi(\mathbf{D}\mathbf{t} - \mathbf{n}) \quad \text{and} \quad \tilde{\phi}(\mathbf{t}) = \sum_{\mathbf{n}} 2\tilde{h}[\mathbf{n}]\tilde{\phi}(\mathbf{D}\mathbf{t} - \mathbf{n}) \quad (6.3)$$

or equivalently, in the frequency domain

$$\hat{\phi}(\boldsymbol{\omega}) = \prod_{i=1}^{\infty} H(\mathbf{D}^{-i}\boldsymbol{\omega}) \quad \text{and} \quad \hat{\tilde{\phi}}(\boldsymbol{\omega}) = \prod_{i=1}^{\infty} \tilde{H}(\mathbf{D}^{-i}\boldsymbol{\omega}) \quad (6.4)$$

where  $h[\mathbf{n}]$  and  $\tilde{h}[\mathbf{n}]$  are the lowpass filters. The highpass filters  $g[\mathbf{n}]$  and  $\tilde{g}[\mathbf{n}]$  are given by

$$G(\boldsymbol{\omega}) = \tilde{H}(-\boldsymbol{\omega} + \boldsymbol{\pi}) \quad \text{and} \quad \tilde{G}(\boldsymbol{\omega}) = H(-\boldsymbol{\omega} + \boldsymbol{\pi}). \quad (6.5)$$

The 2-D perfect reconstruction condition for a quincunx dilation matrix  $\mathbf{D}$  can be expressed as

$$\sum_{\mathbf{n}} h[\mathbf{n}]\tilde{h}[\mathbf{n} + \mathbf{D}\mathbf{k}] = \frac{1}{2}\delta[\mathbf{k}], \quad \forall \mathbf{k} \in \mathbb{Z}^2 \quad (6.6)$$

or equivalently

$$H(\boldsymbol{\omega})\tilde{H}(-\boldsymbol{\omega}) + H(\boldsymbol{\omega} + \boldsymbol{\pi})\tilde{H}(-\boldsymbol{\omega} + \boldsymbol{\pi}) = 1, \quad \forall \boldsymbol{\omega} \in \mathbb{R}^2. \quad (6.7)$$

Figures 6.1 and 6.2 illustrate the analysis and synthesis parts of a quincunx FB, respectively. The symbols  $\downarrow \mathbf{D}$  and  $\uparrow \mathbf{D}$  denote downsampling and upsampling with the matrix  $\mathbf{D}$ , respectively.

## 6.2 Vanishing Moments

We define a sequence of subsets of  $\mathbb{Z}^2$ :

$$\mathbb{P}_L = \{\mathbf{l} : \mathbf{l} \in \mathbb{Z}^2, 0 \leq l_1 \leq L-1, 0 \leq l_2 \leq L-1, l_1 + l_2 \leq L-1\} \quad (6.8)$$

for  $L \in \mathbb{N}$ . The next two theorems state the equivalent descriptions of vanishing moments for the wavelets and scaling functions, respectively.

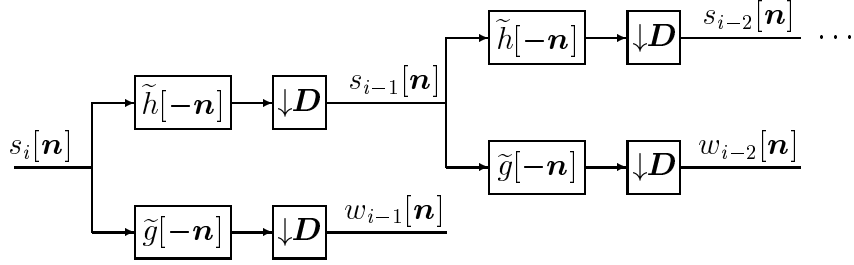


Figure 6.1: Block diagram of the analysis part of a two-dimensional two-channel iterative filterbank

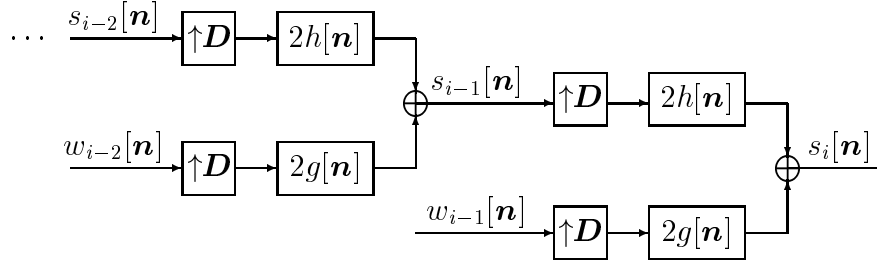


Figure 6.2: Block diagram of the synthesis part of a two-dimensional two-channel iterative filterbank

**Theorem 10** *For a biorthogonal quincunx wavelet system, the following three equations are equivalent:*

$$\int \mathbf{t}^l \tilde{\psi}(\mathbf{t}) d\mathbf{t} = 0 \quad \text{for } \mathbf{l} \in \mathbb{P}_L \quad (6.9)$$

$$\sum_{\mathbf{n}} (-1)^{n_1+n_2} \mathbf{n}^l h[\mathbf{n}] = 0 \quad \text{for } \mathbf{l} \in \mathbb{P}_L \quad (6.10)$$

$$H^{(l_1, l_2)}(\pi, \pi) = \left. \frac{\partial^{l_1+l_2} H(\omega_1, \omega_2)}{\partial \omega_1^{l_1} \partial \omega_2^{l_2}} \right|_{\boldsymbol{\omega}=\boldsymbol{\pi}} = 0 \quad \text{for } \mathbf{l} \in \mathbb{P}_L; \quad (6.11)$$

and similar equivalence holds between  $\psi(\mathbf{t})$  and  $\tilde{h}[\mathbf{n}]$ .

The proof of Theorem 6.9 was given in [34].

**Theorem 11** *For a biorthogonal quincunx wavelet system,*

$$\int \mathbf{t}^l \phi(\mathbf{t}) d\mathbf{t} = \delta[\mathbf{l}] \quad \text{for } \mathbf{l} \in \mathbb{P}_L \quad (6.12)$$

$$\sum_{\mathbf{n}} \mathbf{n}^l h[\mathbf{n}] = \delta[\mathbf{l}] \quad \text{for } \mathbf{l} \in \mathbb{P}_L \quad (6.13)$$

$$H^{(l_1, l_2)}(0, 0) = \left. \frac{\partial^{l_1 + l_2} H(\omega_1, \omega_2)}{\partial \omega_1^{l_1} \partial \omega_2^{l_2}} \right|_{\boldsymbol{\omega}=\mathbf{0}} = \delta[\mathbf{l}] \quad \text{for } \mathbf{l} \in \mathbb{P}_L; \quad (6.14)$$

and similar equivalence holds between  $\tilde{\phi}(\mathbf{t})$  and  $\tilde{h}[\mathbf{n}]$ .

**Proof:** Due to the similarity between  $\{\phi(\mathbf{t}), h[\mathbf{n}]\}$  and  $\{\tilde{\phi}(\mathbf{t}), \tilde{h}[\mathbf{n}]\}$ , we only need to prove the first equivalence.

Let  $[\mathbf{d}_1 \ \mathbf{d}_2] = \mathbf{D}^{-1}$ . Define

$$\mu[\mathbf{l}] = \int \mathbf{t}^l \phi(\mathbf{t}) d\mathbf{t} \quad \text{and} \quad \nu[\mathbf{l}] = \sum_{\mathbf{n}} \mathbf{n}^l h[\mathbf{n}]. \quad (6.15)$$

Using the first dilation equation in (6.3), we infer that for  $\mathbf{l} \in \mathbb{P}_L$ ,

$$\mu[\mathbf{l}] = \int \mathbf{t}^l \sum_{\mathbf{n}} 2h[\mathbf{n}] \phi(\mathbf{D}\mathbf{t} - \mathbf{n}) d\mathbf{t} \quad (6.16)$$

$$= \int 2|\mathbf{D}|^{-1} \sum_{\mathbf{n}} (\mathbf{D}^{-1}\mathbf{s} + \mathbf{n})^l h[\mathbf{n}] \phi(\mathbf{s}) d\mathbf{s} \quad (6.17)$$

$$= \int \sum_{\mathbf{n}} \sum_{\mathbf{p}=0}^l \sum_{\mathbf{q}=0}^r \binom{l}{\mathbf{p}} \binom{r}{\mathbf{q}} \mathbf{d}_1^{\mathbf{p}} \mathbf{d}_2^{l-\mathbf{p}} \mathbf{s}^{\mathbf{q}} \mathbf{n}^{r-\mathbf{q}} h[\mathbf{n}] \phi(\mathbf{s}) d\mathbf{s} \quad (6.18)$$

$$= \sum_{\mathbf{p}=0}^l \sum_{\mathbf{q}=0}^r \binom{l}{\mathbf{p}} \binom{r}{\mathbf{q}} \mathbf{d}_1^{\mathbf{p}} \mathbf{d}_2^{l-\mathbf{p}} \nu[\mathbf{r} - \mathbf{q}] \mu[\mathbf{q}] \quad (6.19)$$

where  $\mathbf{r} = [p_1 + p_2, l_1 + l_2 - p_1 - p_2]^T$ .

If  $\phi(\mathbf{t})$  satisfies (6.12), it follows that

$$\sum_{\mathbf{p}=0}^l \binom{l}{\mathbf{p}} \mathbf{d}_1^{\mathbf{p}} \mathbf{d}_2^{l-\mathbf{p}} \nu[\mathbf{r}] = \delta[\mathbf{l}]. \quad (6.20)$$



For any  $l \in \mathbb{N}$  such that  $l < L$ , we define  $\mathbf{l}_k = [k, l - k]^T$ . Then, (6.20) can be rewritten as

$$\begin{bmatrix} \binom{l_0}{\mathbf{0}} \mathbf{d}_1^0 \mathbf{d}_2^{l_0} & \binom{l_0}{\mathbf{1}} \mathbf{d}_1^1 \mathbf{d}_2^{l_0-1} & \cdots & \binom{l_0}{l_0} \mathbf{d}_1^{l_0} \mathbf{d}_2^0 \\ \binom{l_1}{\mathbf{0}} \mathbf{d}_1^0 \mathbf{d}_2^{l_1} & \binom{l_1}{\mathbf{1}} \mathbf{d}_1^1 \mathbf{d}_2^{l_1-1} & \cdots & \binom{l_1}{l_1} \mathbf{d}_1^{l_1} \mathbf{d}_2^0 \\ \vdots & \vdots & \vdots & \vdots \\ \binom{l_l}{\mathbf{0}} \mathbf{d}_1^0 \mathbf{d}_2^{l_l} & \binom{l_l}{\mathbf{1}} \mathbf{d}_1^1 \mathbf{d}_2^{l_l-1} & \cdots & \binom{l_l}{l_l} \mathbf{d}_1^{l_l} \mathbf{d}_2^0 \end{bmatrix} \begin{bmatrix} \nu[\mathbf{l}_0] \\ \nu[\mathbf{l}_1] \\ \vdots \\ \nu[\mathbf{l}_l] \end{bmatrix} = \begin{bmatrix} 0 \\ 0 \\ \vdots \\ 0 \end{bmatrix}. \quad (6.21)$$

Since  $\mathbf{D}^{-1}$  is non-singular, the above  $(l + 1) \times (l + 1)$  matrix is non-singular. Therefore,  $\nu[\mathbf{l}_k] = 0$  for  $k = 0, 1, \dots, l$ , which implies (6.13).

If  $h[\mathbf{n}]$  satisfies (6.13), it follows that

$$\sum_{p=0}^l \binom{l}{p} \mathbf{d}_1^p \mathbf{d}_2^{l-p} \mu[\mathbf{r}] = \mu[\mathbf{l}]. \quad (6.22)$$

For any  $l \in \mathbb{N}$  such that  $l < L$ , (6.22) can be rewritten as

$$\begin{bmatrix} \binom{l_0}{\mathbf{0}} \mathbf{d}_1^0 \mathbf{d}_2^{l_0} - 1 & \binom{l_0}{\mathbf{1}} \mathbf{d}_1^1 \mathbf{d}_2^{l_0-1} & \cdots & \binom{l_0}{l_0} \mathbf{d}_1^{l_0} \mathbf{d}_2^0 \\ \binom{l_1}{\mathbf{0}} \mathbf{d}_1^0 \mathbf{d}_2^{l_1} & \binom{l_1}{\mathbf{1}} \mathbf{d}_1^1 \mathbf{d}_2^{l_1-1} - 1 & \cdots & \binom{l_1}{l_1} \mathbf{d}_1^{l_1} \mathbf{d}_2^0 \\ \vdots & \vdots & \vdots & \vdots \\ \binom{l_l}{\mathbf{0}} \mathbf{d}_1^0 \mathbf{d}_2^{l_l} & \binom{l_l}{\mathbf{1}} \mathbf{d}_1^1 \mathbf{d}_2^{l_l-1} & \cdots & \binom{l_l}{l_l} \mathbf{d}_1^{l_l} \mathbf{d}_2^0 - 1 \end{bmatrix} \begin{bmatrix} \mu[\mathbf{l}_0] \\ \mu[\mathbf{l}_1] \\ \vdots \\ \mu[\mathbf{l}_l] \end{bmatrix} = \begin{bmatrix} 0 \\ 0 \\ \vdots \\ 0 \end{bmatrix}. \quad (6.23)$$

Since  $\mathbf{D}^{-1}$  is non-singular, the above  $(l + 1) \times (l + 1)$  matrix is non-singular. Therefore,  $\mu[\mathbf{l}_k] = 0$  for  $k = 0, 1, \dots, l$ , which implies (6.12).

Finally, according to the differentiation in frequency property of the 2-D discrete-time Fourier transform, it is trivial to show that (6.13) is equivalent to (6.14). ■

### 6.3 Definition

**Definition 4** A 2-D biorthogonal quincunx wavelet system is a **biorthogonal quincunx Coiflet** system of order  $(L, \tilde{L})$  if

$$\int \mathbf{t}^{\mathbf{l}} \tilde{\phi}(\mathbf{t}) d\mathbf{t} = \delta[\mathbf{l}] \quad \text{for } \mathbf{l} \in \mathbb{P}_L \quad (6.24)$$

$$\int \mathbf{t}^{\mathbf{l}} \tilde{\psi}(\mathbf{t}) d\mathbf{t} = 0 \quad \text{for } \mathbf{l} \in \mathbb{P}_L \quad (6.25)$$

$$\int \mathbf{t}^{\mathbf{l}} \psi(\mathbf{t}) d\mathbf{t} = 0 \quad \text{for } \mathbf{l} \in \mathbb{P}_{\tilde{L}}. \quad (6.26)$$

The definition may be viewed as an extension of the definition of 1-D biorthogonal Coiflet wavelet systems to the quincunx case.

### 6.4 Design

While the method of solving simultaneous equations in the design of biorthogonal Coiflet systems could still be used here, the much larger number of filter coefficients in BQC systems makes it difficult, if not impossible, to derive closed-form formulae for the filter coefficients. As an alternative, we use the McClellan transformation [17], which is a highly efficient method for the design of 2-D zero phase filters.

If  $L$  is even, we rewrite the frequency response of the synthesis lowpass filter in the order- $(L, \tilde{L})$  biorthogonal Coiflet system given in (4.16) as

$$H_L(\omega) = \frac{1}{2} + \sum_{m=1}^{L/2} 2h_L[2m-1] T_{2m-1}(\cos \omega) \quad (6.27)$$

where  $T_n(\cdot)$  denotes the  $n$ th-order Chebyshev polynomial. We choose the transformation function

$$F(\boldsymbol{\omega}) = \frac{1}{2}(\cos \omega_1 + \cos \omega_2). \quad (6.28)$$

Then, the frequency response of the synthesis lowpass filter in the order- $(L, \tilde{L})$  BQC system is given by

$$H_L(\boldsymbol{\omega}) = \frac{1}{2} + \sum_{m=1}^{L/2} 2h_L[2m-1] T_{2m-1}(F(\boldsymbol{\omega})). \quad (6.29)$$

A similar design procedure can be used to construct  $\tilde{H}_{L, \tilde{L}}(\boldsymbol{\omega})$  via transforming  $\tilde{H}_{L, \tilde{L}}(\omega)$  with both  $L$  and  $\tilde{L}$  being even.

If we require  $H_L(\omega)$  and  $\tilde{H}_{L, \tilde{L}}(\omega)$  to satisfy the vanishing moment conditions in the definition, the numbers of vanishing moments for the order- $(L, \tilde{L})$  biorthogonal Coiflet system and BQC system must be identical. It was shown [10], [20] that  $F(\boldsymbol{\omega})$  converts the number of zeros of a 1-D frequency response at  $\omega = \pi$  to the same number of zeros of the transformed 2-D frequency response at the aliasing frequency  $\boldsymbol{\omega} = \boldsymbol{\pi}$ . This implies that  $F(\boldsymbol{\omega})$  preserves vanishing wavelet moments.

If a 1-D zero phase filter  $h[n]$  satisfies

$$H^{(l)}(0) = \delta[l] \quad \text{for } l = 0, 1, \dots, 2K - 1 \quad (6.30)$$

then the frequency response can be expressed as

$$H(\omega) = 1 + (1 - \cos \omega)^K \bar{H}(\omega) \quad (6.31)$$

where  $\bar{H}(\omega)$  is polynomial in  $\cos \omega$ . Hence,  $F(\boldsymbol{\omega})$  converts the  $2K$  zeros of  $(1 - \cos \omega)^K$  at  $\omega = 0$  to the  $2K$  zeros of  $(1 - \frac{1}{2} \cos \omega_1 - \frac{1}{2} \cos \omega_2)^K$  at  $\boldsymbol{\omega} = \mathbf{0}$ . Therefore,  $F(\boldsymbol{\omega})$  preserves vanishing scaling function moments, too. In summary,  $F(\boldsymbol{\omega})$  is a valid transformation function for designing BQC systems.

We now give a design example. The filters  $h[\mathbf{n}]$  and  $\tilde{h}[\mathbf{n}]$  of the order- $(4,2)$  BQC system are obtained from the filters  $h[n]$  and  $\tilde{h}[n]$  of the order- $(4,2)$

biorthogonal Coiflet system, respectively. The filter coefficients  $\{h[\mathbf{n}]\}_n$  and  $\{\tilde{h}[\mathbf{n}]\}_n$  are given by

$$\frac{1}{256} \begin{bmatrix} 0 & 0 & 0 & -1 & 0 & 0 & 0 \\ 0 & 0 & -3 & 0 & -3 & 0 & 0 \\ 0 & -3 & 0 & 39 & 0 & -3 & 0 \\ -1 & 0 & 39 & 128 & 39 & 0 & -1 \\ 0 & -3 & 0 & 39 & 0 & -3 & 0 \\ 0 & 0 & -3 & 0 & -3 & 0 & 0 \\ 0 & 0 & 0 & -1 & 0 & 0 & 0 \end{bmatrix} \quad (6.32)$$

and

$$\frac{1}{1024} \begin{bmatrix} 0 & 0 & 0 & 0 & 1 & 0 & 0 & 0 & 0 \\ 0 & 0 & 0 & 4 & 0 & 4 & 0 & 0 & 0 \\ 0 & 0 & 6 & 0 & -32 & 0 & 6 & 0 & 0 \\ 0 & 4 & 0 & -72 & 128 & -72 & 0 & 4 & 0 \\ 1 & 0 & -32 & 128 & 868 & 128 & -32 & 0 & 1 \\ 0 & 4 & 0 & -72 & 128 & -72 & 0 & 4 & 0 \\ 0 & 0 & 6 & 0 & -32 & 0 & 6 & 0 & 0 \\ 0 & 0 & 0 & 4 & 0 & 4 & 0 & 0 & 0 \\ 0 & 0 & 0 & 0 & 1 & 0 & 0 & 0 & 0 \end{bmatrix} \quad (6.33)$$

respectively, where the largest coefficients  $\frac{128}{256}$  and  $\frac{868}{1024}$  correspond to  $h[\mathbf{0}]$  and  $\tilde{h}[\mathbf{0}]$ , respectively.

## 6.5 Properties

### 6.5.1 Symmetry and Isotropism

The symmetry of  $h[n]$  and  $F(\boldsymbol{\omega})$  results in the following *eight-fold symmetry* of  $h[\mathbf{n}]$ :

$$h[n_1, n_2] = h[-n_1, n_2] \quad (6.34)$$

$$h[n_1, n_2] = h[n_1, -n_2] \quad (6.35)$$

$$h[n_1, n_2] = h[n_2, n_1]. \quad (6.36)$$

This symmetry implies the following spatial-domain isotropism:

$$\|\mathbf{n}_1\| = \|\mathbf{n}_2\| \Rightarrow h[\mathbf{n}_1] = h[\mathbf{n}_2]. \quad (6.37)$$

Similar properties hold for the analysis filter  $\tilde{h}[\mathbf{n}]$ .

### 6.5.2 Interpolating Scaling Functions

A two-dimensional scaling function  $\phi(\mathbf{t})$  is *interpolating* or *cardinal* if

$$\phi(\mathbf{n}) = \delta[\mathbf{n}] \quad \forall \mathbf{n} \in \mathbb{Z}^2. \quad (6.38)$$

For instance, the function

$$\phi(\mathbf{t}) = \frac{\sin(\pi t_1) \sin(\pi t_2)}{\pi^2 t_1 t_2} \quad (6.39)$$

is interpolating. 2-D interpolating functions are desirable in sampling and interpolation of 2-D functions. If we use the uniform samples of a 2-D function  $f$  with a sampling matrix  $\mathbf{D}$ , and a 2-D interpolating function  $\phi$  to reconstruct  $f$  as

$$\tilde{f}(\mathbf{t}) = \sum_{\mathbf{n}} f(\mathbf{D}^{-i}\mathbf{n})\phi(\mathbf{D}^i\mathbf{t} - \mathbf{n}) \quad (6.40)$$

for any  $i \in \mathbb{Z}$ , then

$$\tilde{f}(\mathbf{D}^{-i}\mathbf{n}) = f(\mathbf{D}^{-i}\mathbf{n}) \quad \forall \mathbf{n} \in \mathbb{Z}^2 \quad (6.41)$$

i.e., we obtain an exact reconstruction at those sampling points.

**Theorem 12** *The synthesis scaling function  $\phi$  in a BQC system is interpolating.*

**Proof:** Since the  $(2m - 1)$ th-order Chebyshev polynomial  $T_{2m-1}$  is an odd function for any  $m \in \mathbb{N}$  and

$$F(\boldsymbol{\omega} + \boldsymbol{\pi}) = -F(\boldsymbol{\omega}), \quad (6.42)$$

it follows that

$$H(\boldsymbol{\omega}) + H(\boldsymbol{\omega} + \boldsymbol{\pi}) = 1. \quad (6.43)$$

For  $k \in \mathbb{N}$ , let

$$U_k(\boldsymbol{\omega}) = \prod_{i=1}^k H(\mathbf{D}^{-i}\boldsymbol{\omega}) I_{[-\pi, \pi]^2}(\mathbf{D}^{-k}\boldsymbol{\omega}) \quad (6.44)$$

where  $I_{\mathbb{I}}(\boldsymbol{\omega})$  is the indicator function

$$I_{\mathbb{I}}(\boldsymbol{\omega}) = \begin{cases} 1 & \text{if } \boldsymbol{\omega} \in \mathbb{I} \\ 0 & \text{otherwise.} \end{cases} \quad (6.45)$$

Let  $u_k$  be the inverse Fourier transform of  $U_k(\boldsymbol{\omega})$ . Thus, from (6.4) we deduce that, as  $k$  tends to infinity,  $U_k(\boldsymbol{\omega})$  converges to  $\hat{\phi}(\boldsymbol{\omega})$  pointwise and

$$\lim_{k \rightarrow \infty} u_k(\mathbf{n}) = \lim_{k \rightarrow \infty} \frac{1}{4\pi^2} \int U_k(\boldsymbol{\omega}) e^{j\boldsymbol{\omega}^T \mathbf{n}} d\boldsymbol{\omega} \quad (6.46)$$

$$= \frac{1}{4\pi^2} \int \hat{\phi}(\boldsymbol{\omega}) e^{j\boldsymbol{\omega}^T \mathbf{n}} d\boldsymbol{\omega} \quad (6.47)$$

$$= \phi(\mathbf{n}). \quad (6.48)$$

We define a sequence of subsets of  $\mathbb{R}^2$ :

$$\mathbb{W}_k = \{\boldsymbol{\omega} : \mathbf{D}^{-k}\boldsymbol{\omega} \in [-\pi, \pi]^2\} \quad (6.49)$$

with  $k \in \mathbb{Z}$ . We infer that for any  $\mathbf{n} \in \mathbb{Z}^2$ ,

$$u_k(\mathbf{n}) = \frac{1}{4\pi^2} \int_{\mathbb{W}_k} \prod_{i=1}^k H(\mathbf{D}^{-i}\boldsymbol{\omega}) e^{j\boldsymbol{\omega}^T \mathbf{n}} d\boldsymbol{\omega} \quad (6.50)$$

$$= \frac{|\mathbf{D}|^k}{4\pi^2} \int_{[-\pi, \pi]^2} \prod_{i=1}^k H(\mathbf{D}^{k-i}\boldsymbol{\xi}) e^{j(\mathbf{D}^k \boldsymbol{\xi})^T \mathbf{n}} d\boldsymbol{\xi} \quad (6.51)$$

$$= \frac{|D|^k}{4\pi^2} \int_{[-\pi, \pi]^2} \prod_{i=1}^{k-1} H(D^i \boldsymbol{\xi}) e^{j(D^k \boldsymbol{\xi})^T \mathbf{n}} H(\boldsymbol{\xi}) d\boldsymbol{\xi} \quad (6.52)$$

$$= \frac{|D|^k}{4\pi^2} \int_{\mathbb{W}_{-1}} \prod_{i=1}^{k-1} H(D^i \boldsymbol{\xi}) e^{j(D^k \boldsymbol{\xi})^T \mathbf{n}} (H(\boldsymbol{\xi}) + H(\boldsymbol{\xi} + \boldsymbol{\pi})) d\boldsymbol{\xi} \quad (6.53)$$

since  $\prod_{i=1}^{k-1} H(D^i \boldsymbol{\xi}) e^{j(D^k \boldsymbol{\xi})^T \mathbf{n}}$  is periodic with period  $\pi$  in both  $\xi_1$  and  $\xi_2$ . Due to (6.43), it follows that

$$u_k(\mathbf{n}) = \frac{|D|^k}{4\pi^2} \int_{\mathbb{W}_{-1}} \prod_{i=1}^{k-1} H(D^i \boldsymbol{\xi}) e^{j(D^k \boldsymbol{\xi})^T \mathbf{n}} d\boldsymbol{\xi} \quad (6.54)$$

$$= \frac{|D|^{k-1}}{4\pi^2} \int_{[-\pi, \pi]^2} \prod_{i=0}^{k-2} H(D^i \boldsymbol{\theta}) e^{j(D^{k-1} \boldsymbol{\theta})^T \mathbf{n}} d\boldsymbol{\theta}. \quad (6.55)$$

Comparing (6.52) and (6.55), we conclude that

$$u_k(\mathbf{n}) = u_{k-1}(\mathbf{n}). \quad (6.56)$$

On the other hand,

$$u_1(\mathbf{n}) = \frac{1}{4\pi^2} \int_{\mathbb{W}_1} H(D^{-1} \boldsymbol{\omega}) e^{j\boldsymbol{\omega}^T \mathbf{n}} d\boldsymbol{\omega} \quad (6.57)$$

$$= \frac{1}{4\pi^2} \int_{[-\pi, \pi]^2} \left( H(D^{-1} \boldsymbol{\omega}) e^{j\boldsymbol{\omega}^T \mathbf{n}} + H(D^{-1}(\boldsymbol{\omega} + 2\boldsymbol{\pi})) e^{j(\boldsymbol{\omega} + 2\boldsymbol{\pi})^T \mathbf{n}} \right) d\boldsymbol{\omega} \quad (6.58)$$

$$= \frac{1}{4\pi^2} \int_{[-\pi, \pi]^2} e^{j\boldsymbol{\omega}^T \mathbf{n}} d\boldsymbol{\omega} \quad (6.59)$$

$$= \delta[\mathbf{n}] \quad (6.60)$$

which implies (6.38). ■

The theorem states that the transformation function  $F(\boldsymbol{\omega})$  preserves the property of interpolating scaling functions.

### 6.5.3 Asymptotic Convergence of Filters

Based on the asymptotic convergence of 1-D biorthogonal Coiflet systems discussed in Chapter 4, it is straightforward to establish the theorem below by

considering the transformation function given in (6.28).

**Theorem 13** *The frequency responses of the filters in biorthogonal quincunx Coiflet systems converge pointwise to ideal diamond-shaped halfband lowpass frequency responses as the orders of the systems tend to infinity:*

$$\lim_{L \rightarrow \infty} H_L(\boldsymbol{\omega}) = \begin{cases} 1 & \text{if } |\omega_1| + |\omega_2| < \pi \\ 1/2 & \text{if } |\omega_1| + |\omega_2| = \pi \\ 0 & \text{if } |\omega_1| + |\omega_2| > \pi, |\omega_1| \leq \pi, |\omega_2| \leq \pi \end{cases} \quad (6.61)$$

$$\lim_{L, \tilde{L} \rightarrow \infty} \widetilde{H}_{L, \tilde{L}}(\boldsymbol{\omega}) = \begin{cases} 1 & \text{if } |\omega_1| + |\omega_2| \leq \pi \\ 0 & \text{if } |\omega_1| + |\omega_2| > \pi, |\omega_1| \leq \pi, |\omega_2| \leq \pi; \end{cases} \quad (6.62)$$

the convergence of  $H_L(\boldsymbol{\omega})$  is monotonic in the sense that

$$H_L(\boldsymbol{\omega}) \leq H_{L+2}(\boldsymbol{\omega}) \quad \text{if } |\omega_1| + |\omega_2| \leq \pi \quad (6.63)$$

$$H_L(\boldsymbol{\omega}) \geq H_{L+2}(\boldsymbol{\omega}) \quad \text{if } |\omega_1| + |\omega_2| > \pi, |\omega_1| \leq \pi, |\omega_2| \leq \pi; \quad (6.64)$$

the convergence of  $H_L(\boldsymbol{\omega})$  does not exhibit any Gibbs-like phenomenon and the convergence of  $\widetilde{H}_{L, \tilde{L}}(\boldsymbol{\omega})$  exhibits a one-sided Gibbs-like phenomenon.

#### 6.5.4 Dyadic Rational Filter Coefficients

From the aforementioned McClellan transformation-based design with the transformation function  $F(\boldsymbol{\omega})$  given in (6.28), it is trivial to check that the filterbanks of BQC systems possess dyadic rational filter coefficients. Thus, the filterbanks permit multiplication-free DWT's.

## 6.6 Application to Image Data Compression

Since we have demonstrated in Chapter 4 that several 1-D biorthogonal Coiflet systems are comparable with the popular CDF-9/7 for image data compres-



sion, we expect that BQC systems, which are constructed based on biorthogonal Coiflet systems, are also excellent for image coding. We attempt to compare systems in the new family with the state-of-the-art quincunx wavelet systems. Very few quincunx wavelet systems have been recommended for image coding. The state-of-the-art filterbank is the 9/7-tapped<sup>1</sup> filterbank by Barlaud, Solé, Gaidon, Antonini, and Mathieu [3]. We refer to their filterbank as BSGAM-9/7. In fact, BSGAM-9/7 was constructed from CDF-9/7 via McClellan transformation with the transformation function given in (6.28). From the new BQC family, we choose an filterbank of the same size as BSGAM-9/7 for comparison. This filterbank is denoted by WEB-9/7, for it was first designed and studied by Wei, Evans, and Bovik [53]. The coefficients of its two lowpass filters are given in (6.32) and (6.33), respectively. In fact, WEB-9/7 was constructed from WTWB-9/7 via McClellan transformation with the transformation function given in (6.28).

The images used in our simulations are “Lena”, “Barbara”, “Goldhill”, and “Peppers”, which are all 8-bit grayscale images of size  $512 \times 512$ . Since no high-performance image coder exists for quincunx wavelet systems, we take the following steps to simulate a wavelet transform coding for a given image:

1. choose a preservation percentage  $p$ ;
2. take a forward DWT on the original image;
3. keep the  $p\%$  of DWT coefficients with the largest absolute values unchanged and set the others to zero;

---

<sup>1</sup>A 2-D 9/7-tapped filterbank means that the sizes of its analysis and synthesis lowpass filters are  $9 \times 9$  and  $7 \times 7$ , respectively.

4. take a inverse DWT on the thresholded DWT coefficients to reconstruct the image.

Such a procedure measures the energy compaction capability of wavelet systems, which is generally consistent with their performance in terms of PSNR versus bit rate.

In Figure 6.3, we plot the rate-distortion performance of the two filterbanks in terms of PSNR (defined in (4.67)) versus percentage of thresholded DWT coefficients. Figure 6.4 depicts the “Lena” and “Barbara” images reconstructed with 7% and 20% of DWT coefficients, respectively. The figures show that WEB-9/7 achieved both significantly better objective and subjective image quality than BSGAM-9/7 for all four images. It is interesting to note that, while both WTWB-9/7 and CDF-9/7 are comparable in terms of compression performance, the 2-D transformed version of the former, i.e., WEB-9/7, remarkably outperforms that of the latter, i.e., BSGAM-9/7.

## 6.7 Extension to Higher Dimensions

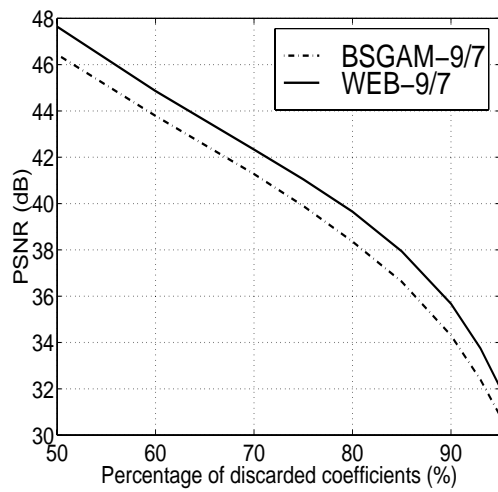
It is straightforward to extend the aforementioned design to higher dimensions. To construct  $m$ -dimensional biorthogonal Coiflet systems, we can simply use the transformation function

$$F(\omega_1, \omega_2, \dots, \omega_m) = \frac{1}{m} \sum_{d=1}^m \cos \omega_d. \quad (6.65)$$

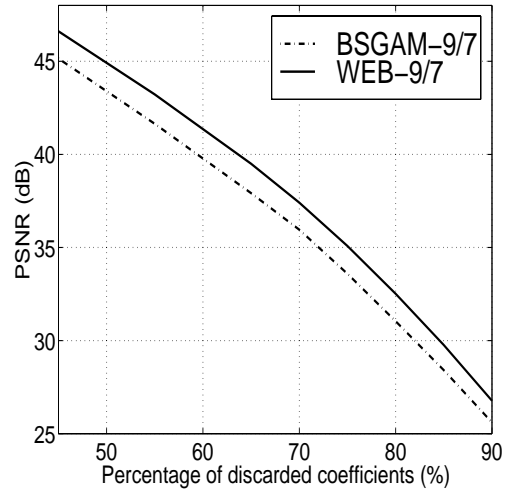
Apparently, the resulting filterbanks have dyadic rational filter coefficients if and only if  $m = 2^k$  for some  $k \in \mathbb{N}$ .

## 6.8 Summary

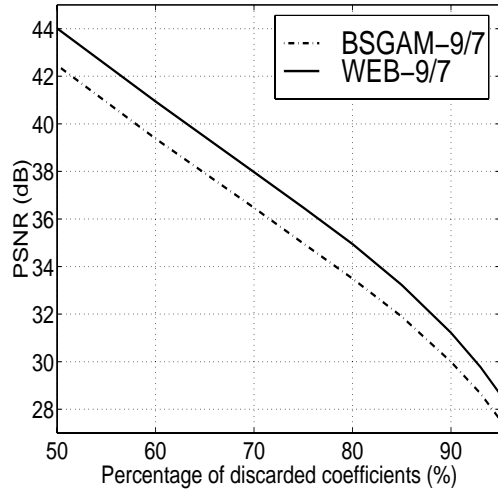
We have presented the design of a novel class of biorthogonal quincunx wavelet systems, which enjoys several remarkable properties. In particular, one filterbank in this family has been shown to have a significantly better rate-distortion performance than the state-of-the-art nonseparable filterbank in DWT-based image data compression and enjoy a much lower computational complexity, due to the former's fast implementation of a multiplication-free DWT. Therefore, these BQC systems are promising for the choice of nonseparable wavelet systems in image and multidimensional signal processing applications.



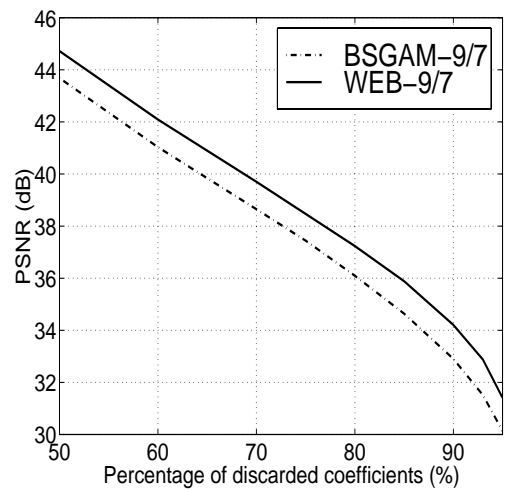
(a)



(b)



(c)



(d)

Figure 6.3: PSNR performance of two filterbanks: (a) “Lena”; (b) “Barbara”; (c) “Goldhill”; and (d) “Peppers”.



(a)



(b)



(c)



(d)

Figure 6.4: The reconstructed “Lena” and “Barbara” images with 7% and 20% of DWT coefficients, respectively. (a) “Lena” compressed by BSGAM-9/7; (b) “Lena” compressed by WEB-9/7; (c) “Barbara” compressed by BSGAM-9/7; and (d) “Barbara” compressed by WEB-9/7.

## Chapter 7

### Generalized Biorthogonal Quincunx Coiflets

In this chapter, we address the design of *generalized biorthogonal quincunx Coiflet* systems, which could be defined with the generalized Coifman criterion. Naturally, we would expect to construct the new filterbanks (FB's) via transforming the FB's associated with generalized biorthogonal Coiflet systems, which were addressed in Chapter 5. The latter FB's are half-point symmetric and of even length. We shall study the design problem in a more general sense.

Two extensions of the McClellan transformation have been proposed to transform even-length half-point symmetric one-dimensional (1-D) prototype filters into even/odd-size multidimensional (M-D) filters [25], [18]. Since numerous even-length symmetric 1-D perfect reconstruction (PR) FB's and wavelets having useful properties have been constructed (e.g., both real-valued biorthogonal PRFB's and complex-valued orthogonal PRFB's can possess both even length and symmetry), it is natural to ask whether they can be transformed into M-D PRFB's using the two extended McClellan transformations. In this chapter, we answer the general question by showing that, unlike the original McClellan transformation, the two extended McClellan transforma-

tions suffer from a limitation in the design of multidimensional two-channel FIR PRFB's and wavelets in the sense that there does *not* exist any transformation function that can preserve PR after transformation. For one of the transformations, we point out that near-PR FB's are possible.

Assume that  $H(\boldsymbol{\omega})$  and  $\widetilde{H}(\boldsymbol{\omega})$  are the frequency responses of the dual lowpass filters in a two-channel  $m$ -dimensional ( $m$ -D) PRFB. They satisfy

$$H(\mathbf{0}) = \widetilde{H}(\mathbf{0}) = 1, \quad H(\boldsymbol{\eta}) = \widetilde{H}(\boldsymbol{\eta}) = 0 \quad (7.1)$$

and the perfect reconstruction condition (see [44])

$$H(\boldsymbol{\omega})\widetilde{H}^*(\boldsymbol{\omega}) + H(\boldsymbol{\omega} + \boldsymbol{\eta})\widetilde{H}^*(\boldsymbol{\omega} + \boldsymbol{\eta}) = 1 \quad (7.2)$$

for any  $\boldsymbol{\omega} \in \mathbb{R}^m$ , where the symbol “\*” denotes complex conjugation and  $\boldsymbol{\eta}$  is the aliasing frequency associated with the  $m$ -D downsampling pattern of the FB (e.g.,  $\boldsymbol{\eta} = [\pi, \pi]$  for 2-D quincunx downsampling lattice).

## 7.1 Design of Even-Size Filterbanks via an Extended McClellan Transformation

The frequency response of an even-length symmetric 1-D FIR filter  $h_0[n]$  centered at  $n = \frac{1}{2}$  can be expressed as [25]

$$H_0(\omega) = (1 + e^{-j\omega})P(\cos \omega) \quad (7.3)$$

where  $P(\cdot)$  is a polynomial on the interval  $[-1, 1]$ , and  $P(\cos \omega)$  can be viewed as the frequency response of a 1-D odd-length symmetric filter. Then, the desired  $m$ -D even-size filter can be constructed by [25], [18]

$$H(\boldsymbol{\omega}) = \prod_{i=1}^m (1 + e^{-j\omega_i})P(F(\boldsymbol{\omega})) \quad (7.4)$$

where  $F(\boldsymbol{\omega})$  is a transformation function used to substitute for  $\cos \omega$ .

Assume that a transformation function  $F(\boldsymbol{\omega})$  is used to transform a pair of 1-D even-length dual filters  $H_0(\omega)$  and  $\widetilde{H}_0(\omega)$  having the PR property into a pair of  $m$ -D even-size dual filters  $H(\boldsymbol{\omega})$  and  $\widetilde{H}(\boldsymbol{\omega})$ ; i.e.,  $H(\boldsymbol{\omega})$  is given by (7.4) and  $\widetilde{H}(\boldsymbol{\omega})$  is given by

$$\widetilde{H}(\boldsymbol{\omega}) = \prod_{i=1}^m (1 + e^{-j\omega_i}) \widetilde{P}(F(\boldsymbol{\omega})) \quad (7.5)$$

where the polynomial  $\widetilde{P}(\cdot)$  is defined similarly as  $P(\cdot)$ . Since  $H_0(\omega)$  and  $\widetilde{H}_0(\omega)$  satisfy the PR condition (7.2), it follows that

$$2(1 + \cos \omega) P(\cos \omega) \widetilde{P}^*(\cos \omega) + 2(1 - \cos \omega) P(-\cos \omega) \widetilde{P}^*(-\cos \omega) = 1 \quad (7.6)$$

for any  $\omega \in \mathbb{R}$ . If  $H(\boldsymbol{\omega})$  and  $\widetilde{H}(\boldsymbol{\omega})$  are required to satisfy the PR condition (7.2), then it follows that

$$\begin{aligned} 2^m \prod_{i=1}^m (1 + \cos \omega_i) P(F(\boldsymbol{\omega})) \widetilde{P}^*(F(\boldsymbol{\omega})) \\ + 2^m \prod_{i=1}^m (1 - \cos \omega_i) P(F(\boldsymbol{\omega} + \boldsymbol{\eta})) \widetilde{P}^*(F(\boldsymbol{\omega} + \boldsymbol{\eta})) = 1 \end{aligned} \quad (7.7)$$

for any  $\boldsymbol{\omega} \in \mathbb{R}^m$ . Since the 1-D aliasing frequency  $\pi$  should map to the  $m$ -D aliasing frequency  $\boldsymbol{\eta}$ ,  $\cos(\omega + \pi) = -\cos \omega$  maps to  $F(\boldsymbol{\omega} + \boldsymbol{\eta})$ . Therefore, for any  $\boldsymbol{\omega} \in \mathbb{R}^m$ ,

$$F(\boldsymbol{\omega} + \boldsymbol{\eta}) = -F(\boldsymbol{\omega}). \quad (7.8)$$

Comparing (7.6) and (7.7), we infer that the transformation function  $F(\boldsymbol{\omega})$  must satisfy

$$F(\boldsymbol{\omega}) = -1 + 2^{m-1} \prod_{i=1}^m (1 + \cos \omega_i) \quad (7.9)$$

$$F(\boldsymbol{\omega}) = 1 - 2^{m-1} \prod_{i=1}^m (1 - \cos \omega_i) \quad (7.10)$$



which are apparently conflict with each other for any  $m$  such that  $m > 1$ . Thus,  $H(\boldsymbol{\omega})$  and  $\widetilde{H}(\boldsymbol{\omega})$  cannot satisfy the PR condition. Therefore, we have established the theorem below.

**Theorem 14** *There does not exist any transformation function by which a pair of 1-D even-length dual filters can be transformed to a pair of  $m$ -D even-size dual filters having the perfect reconstruction property.*

## 7.2 Design of Odd-Size Filterbanks via an Extended McClellan Transformation

Define a polynomial  $Q(\cdot)$  on the interval  $[0, 1]$  by

$$Q(x) = 2P(2x - 1). \quad (7.11)$$

Then, the frequency response of an even-length symmetric 1-D FIR filter given in (7.3) can be rewritten as

$$H_0(\omega) = e^{-j\omega/2} \cos(\omega/2) Q(\cos^2(\omega/2)). \quad (7.12)$$

By substituting a transformation function  $F(\boldsymbol{\omega})$  for  $\cos(\omega/2)$ , we can obtain the frequency response of an  $m$ -D odd-size filter [18]

$$H(\boldsymbol{\omega}) = F(\boldsymbol{\omega}) Q(F^2(\boldsymbol{\omega})). \quad (7.13)$$

Assume that a transformation function  $F(\boldsymbol{\omega})$  is used to transform a pair of 1-D even-length dual filters  $H_0(\omega)$  and  $\widetilde{H}_0(\omega)$  having the PR property into a pair of  $m$ -D odd-size dual filters  $H(\boldsymbol{\omega})$  and  $\widetilde{H}(\boldsymbol{\omega})$ ; i.e.,  $H(\boldsymbol{\omega})$  is given by (7.13) and  $\widetilde{H}(\boldsymbol{\omega})$  is given by

$$\widetilde{H}(\boldsymbol{\omega}) = F(\boldsymbol{\omega}) \widetilde{Q}(F^2(\boldsymbol{\omega})) \quad (7.14)$$

where the polynomial  $\tilde{Q}(\cdot)$  is defined similarly as  $Q(\cdot)$ . From the transformation mapping of the origin and aliasing frequency we infer

$$F(\mathbf{0}) = 1 \quad \text{and} \quad F(\boldsymbol{\eta}) = 0. \quad (7.15)$$

Since  $H_0(\omega)$  and  $\tilde{H}_0(\omega)$  satisfy the PR condition given by (7.2), it follows that

$$\cos^2\left(\frac{\omega}{2}\right) Q\left(\cos^2\left(\frac{\omega}{2}\right)\right) \tilde{Q}^*\left(\cos^2\left(\frac{\omega}{2}\right)\right) + \sin^2\left(\frac{\omega}{2}\right) Q\left(\sin^2\left(\frac{\omega}{2}\right)\right) \tilde{Q}^*\left(\sin^2\left(\frac{\omega}{2}\right)\right) = 1 \quad (7.16)$$

for any  $\omega \in \mathbb{R}$ . If  $H(\boldsymbol{\omega})$  and  $\tilde{H}(\boldsymbol{\omega})$  are required to satisfy the PR condition (7.2), then it follows that

$$F^2(\boldsymbol{\omega}) Q(F^2(\boldsymbol{\omega})) \tilde{Q}^*(F^2(\boldsymbol{\omega})) + F^2(\boldsymbol{\omega} + \boldsymbol{\eta}) Q(F^2(\boldsymbol{\omega} + \boldsymbol{\eta})) \tilde{Q}^*(F^2(\boldsymbol{\omega} + \boldsymbol{\eta})) = 1 \quad (7.17)$$

for any  $\boldsymbol{\omega} \in \mathbb{R}^m$ . Comparing (7.16) and (7.17), we infer that the transformation function  $F(\boldsymbol{\omega})$  must satisfy

$$R(1 - F^2(\boldsymbol{\omega})) = R(F^2(\boldsymbol{\omega} + \boldsymbol{\eta})) \quad (7.18)$$

where  $R(x) = xQ(x)\tilde{Q}^*(x)$  is a polynomial on  $[0, 1]$ . From (7.13), (7.14), (7.15), and (7.1), it is easy to check that  $R(0) = 0$  and  $R(1) = 1$ . Therefore,  $F(\boldsymbol{\omega})$  must satisfy

$$F^2(\boldsymbol{\omega}) + F^2(\boldsymbol{\omega} + \boldsymbol{\eta}) = 1 \quad (7.19)$$

for any  $\boldsymbol{\omega} \in \mathbb{R}^m$ . The  $m$ -D filter  $F(\boldsymbol{\omega})$  satisfying both (7.15) and (7.19) is an odd-size symmetric filter (recall that  $F(\boldsymbol{\omega})$  is real-valued) and should correspond to an orthogonal wavelet. It has been shown [20, Proposition 4.6] that such a filter does not exist for any dimension. Therefore, we have established the theorem below.

**Theorem 15** *There does not exist any transformation function by which a pair of 1-D even-length dual filters can be transformed to a pair of  $m$ -D odd-size dual filters without losing the PR property.*

Although the exact solution to (7.19) does not exist, approximate solutions are possible. In fact, such an approximation problem is similar to the design of near-PR linear-phase quadrature mirror FB's, which has been successfully solved [44]. Since often both  $Q$  and  $\tilde{Q}$  are smooth functions, if (7.19) is approximately satisfied, then so is (7.17). Therefore, we are able to construct  $m$ -D near-PR FB's using the transformation.

### 7.3 Summary

We have presented a limitation of the application of two extended McClellan transformations to the design of two-channel M-D PRFB's and wavelet systems, which is due to the fact that when transforming 1-D even-length PRFB's, PR cannot be preserved for the resulting M-D FB's. Thus, the existence of the M-D non-separable counterparts corresponding to those 1-D even-length PRFB's remains an open question for further research. In this sense, we conclude that the generalized biorthogonal quincunx Coiflet systems, if they exist, cannot be constructed via the two extended McClellan transformations.

## Chapter 8

### Conclusion

We have presented a systematic study of the theory, design, and applications of several novel classes of Coiflet-type wavelet systems. We briefly review the key contributions of this dissertation below.

In Chapter 2, we established the Mathematical theory of Coiflet-type wavelet systems.

In Chapter 3, we designed generalized orthogonal Coiflet systems, discussed their useful properties such as nearly linear phase filterbank, addressed their advantages over the original orthogonal Coiflet systems, and studied their application to sampling and approximation of smooth functions.

In Chapter 4, we designed biorthogonal Coiflet systems, discussed their useful properties such as whole-point symmetric filterbanks, interpolating scaling functions, dyadic rational filter coefficients, and asymptotic convergence, and studied their application to image data compression.

In Chapter 5, we designed generalized biorthogonal Coiflet systems, discussed their useful properties such as half-point symmetric filterbanks and extra vanishing moments, and studied their application to image data compression.

In Chapter 6, we designed biorthogonal quincunx Coiflet systems, discussed their useful properties such as zero phase filterbanks, spatial-domain isotropism, interpolating scaling functions, dyadic rational filter coefficients, and asymptotic convergence, and studied their application to image data compression.

In Chapter 7, we proved that multidimensional two-channel perfect reconstruction filterbanks including the filterbanks of generalized biorthogonal quincunx Coiflet systems cannot be designed via extended McClellan transformations.

Since Coiflet-type wavelet systems possess both vanishing wavelet moments and vanishing scaling function moments, they are outstanding for digital signal processing applications. In particular, they generally outperform wavelet systems having vanishing wavelet moments only. For image coding applications, some of the new wavelet systems achieve better performance than the state-of-the-art wavelet systems.

We propose a number of open problems related to Coiflet-type wavelet systems, which may be worth future research.

1. Due to the lack of closed-form formulae for biorthogonal Coiflet systems for the case that one wavelet has higher degree of vanishing moments than the two scaling functions, the properties of those wavelet systems have not been studied rigorously.
2. The existence and uniqueness of the analysis lowpass filters in generalized biorthogonal Coiflet systems have not been proved.

3. The McClellan transformation-based design of biorthogonal quincunx Coiflet systems may not lead to minimum-size filterbanks. Other design methods need to be studied.
4. The existence, design, and properties of generalized biorthogonal quincunx Coiflet systems remain open.

It is our hope that the dissertation provides a rich collection of high-performance wavelet systems, which can be promising in solving various scientific and engineering problems.

## Appendix

# Appendix A

## Original Images



Figure A.1: The original “Boats” image.





(a)



(b)



(c)



(d)

Figure A.2: The original images: (a) “Lena”; (b) “Barbara”; (c) “Goldhill”; and (d) “Peppers”.

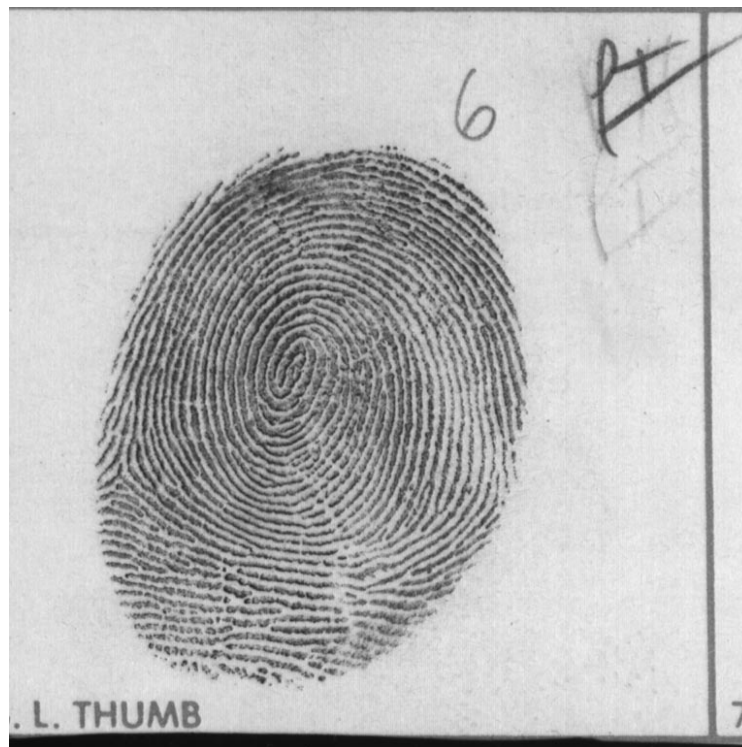


Figure A.3: The original “Fingerprint-1” image.



Figure A.4: The original “Fingerprint-2” image.

## Bibliography

- [1] P. Abry and P. Flandrin, “On the initialization of the discrete wavelet transform algorithm”, *IEEE Signal Processing Letters*, vol. 1, no. 2, pp. 32–34, Feb. 1994.
- [2] R. Ansari, C. Guillemot, and J. F. Kaiser, “Wavelet construction using Lagrange halfband filters”, *IEEE Trans. Circuits Syst.*, vol. 38, no. 9, pp. 1116–1118, Sept. 1991.
- [3] M. Barlaud, P. Solé, T. Gaidon, M. Antonini, and P. Mathieu, “Pyramidal lattice vector quantization for multiscale image coding”, *IEEE Trans. Image Processing*, vol. 3, no. 4, pp. 367–381, July 1994.
- [4] G. Beylkin, R. R. Coifman, and V. Rokhlin, “Fast wavelet transforms and numerical algorithms”, *Commun. Pure Appl. Math.*, vol. 44, pp. 141–183, 1991.
- [5] C. M. Brislawn, J. N. Bradley, R. J. Onyschczak, and T. Hopper, “The FBI compression standard for digitized fingerprint images”, in *Proc. SPIE Conf. Applications of Digital Image Processing XIX*, Denver, CO, Aug. 1996, vol. 2847, pp. 344–355.
- [6] C. S. Burrus, R. A. Gopinath, and H. Guo, *Introduction to Wavelets and Wavelet Transforms: A Primer*, Prentice-Hall, Upper Saddle River, NJ,

1997.

- [7] C. S. Burrus and J. E. Odegard, “Coiflet systems and zero moments”, *IEEE Trans. Signal Processing*, vol. 46, no. 3, pp. 761–766, Mar. 1998.
- [8] P. J. Burt and E. H. Adelson, “The Laplacian pyramid as a compact image code”, *IEEE Trans. Commun.*, vol. 31, no. 4, pp. 532–540, Apr. 1983.
- [9] S. Cambanis and E. Masry, “Wavelet approximation of deterministic and random signals: Convergence properties and rates”, *IEEE Trans. Inform. Theory*, vol. 40, no. 4, pp. 1013–1029, July 1994.
- [10] A. Cohen and I. Daubechies, “Non-separable bidimensional wavelet bases”, *Revista Matemática Iberoamericana*, vol. 9, no. 1, pp. 51–137, 1993.
- [11] A. Cohen, I. Daubechies, and J.-C. Feauveau, “Biorthogonal bases of compactly supported wavelets”, *Commun. Pure Appl. Math.*, vol. 45, pp. 485–560, 1992.
- [12] I. Daubechies, “Orthonormal bases of compactly supported wavelets”, *Commun. Pure Appl. Math.*, vol. 41, pp. 909–996, 1988.
- [13] I. Daubechies, *Ten Lectures on Wavelets*, Soc. Indus. Appl. Math., Philadelphia, PA, 1992.
- [14] I. Daubechies, “Orthonormal bases of compactly supported wavelets II. variations on a theme”, *SIAM J. Math. Anal.*, vol. 24, no. 2, pp. 499–519, Mar. 1993.

- [15] G. Deslauriers and S. Dubuc, “Symmetric iterative interpolation process”, *Constr. Approx.*, vol. 5, no. 1, pp. 49–68, 1989.
- [16] D. L. Donoho, “De-noising by soft-thresholding”, *IEEE Trans. Inform. Theory*, vol. 41, no. 3, pp. 613–627, May 1995.
- [17] D. E. Dudgeon and R. M. Mersereau, *Multidimensional Digital Signal Processing*, Prentice-Hall, Englewood Cliffs, NJ, 1983.
- [18] L. J. Karam, “Design of complex multi-dimensional FIR filters by transformation”, in *Proc. IEEE Int. Conf. Image Processing*, Lausanne, Switzerland, Sept. 1996, pp. 573–576.
- [19] S. E. Kelly, “Pointwise convergence of wavelet expansions”, *Bull. Amer. Math. Soc.*, vol. 30, no. 1, pp. 87–94, Jan. 1994.
- [20] J. Kovačević and M. Vetterli, “Nonseparable multidimensional perfect reconstruction filter banks and wavelet bases for  $R^n$ ”, *IEEE Trans. Inform. Theory*, vol. 38, no. 2, pp. 533–555, Mar. 1992.
- [21] M. Lai, “On the digital filter associated with Daubechies’ wavelets”, *IEEE Trans. Signal Processing*, vol. 43, no. 9, pp. 2203–2205, Sept. 1995.
- [22] S. G. Mallat, “Multiresolution approximation and wavelet orthonormal bases of  $L^2(\mathbf{R})$ ”, *Trans. Amer. Math. Soc.*, vol. 315, no. 1, pp. 69–87, Sept. 1989.

- [23] S. G. Mallat, “A theory for multiresolution signal decomposition: the wavelet representation”, *IEEE Trans. Pattern Anal. Machine Intell.*, vol. 11, no. 7, pp. 674–693, July 1989.
- [24] S. G. Mallat and W. L. Hwang, “Singularity detection and processing with wavelets”, *IEEE Trans. Inform. Theory*, vol. 38, no. 2, pp. 617–643, Mar. 1992.
- [25] R. M. Mersereau, W. F. G. Mecklenbrauker, and T. F. Quatieri, Jr., “McClellan transformations for two-dimensional digital filtering: I – design”, *IEEE Trans. Circuits Syst.*, vol. CAS-23, no. 7, pp. 405–414, July 1976.
- [26] A. V. Oppenheim and R. W. Schaffer, *Discrete-Time Signal Processing*, Prentice-Hall, Englewood Cliffs, NJ, 1989.
- [27] J. M. Ortega and W. C. Rheinboldt, *Iterative Solution of Nonlinear Equations in Several Variables*, Academic Press, New York, NY, 1970.
- [28] S.-M. Phoong, C. W. Kim, P. P. Vaidyanathan, and R. Ansari, “A new class of two-channel biorthogonal filter banks and wavelet bases”, *IEEE Trans. Signal Processing*, vol. 43, no. 3, pp. 649–665, Mar. 1995.
- [29] O. Rioul and P. Duhamel, “Fast algorithms for discrete and continuous wavelet transforms”, *IEEE Trans. Inform. Theory*, vol. 38, no. 2, pp. 569–586, Mar. 1992.
- [30] A. Said and W. A. Pearlman, “A new, fast, and efficient image codec based on set partitioning in hierarchical trees”, *IEEE Trans. Circuits Syst. Video Tech.*, vol. 6, no. 3, pp. 243–250, June 1996.

- [31] N. Saito and G. Beylkin, “Multiresolution representation using the auto-correlation functions of compactly supported wavelets”, *IEEE Trans. Signal Processing*, vol. 41, no. 12, pp. 3584–3590, Dec. 1993.
- [32] I. W. Selesnick, J. E. Odegard, and C. S. Burrus, “Nearly symmetric orthogonal wavelets with non-integer DC group delay”, in *Proc. 7th IEEE DSP Workshop*, Loen, Norway, Sept. 1996, pp. 431–434.
- [33] M. J. Shensa, “The discrete wavelet transform: Wedding the à trous and Mallat algorithms”, *IEEE Trans. Signal Processing*, vol. 40, no. 10, pp. 2464–2482, Oct. 1992.
- [34] D. Stanhill and Y. Y. Zeevi, “Two-dimensional orthogonal wavelets with vanishing moments”, *IEEE Trans. Signal Processing*, vol. 44, no. 10, pp. 2579–2590, Oct. 1996.
- [35] G. Strang, “Wavelets and dilation equations: A brief introduction”, *SIAM Rev.*, vol. 31, no. 4, pp. 614–627, 1989.
- [36] G. Strang and T. Nguyen, *Wavelets and Filter Banks*, Wellesley-Cambridge, Wellesley, MA, 1996.
- [37] W. Sweldens, “The lifting scheme: a custom-design construction of biorthogonal wavelets”, *Appl. Comput. Harmon. Anal.*, vol. 3, no. 2, pp. 186–200, 1996.
- [38] W. Sweldens and R. Piessens, “Wavelet sampling techniques”, in *Proc. Statistical Computing Section*, 1993, pp. 20–29, American Statistical Association.

- [39] W. Sweldens and R. Piessens, “Asymptotic error expansions of wavelet approximations of smooth functions II”, *Numer. Math.*, vol. 68, no. 3, pp. 377–401, 1994.
- [40] W. Sweldens and R. Piessens, “Quadrature formulae and asymptotic error expansions for wavelet approximations of smooth functions”, *SIAM J. Numer. Anal.*, vol. 31, no. 4, pp. 1240–1264, Aug. 1994.
- [41] J. Tian and R. O. Wells, Jr., “Vanishing moments and wavelet approximation”, Tech. Rep. CML TR95-01, Computational Mathematics Laboratory, Rice University, Houston, TX, 1995.
- [42] M.-J. Tsai, J. D. Villasenor, and F. Chen, “Stack-run image coding”, *IEEE Trans. Circuits Syst. Video Tech.*, vol. 6, no. 5, pp. 519–521, Oct. 1996.
- [43] M. Unser, “Approximation power of biorthogonal wavelet expansion”, *IEEE Trans. Signal Processing*, vol. 44, no. 3, pp. 519–527, Mar. 1996.
- [44] P. P. Vaidyanathan, *Multirate Systems and Filter Banks*, Prentice-Hall, Englewood Cliffs, NJ, 1992.
- [45] M. Vetterli and C. Herley, “Wavelets and filter banks: Theory and design”, *IEEE Trans. Acoust. Speech Signal Processing*, vol. 40, no. 9, pp. 2207–2232, Sept. 1992.
- [46] M. Vetterli and J. Kovačević, *Wavelets and Subband Coding*, Prentice-Hall, Englewood Cliffs, NJ, 1995.



- [47] J. D. Villasenor, B. Belzer, and J. Liao, “Wavelets filter evaluation for image compression”, *IEEE Trans. Image Processing*, vol. 4, no. 8, pp. 1053–1060, Aug. 1995.
- [48] D. Wei and A. C. Bovik, “Asymptotic convergence of biorthogonal wavelet filters”, in *Proc. Asilomar Conf. Signals, Systems, and Computers*, Pacific Grove, Nov. 1997, vol. 2, pp. 1244–1248.
- [49] D. Wei and A. C. Bovik, “On asymptotic convergence of the dual filters associated with two families of biorthogonal wavelets”, *IEEE Trans. Signal Processing*, vol. 45, no. 12, pp. 2928–2940, Dec. 1997.
- [50] D. Wei and A. C. Bovik, “Enhancement of compressed images by optimal shift-invariant wavelet packet basis”, *J. Visual Commun. Image Represent.*, vol. 9, no. 4, pp. 15–24, Mar. 1998, Special Issue on High-Fidelity Media Processing.
- [51] D. Wei and A. C. Bovik, “Generalized Coiflets with nonzero-centered vanishing moments”, *IEEE Trans. Circuits Syst. II*, vol. 45, no. 8, Aug. 1998, Special Issue on Multirate Systems, Filter Banks, Wavelets, and Applications.
- [52] D. Wei and A. C. Bovik, “Sampling approximation of smooth functions via generalized Coiflets”, *IEEE Trans. Signal Processing*, vol. 46, no. 4, pp. 1133–1138, Apr. 1998, Special Issue on Theory and Applications of Filter Banks and Wavelet Transforms.
- [53] D. Wei, B. L. Evans, and A. C. Bovik, “Biorthogonal quincunx Coifman

- wavelets”, in *Proc. IEEE Int. Conf. Image Processing*, Santa Barbara, CA, Oct. 1997, vol. II, pp. 246–249.
- [54] D. Wei, A. C. Bovik, and B. L. Evans, “Generalized Coiflets: A new class of orthonormal wavelets”, in *Proc. Asilomar Conf. Signals, Systems, and Computers*, Pacific Grove, CA, Nov. 1997, vol. 2, pp. 1259–1263.
- [55] D. Wei, B. L. Evans, and A. C. Bovik, “Loss of perfect reconstruction in multidimensional filterbanks and wavelets designed via extended McClellan transformations”, *IEEE Signal Processing Letters*, vol. 4, no. 10, pp. 295–297, Oct. 1997.
- [56] D. Wei, H.-T. Pai, and A. C. Bovik, “Antisymmetric biorthogonal Coiflets for image coding”, in *Proc. IEEE Int. Conf. Image Processing*, Chicago, IL, Oct. 1998.
- [57] D. Wei, J. Tian, R. O. Wells, Jr., and C. S. Burrus, “A new class of biorthogonal wavelet systems for image transform coding”, *IEEE Trans. Image Processing*, vol. 7, no. 7, pp. 1000–1013, July 1998.
- [58] X.-G. Xia, C.-C. J. Kuo, and Z. Zhang, “Wavelet coefficient computation with optimal prefiltering”, *IEEE Trans. Signal Processing*, vol. 42, no. 8, pp. 2191–2196, Aug. 1994.

## Vita

Dong Wei was born in Beijing, China, on May 9, 1968, the son of Qinfang Zheng and Guangyi Wei. After completing his work at the Experimental High School attached to Beijing Normal University in Beijing in 1987, he entered Tsinghua University in Beijing. He received the degree of Bachelor of Engineering from Tsinghua University in July 1992. During the following year he was employed as an engineer in Tsinghua University. In August 1993, he entered the Graduate School of Rice University in Houston, Texas, where he received the degree of Master of Science in Electrical Engineering in May 1995. During the summer of 1995, he worked for Schlumberger Austin Research Center, Austin, Texas. In August 1995, he entered the Graduate School of The University of Texas at Austin.

Permanent address: 3473-A Lake Austin Blvd.  
Austin, Texas 78703 U.S.A.

This dissertation was typeset with L<sup>A</sup>T<sub>E</sub>X<sup>†</sup> by the author.

---

<sup>†</sup>L<sup>A</sup>T<sub>E</sub>X is a document preparation system developed by Leslie Lamport as a special version of Donald Knuth's T<sub>E</sub>X Program.